Chapter 4 Nation-Wide Survey for Geothermal Resources

Chapter 4 Nation-Wide Survey for Geothermal Resources

4.1 Preliminary Evaluation of 73 Geothermal Fields and Selection of Supplemental Survey Fields

4.1.1 Preliminary Evaluation of Geothermal Resources

(1) Research Area

In the preliminary evaluation stage, processing, analysis and interpretation of the collected data for 73 fields were conducted. Following to a request from the Indonesian side, three additional fields, Sipaholon in North Sumatra, Iyan Argopuro in East Java and Suwawa in Gorontaro, were added to 70 initial target fields (Fig. 4.1.1-1).

(2) Data collection and Methodology of Preliminary Evaluation

Geological data of regional geology, tectonic structure and well geology, geochemical data on thermal fluids from hot springs, fumaroles and wells, and geothermal conceptual model for the 73 prospective fields were collected from CGR and by literature searches. The data and information were compiled and integrated.

Geological data on regional geologic map covered the whole Indonesia, geological sections, and alteration distribution maps in each target field were collected in digital format as much as possible. The study results were summarized as conceptual model of geothermal systems in each field. However, the conceptual model in some prospective fields could not be prepared due mainly to lack of detailed survey data. Surface alteration maps and resistivity distribution map were used for resource evaluation in such fields.

In geochemical study, major chemical composition data of 196 for hot spring water, 20 for well water, 31 for fumarolic gas and 6 for well gas were collected. For hydrogen and oxygen isotopic composition, the data of 24 for hot spring water and 4 for well water were collected. The chemical data for hot spring water were available for evaluation of 51 fields, but data for the other 22 fields could not be used. For the fields where raw analytical data were not available, in case that processed chemical data or information including geochemical temperatures was available in the CGR's internal reports, the data or information were used for geochemical interpretation in this study.

(3) Geological Study

Indonesia is a huge archipelagic country extending 5,120km from east to west and 1,760 kilometers from north to south. It encompasses 13,667 islands (some sources say as many

as 18,000), only 6,000 of which are inhabited. There are five main islands (Sumatra, Java, Kalimantan, Sulawesi, and Irian Jaya), two major archipelagoes (Nusa Tenggara and the Maluku Islands), and sixty smaller archipelagos. Two of the islands are shared with other nation; Kalimantan (known in the colonial period as Borneo, the world's third largest island) is shared with Malaysia and Brunei, and Irian Jaya shares the island of New Guinea with Papua New Guinea. Indonesia's total land area is 1,919,317 square kilometers of islands. Included in Indonesia's total territory is another 93,000 square kilometers of inlands sea (straits, bays, and other bodies of water). The additional surrounding sea areas bring Indonesia's generally recognized territory (land and sea) to about 5 million square kilometers. The government, however, also claims an exclusive economic zone, which brings the total to about 7.9 million square kilometers.

In geography, there are Sumatra, Java (and Madura), Kalimantan (formerly Borneo), and Sulawesi (formerly Celebes) in the Greater Sunda Islands. These islands, except for Sulawesi, lie on the Sunda Shelf—an extension of the Malay Peninsula and the Southeast Asian mainland. Far to the east is Irian Jaya, which takes up the western half of the world's second largest island—New Guinea—on the Sahul Shelf. Sea depths in the Sunda and Sahul shelves are in average 200 meters or less. Between these two shelves lie Sulawesi, Nusa Tenggara (also known as the Lesser Sunda Islands), the Maluku Islands (or the Moluccas).

Tectonically, this region—especially Java—is highly unstable, and although the volcanic ash has resulted in fertile soils, it makes agricultural conditions unpredictable to some areas. The country has numerous mountains and some 400 volcanoes, of which approximately 100 are active. Since 1970's, more than forty volcanic eruptions were recorded, mostly in Java. The most violent volcanic eruptions in modern times occurred in Indonesia is in 1815 a volcano eruption in Gunung Tambora on the north coast of Sumbawa, Nusa Tenggara Barat Province and claimed 92,000 injured and created " the year without a summer" in various parts of the world. In 1883 Krakatau explosion in the Sunda Strait between Java and Sumatra generates some 36,000 West Javanese died from the resulting tidal wave. Sound of the explosion was reported as far away as Turkey and Japan. For almost a century following that eruption, Krakatau was quiet, until the date. Recently, a gigantic earthquake attached the surrounding Jogyakarta and died 6,000 people over. With relation to the current earthquake, Merapi volcano, which situated to the north of Jogyakarta, increases the activities of pyroclastic as flow eruption.

Mountains ranging between 3,000 and 3,800 meters above sea level can be found on the islands of Sumatra, Java, Bali, Lombok, Sulawesi, and Seram. The country's tallest mountains, which reach between 4,700 and 5,000 meters, are located in the Jayawijaya Mountains and the Sudirman Mountains in Irian Jaya. The highest peak, Puncak Jaya, which reaches 5,039 meters, is located in the Sudirman Mountains.

Nusa Tenggara consists of two strings of islands stretching eastward from Bali toward Irian Jaya. The inner arc of Nusa Tenggara is a continuation of the chain of mountains and volcanoes extending from Sumatra through Java, Bali, and Flores, and trailing off in the Banda Islands. The outer arc of Nusa Tenggara is a geological extension of the chain of islands west of Sumatra that includes Nias, Mentawai, and Enggano. This chain resurfaces in Nusa Tenggara in the ruggedly mountainous islands of Sumba and Timor.

The Maluku Islands are geologically among the most complex of the Indonesian Islands. They are located in the northeast sector of the archipelago, bounded by the Philippines to the north, Irian Jaya to the east, and Nusa Tenggara to the south. The largest of these island include Halmahera, Seram, and Buru, all of which rise steeply out of very deep seas. This abrupt relief pattern from sea to high mountains means that there are very few level coastal plains.

Geological tectonic zones in Indonesia are divided into following five zones: Malay Tectonic Zone, Sumatra Tectonic Zone, Sunda Tectonic Zone, Maruku Tectonic Zone and Irian Jaya Tectonic zone (Fig. 4.1.1-2).

(a) Malay Tectonic Zone

This zone mainly consists of granitic rocks in the period of Late Paleozoic to Early Mesozoic and distributes in Malay Peninsula, West Kalimantan, Bangka and Belitung. Sedimentary rocks deposits at the western portion and the eastern portion of Malay Peninsula. Among them, non-marine sediment under the circumstances of old continental crust exists in the western portion of Peninsula. In Triassic period, the presence of granitic intrusion is reported. On the contrary, shale extends dominantly and regional acidic volcanic activity and granitic intrusion are recognized in the period of Carboniferous and Triassic in eastern portion. Bintang Island, Bangka Island and Belitung are famous for tin deposits.

(b) Sumatra Tectonic Zone

Sumatra Tectonic Zone encloses Malay Tectonic Zone and exists in almost all of Sumatra, northern Java, southeastern part and eastern part of Kalimantan. Its basement is various kinds of rocks in the time from Paleozoic to Mesozoic period. In Sumatra, sedimentary rocks and volcanic rocks of Cenozoic period overlie the sediments from Paleozoic to Triassic era.

(c) Sunda Tectonic Zone

Sunda Tectonic Zone is at the outer side of Sumatra Tectonic Zone and runs at western coast of Sumatra, southern Java, Small Sunda Islands and bends towards the north to SE Sulawesi and Minahasa Peninsula. Regional depression proceeded in early Miocene and thick shale

deposited in middle Miocene. In southwestern portion of Sumatra, rhyolitic rock and andesitic volcanic rocks and breccias appear under the marine regression circumstances.

Most of target geothermal fields in Sumatra, Java, Bali and Nusa Tenggarah Islands were included in this tectonic zone.

(d) Maluku Tectonic Zone

Maruku Tectonic Zone exists in the outer-most side of above three tectonic zones and runs at Muntawai Islands of Sumatra, Timor Island, Tanimbar Islands, Seram Island and Tariabu Islands and reaches to eastern part of Sulawesi. Although there are no active volcanoes, ultra-basic rocks consist of ophyolite partly.

Teluhu in Ambon Island and Lainea, Marana, Bora and Bituang in Sulawesi Island among 73 target fields were located in this tectonic zone.

(e) Irian Jaya Tectonic Zone

Irian Jaya Tectonic Zone forms the north edge of the Australian continental plate. This zone consists of three mountain ridges, northern, central and southern mountains. In northern ridge, volcanic rocks in Mesozoic and Neogene sedimentary rocks spread widely on the basement of metamorphic rocks and ultra basic rocks in Paleozoic. In central mountains, sedimentary rocks that consist of limestone, sandstone, shale and so on from Paleozoic to Cenozoic, deposited thickly and granitic rocks intruded at the period of Neogene. On the contrary, limestone in Mesozoic and Quaternary sedimentary rocks mainly distributes in the portion of southern ridge.

Geothermal fields in Lahendong, Tompaso, Kotamobagu and Suwawa in northern Sulawesi, Jailolo in Halmahera Island and Tonga Wayana in Bacan Island belong to an unique tectonic zone, which is different from above 5 tectonic zones. These geothermal fields were created as result of movement of Celebes Sea plate from north and Moluccas ocean plate. The effect of the two stresses from north and south, the north arm of Sulawesi plate moved eastward that collides with westward movement of Moluccas ocean plate (K-shape Halmahera Island).

(4) Geochemical Analysis

The collected chemical data of thermal waters and gases have been compiled and studied, and the results combined with information from CGR's internal reports provides geothermal indices for the 73 prospective fields as shown in Table 4.1.1-1.

(a) Surface Thermal Manifestations

The measured maximum temperature of surface thermal manifestations (hot springs or fumaroles) in each fields is close to the boiling point (above 90℃) at more than half of the 73 prospective fields. At the other fields except for a few fields, the maximum temperature over 50℃ has been observed.

More than one hot spring or fumaroles was observed in most of the prospective fields. In the Tulehu field where the largest number of chemical data on hot spring water was available, the chemical data of 22 individual spring waters were obtained. The chemical data on fumarolic gases were available only for 16 fields, but existing of fumarole or sulfatara in the other numerous fields had been recorded in the CGR's internal reports. The existing of natural fumaroles implies that occurrence of thermal fluids of the temperature above 100℃ at relatively shallow level.

(b) Origin of Thermal Fluids

Origin of the water from hot springs and wells was examined from their hydrogen and oxygen isotopic composition (App.4.1.1-1). Most of the data for hot springs show isotopic compositions similar to those of *Meteoric Waters* , whose values were deduced from t the isotopic compositions of typical meteoric water in the world. These results suggest that the hot spring waters originate mainly in meteoric water (rainwater infiltrated into subsurface).

Among the hot spring waters having isotopic composition different from the *Meteoric Watere*, the waters in the Bena-Mataloko field are likely to be affected by isotopic fractionation due to surface evaporation (steam separation), though they must originate essentially in meteoric water.

One of the hot spring waters in the Wai Sano field exhibits an isotopic composition similar to *Andesitic Magma Water*. This indicates that the spring water possibly contains magma-derived water.

Some hot spring waters in the Iboi-Jaboi and Lempur/Kerinci fields and all the well waters in the Lempur/Kerinci have isotopic compositions that oxygen isotope ratio ($\delta\ ^{18}O$) shows positive oxygen shifts of 1-2‰ from the *Meteoric Water*. This suggests that the waters originate in meteoric water and have had isotope exchange reaction at high temperature with rock-forming minerals, which have high (isotopically heavy) oxygen isotope ratio in general. The occurrence of those waters implies that geothermal reservoir fluids having well reacted with host rocks may exist in the two fields.

In addition to the data represented in App.4.1.1-1, hydrogen and oxygen isotopes of thermal waters in five fields (Seulawah Agam, Hu'u Daha, Marana, Jailolo and

Suwawa-Gorontalo) have been represented in figures in CGR's internal reports (though raw data are not shown). According to the figures, most of the thermal waters seem to originate in meteoric water. Some of the thermal waters in the Hu'u Daha and Jailolo, however, have isotopic compositions indicating some contribution of seawater. Regarding the contribution of seawater into thermal water, it will be also examined below in the discussion on water chemistry.

(c) Occurrence of Acid Sulfate Water

In general, sulfate-rich thermal acid water is derived from mixture of steam and gases (including H_2S) ascending from depth with shallow groundwater or surface water, and the acid water contains sulfate ion (SO_4^{2-}) with high concentration due to air-oxidation of the H_2S gas. Therefore, the existing of acid sulfate thermal-water at the surface suggests that deep thermal fluid occurs with boiling at a temperature above 100℃.

Diagrams for major anions and Cl/SO_4 molar ratio vs. pH of thermal waters constructed with using the data collected in this study are shown in App.4.1.1-2 and App.4.1.1-3 respectively. These diagrams reveal that acidic (pH<4) thermal water classified into SO_4-type occurred in 18 fields listed below (cf. Table 4.1.1-1).

Iboih-Jaboi	Sarula	Merapi-Sampuraga
Pusuk Bukit-Danau Toba	Simbolon-Samosir	Lempur/Kerinci
Air Dikit	B. Gedung Hulu Lais	Bukit Daun
Lumut Balai	Kamojang	Darajat
Tangkubanperahu	Hu'u Daha	Ulumbu
Bena-Mataloko	Sokoria-Mutubusa	Oka-Larantuka

The lowest pH (1.9) was observed at a hot spring (95℃) in the Sokoria-Mutubasa field. The highest concentration of SO_4 ion(5,485mg/L) was determined for a hot spring (96℃, Cl/SO_4=0.004) in the Iboi-Jaboi field.

Among the fields listed above, in the five fields (S. Merapi-Sampuraga, Pusuk Bukit-Danau Toba, Tangkubanperahu, Hu'u Daha and Sokoria-Mutubusa), hot spring waters rich in chloride ion as well as sulfate ion and of Cl/SO_4 molar ratios over 1.0 are also present. These waters are possibly admixture of the meteoric water with magma-derived strongly acidic gases (HCl, SO_2, etc.) or seawater (having high chloride concentration).

(d) Occurrence of Neutral Chloride Water and Contribution of Seawater

Generally, deep geothermal reservoir water utilized to power generation is of neutral-pH (or

weakly alkaline) and its major anion is dominated by chloride ion (the water is classified into Cl-type, Cl-SO_4-type or Cl-HCO_3-type in the ternary plot shown in App.4.1.1-2). This kind of thermal water is yielded by dissolution of chlorine from host rocks into meteoric thermal water or neutralization of chloride-rich acidic magma-derived water reacting with host rocks. In the field where the neutral chloride thermal water occurs at the surface as hot spring or shallow well water, geothermal reservoir water with high temperature is likely to exist at the depth.

According to the classification of thermal waters using chemical data collected in this study, neutral-pH (or weakly alkaline) and chloride type thermal-waters are recognized in 25 fields listed below (App.4.1.1-2, App.4.1.1-3 and Table 4.1.1-1).

Iboih-Jaboi	Lho Pria Laot	Seulawah Agam
G. Kembar	Sarula	Sibual Buali
S. Merapi-Sampuraga	Muaralabuh	Sungai Tenang
Sungai Penuh	Tambang Sawah	Suoh Antatai
G. Sekincau	Rajabasa	Wai Ratai
Cisolok-Cisukarame	Tangkubanperahu	Ungaran
Wilis/Ngebel	Hu'u Daha	Wai Sano
Sokoria-Mutubusa	Oka-Larantuka	Marana
Tulehu	Jailolo	Sipaholon-Tarutung
Suwawa-Gorontalo		

It is noteworthy fact that the neutral chloride type thermal-water also occurs in case of existing of seawater contribution even if the water is not derived from deep geothermal reservoir. The contribution of seawater in thermal waters was examined with constructing cross plots of boron (B) vs. Cl (App.4.1.1-4) and total silica (T-SiO_2) vs. Cl (App.4.1.1-5). Unaltered seawater has a very low B/Cl molar ratio (ca. 0.001) and T-SiO_2 content compared to those of typical thermal waters. In addition to those parameters, hydrogen and oxygen isotopic ratios of thermal waters were utilized for examining the contribution of seawater. As a result, it is suggested that hot spring waters in the 6 fields being underlined among the 25 fields listed above are likely to be contributed by seawater. All the 6 fields are geothermal field located at seashore or in small remote islands, and the hot spring waters in those fields are generally high in chloride ion concentration.

Therefore, in the 19 fields listed above excluding the 6 fields where the thermal waters are possibly contributed by seawater, possibility of occurrence of deep geothermal reservoir water originating mainly in meteoric water is thought to be very high. Nevertheless, contribution of seawater at the 19 fields has not been denied entirely, so that further detailed study is needed in the future. On the other hand, the possibility of occurrence of deep

geothermal reservoir water still remains for the 6 fields where the thermal waters are possibly contributed by seawater, and the 6 fields are not wholly evaluated to be non-promising.

(e) Fluid Temperature Estimation by Geothemometries

In a geothermal field under early exploration stage, geochemical temperatures calculated by using chemical data of hot spring water or fumarolic gas, regardless of origin or chemical characteristics of the thermal fluids, are the most valuable chemical indices to evaluate resource potential in the field.

Geochemical temperatures calculated from the data for hot spring and well waters and fumarolic and well gases are shown in Table 4.1.1-1. Geothermometers adopted for calculating the temperature are as follows.

Silica temperature

T (SiO_2) : T- α -cristobalite, T-chalcedony and T-quartz : Fournier (1977)

Cation temperature

T (Na/K) : Truesdell (1976) and Fournier (1979)

T (NaKCa-dMg) : Fournier and Potter (1979)

T (K/Mg) : Giggenbach (1988)

Gas chemical temperature

T (CO_2-H_2S-H_2-CH_4): D'Amor and Panichi (1980)

Silica temperatures, which are calculated from silica content in water that is rapidly re-equilibrated for temperature change of the water, tend to reflect a temperature at relatively shallow level under the ground. Accordingly, most of the calculated silica temperatures for thermal waters in each field were relatively low at below 200℃. High silica temperatures above 200℃ (257℃ in maximum in G. Sekincau), however, were calculated for hot spring waters in 6 fields (Sarula, Sungai Penuh, Suoh Antatai, G. Sekincau, Wai Ratai and Lahendong). In those fields excluding the Lahendong field, neutral-pH chloride spring waters were observed, suggesting that hot reservoir fluid was likely to occur at the depth.

Regarding the silica temperature (T-quartz) for well waters, high temperatures above 200℃ were calculated for the waters in Lempur/Kerinci, G. Salak, G. Wayang-Windu and G. Karaha.

Among the cation temperatures, T(Na/K) is thought to reflect fluid temperature at a relatively deeper level under the ground. The highest temperature of calculated T(Na/K)s in

each field is above 200℃ at numerous fields. However, the reliability of T(Na/K) for estimating fluid temperature at a deeper level is restricted when the surface thermal water is contributed by deep hot water well-reacted with reservoir host rocks. To examine the reliability of T(Na/K) for all the data, ternary plot of Na-K-Mg composition was constructed (App.4.1.1-6). In that diagram, the data plotted closer to a curve indicating *full equilibrium* have higher reliability of its T(Na/K). Only the T(Na/K)s thought to have high reliability are represented in Table 4.1.1-1. The highest temperature of T(Na/K)s in each field ranges from 170 to 300℃, and is above 200℃ in most of the fields.

The gas chemical temperature is also considered to reflect fluid temperature at a relatively deeper level. The highest gas chemical-temperature is above 200℃ in most of the fields in where gas chemical data have been obtained. Cross-plots of H_2/CH_4 molar ratio, which is one of the temperature indices of gas chemistry, vs. gas chemical temperature are shown in App.4.1.1-7.

(5) Geothermal Conceptual Model

In order to construct the geothermal conceptual model, data and information of three essential components, such as reservoir structure (underground geological structure), heat source (geothermal activity history), and water supply (water availability & flow pattern), should be basically collected, analyzed and integrated from geoscientific studies. The schematic process for geothermal interpretations is shown to Fig. 4.1.1-3.

Fluid behavior in most geothermal reservoirs are regarded to be controlled by fracture system, even in horizontal permeability type reservoir. Therefore, detection of location and extent of permeability of fracture along faults are important. In this study, evaluation of permeability of fracture was conducted from the geological viewpoints using exiting data and collected data in the field work. . In order to exploit such geothermal resources efficiently, it is first necessary to locate the reservoir and to identify reservoir structure. Behavior and extent of geothermal fluid in permeability along those fractures and so on were inferred using geological information such as geology, geological structure, manifestation and alteration and geochemical information such as hot spring waters, fumarolic gases and well discharges. To construct the model, a variety of geoscientific field data, such as geological, hydrological, geophysical and geochemical data were used.

Geology and geological structure at the exploitable depth of geothermal development were integrated on a 2-dimension or 3-dimensional model with data of the surface geology and geological structure in addition to geophysical survey data (gravity, resistivity and etc.) and well test data. In case that the data of well drilling and results of well test could be collected, the precise and detailed geological conditions, such as lithological correlation, trends of faults and distribution of alteration zone, were studied for the modeling.

In order to clarify the thermal structure in a geothermal system, heat source of the geothermal system related to regional magmatic activities, that is, feature and location of heat supply to the hydrothermal system in the geothermal system was studied considering volcanic activity history. Heat supply to the hydrothermal system was illustrated by intrusion of magma, conductive heat flow, and/or fluid convection along deep fracturing etc. Some case studies for deep geothermal development had showed the existence of intrusion as a heat source in the geothermal system and existence of reservoirs in fracture zones around the intrusion. In such geothermal fields, data of geophysical survey (gravity, magnetic, seismic) is generally of help in structural interpretation and preparation of conceptual model. Clarification of volcanic activity history based on rock age is generally utilized in estimation of the effect of remnant magma.

Characteristics of hydrothermal systems in the target fields were inferred mainly based on chemical data of well discharges, hot springs, fumaroles with reference to geological structure and geology. Geothermal fluid behaviors estimated for making geothermal conceptual models in this study are listed as follows:

- Type classification of hydrothermal system.
- Origin /formation mechanism of geothermal fluid
- Extent/center of each hydrothermal system
- Regional flow patterns of geothermal water and groundwater
- Recharge area and discharge area of the hydrothermal system
- Relationship between the behavior of the fluid and geological structure

In this Master-Plan Study, the simplified economic evaluation of the geothermal development project in each field was supposed to be conducted, based on the exploitable geothermal potential. In order to evaluate the economy of each project, potential of geothermal power development in the field was calculated using the conceptual model. In some field where the model could not be prepared adequately due mainly to shortage of geoscientific data, data on geothermal surface manifestations (fumaroles, hot springs, and surface features, etc) and resistivity maps of Schulumberger survey and MT survey were used for delineating geothermal reservoir in the field.

(6) Calculation of Resource Potential by Stored Heat Method

Fig. 4.1.1-4 shows the flow chart of resource potential evaluation. The geothermal resource potential was calculated by means of the Stored Heat Method based on the geothermal

reservoir conceptual model. The Stored Heat Method is usually used at the preliminary stage of geothermal development as a simple method for evaluating the resource potential. This method estimates first the reservoir volume and its average temperature to calculate the stored heat in the reservoir, and then calculates the equivalent electric power generation assuming the recovery factor that is an extractable energy ratio from the reservoir. The equations are as follows.

Stored Heat= $(T_r - T_a) \times \{(1-\phi) C_{pr} \rho_r + \phi C_{pw} \rho_w\} \times V$

Heat Recovery(H.R)=Stored Heat × Recovery Factor

Resource Potential= (H.R. x C.E.) / (Lf x P.L.)

T_r, T_a : Reservoir temperature (℃), Abandonment temperature (℃)

ϕ : Rock porosity (%)

ρ_r, ρ_w : Rock density (kg/m^3), Fluid density (kg/m^3)

C_{pr}, C_{pw} : Rock specific heat(kJ/kg-℃), Fluid specific heat (kJ/kg-℃)

V : Reservoir volume (km^3)

C.E. : Heat/electricity conversion factor (%)

Lf : Plant capacity factor (%)

P.L. : Plant operation period (year)

In this calculation, it is difficult to select a unique value of each parameter because of the expected range. Accordingly, the resource potential itself estimated by the Stored Heat Method should have a range. In addition, we should notice that the Stored Heat Method gives conservative estimate of the resource potential, because this method supposes that the geothermal reservoir is a closed system ignoring the recharge of geothermal fluids.

Considering the range of each parameter for the Stored Heat Method, Monte Carlo Analysis was combined to this method to evaluate the most probable resource potential statistically. The Monte Carlo Analysis is a method that statistically analyzes the probability of resource potential by combining values of each parameter for the Stored Heat Method within the expected range using random generator. In this study, the resource potential of which the probability is 20-80% was evaluated by calculating 100,000 patterns of parameter combinations for each field.

The evaluation was carried out after the preliminary evaluation and after supplemental study. Finally, the resource potentials in 39 fields were evaluated because these fields have enough data for calculating the resource potential. The results of evaluation are shown in Table 4.7.1-1, and the results of Monte Carlo Analysis of each field are attached in Appendix (App.4.7.1-1).

The fields under development were excluded for evaluating resource potential by the Stored

Heat Method, and their planning power outputs, which were decided through detailed evaluation such as reservoir simulation study, were adopted as their resource potentials for this study.

(7) Simplified Economical Evaluation

Simplified economical evaluation was conducted after the preliminary geothermal resource evaluation at first. After the supplementary study, simplified economical evaluation was conducted in consideration of supplementary study. In the simplified economical evaluation, the initial capital investment per kW, which is a cost per kW required for constructing a geothermal power plant, was roughly estimated. Main parameters that remarkably affect the generation cost of geothermal power plant are plant cost and well drilling cost. According to the report of Geothermal Energy Association, the typical cost breakdown of geothermal power project indicates that the ratio of plant cost and well drilling cost is 54% and 23%, respectively, which occupies in total 77% of the total cost (Hence, 2005). Calculating plant and well drilling costs can, therefore, roughly estimate the initial capital investment. In the simplified economical evaluation, the sum of plant cost and well drilling cost was assumed as an initial capital investment, and then the initial capital investment cost per kW was calculated by dividing the initial capital investment by the scale of power plant, which was estimated within each resource potential considering its power demand of the area. Fig. 4.1.1-5 shows the flow chart of simplified economical evaluation.

First, plant cost was calculated considering the scale of the power plant, and well drilling cost was estimated by multiplying the number of well by a single-well-drilling-cost that was calculated by multiplying the drilling length by a drilling-unit-cost. In order to estimate the required number of well it is necessary to know the averaged productivity of a well (single-well-productivity). However, the available measured data of an averaged single-well-productivity is very limited to the filed only where is under development such as Kamojang field, West Jawa. Majority of the other fields hardly have production data of well. Accordingly, the single-well-productivity (power output) was predicted using wellbore simulator WELLFLOW by assuming the depth of geothermal reservoir, temperature, and permeability (kh value). The depth and temperature of the reservoir were estimated based on the reservoir conceptual model, and the reservoir pressure was estimated from the reservoir depth. On the other hands, the permeability range of kh=1-5 darcy-m was assumed because of no measured data, considering the ordinary range of kh for the geothermal reservoir in the world, and also the tendency that the kh value of the deeper should be smaller than the shallower one was considered. The prospective production rate (the expected steam and water flow rate with its power output) was predicted based on the above reservoir conditions, using well bore simulator WELLFLOW.

The following assumptions of the relationships between the reservoir temperatures, wellhead pressure of production wells and turbine inlet pressures were made.

Reservoir Temp.	Wellhead Press.	Turbine Inlet Press.
Under 250℃	4 kg/cm^2 Abs	2 kg/cm^2 Abs
250℃ - 290℃	8 kg/cm^2 Abs	6 kg/cm^2 Abs
Over 290℃	12 kg/cm^2 Abs	10 kg/cm^2 Abs

The relationship between the reservoir depth, temperature, and predicted production rate of a well is shown in Table 4.7.2-1.

Next, the number of production wells and reinjection wells required for constructing a geothermal power plant of the developable scale at each field was estimated using the above table. The required number of reinjection well was calculated by dividing the expected total discharge water rate at each field by the single-well-injectibity that is assumed to be constant. Eventually, the required total number of production and reinjection wells was estimated, and then the initial capital investment was calculated by summing plant cost and well drilling cost.

The initial capital investments per kW of 49 fields are shown in Table 4.7.2-2. The results of the calculation indicate that the initial capital investment per kW has a range from about 1460 US$/kW to 2850 US$/kW. Properly speaking, we should notice that the initial capital investment actually increases because it is necessary to consider the construction costs of access roads, pipelines, and transmission lines in addition to the plant cost and well drilling cost. However, we judged that the general values of initial capital investment estimated from the plant cost and well drilling cost is available to compare the economical aspects of each field for selecting 16 prospective fields.

4.1.2 Selection of Supplemental Survey Fields

(1) Selection Criteria of the Fields

Based on the documents collected in Japan and provided by the Indonesian side at the time of the 1st work in Indonesia as well as hearing from various institutions of Indonesian government, evaluation criteria was considered for selection of 16 supplemental survey areas among 73 prospective fields. Basic concepts for the selection of geothermal prospective field are regarded as follows.

- Field where sufficient geothermal capacity is estimated from geothermal structures and resource evaluation.

- Field where economical development can be done.

- Field where geothermal energy development accords with power demand and development policies.

- Field where social and environmental constraints are not notable in geothermal energy development.

The consideration items for the selection of 16 survey fields are summarized as follows (Table 4.1.2-1):

(a) Economy

Cost ranking on the simplified economic evaluation based on the initial investment cost per kW (US$/kW) and characteristics of each geothermal reservoir (drilling depth, productivity and reinjectivity)

(b) Security

Geothermal developments in the fields where security is poor are likely to be delayed due to high risk of exploration and employment. Following the safety instruction by Foreign Ministry of Japan, the JICA study team could not visit geothermal fields situated in the following provinces.

- Nanggroe Aceh Darussalam

- Central Sulawesi, West Timor of East Nusa Tenggara

- Maruku, North Maruku, Papua

(c) Development Stage

Since the purpose of this study project is to prepare the future development plans as Geothermal Master Plan in accordance with Geothermal Road Map, the following fields were excluded in the field reconnaissance.

- Fields already installed the generating facilities.

- Joint Operation Contract fields.

- Detailed-explored fields with the development plan (on the Road Map 2025).

- Fields with natural/social/environmental problems and the restricted areas on regulation.

(d) Purpose of Development

Field classification between large-scale power plant connecting regional power grid and independent power plants for rural electrification (small-scale power plant in multipurpose utilization)

(e) Corporate Structure for Geothermal Power Development

Corporate structure for geothermal power development was categorized by the following three schemes.

- IPP by private investors
- Government developer financially supported by ODA (ex. Soft-Loan)
- Government developer by public support and/or local government

(f) Difficulty in Development

Necessity of supplemental field survey was finally considered on condition of infrastructure construction, power demand, access to the site, distance to the grid-line, development condition of surrounding areas, etc.

(2) Supplemental Survey Fields

In the procedure of the above-mentioned consideration items, 16 supplemental geological and geochemical survey fields (18 fields) were selected and shown below.

Sipaholon-Tarutung（N. Sumatra）, Muara Labuh and G. Talang（W. Sumatra）, Sungai Penuh（Jambi）, Bukit Gedung Hulu Lais（Bengkulu）, Marga Bayur（S. Sumatra）, Suoh Antatai and Genung Sekincau（Lampung）, Cisolok-Cisukarame and Tangkuban Perahu（W. Java）, Citamang-G. Karang（Banten）, Telomoyo and Ungaran（C. Java）, Wilis-Ngebel and Ijen（E. Java）, Sokoria-Mutubusa（E. Nusa Tenggara）, Tompaso（N. Sulawesi）, Suwawa（Golontaro）

In the 2nd Workshop/Steering Committee, additional field studies for evaluation of geothermal resources were required by the counterparts. Considering this request, 23 fields were studied as the nationwide study (data collection by conducting supplementary geological and geochemical surveys) of 2nd Work in Indonesia (Fig. 4.1.2-1).

Pusuk Bukit-Danau Toba, Simbolon-Samosir（N. Sumatra）, Tambang Sawah（Bengkulu）, Raja Basa（Lampung）, Kotamobagu（N. Sulawesi）

4.2 Supplemental Geological Field Survey

4.2.1 Methodology

In the field, a fracture survey for detecting fluid flow and a geological mapping for rock distribution was done to collect the direct evidence of the presence of faults in situ. In case of occurrence of the recent volcanic rock and the intrusive rock, the relation of geothermal activity and fault formation in connection with fluid passage was interpreted. From outcrops of surface alteration zone, the possibility of the up-flow zone (discharge zone) of geothermal fluid was estimated.

To each field, the following analysis and interpretation were done. App.4.2.2-1 shows contents of geological study.

(1) Surface Geology Analysis

Rock sequence, geological structure, basement structure and distribution of recent volcanic rocks were investigated. In this analysis, following information will be noted in particular:

- Permeability resulted in fault trend and porous sequence distribution,

- Geological structure controlling the hydrogeology

Heat source derived from the volcanic activity and magma reservoir movement in greater depth

(2) Analysis of the Alteration Area

To grasp the relation to the up-flow (discharge) zone of geothermal hot fluid, geothermal manifestation and the altered zone on surface will be studied. In additon to considering the distribution and alingnment of hot springs and fumaroles, geological structure will be investigated with reference to their distribution. Furthermore, the hydrothermal activity is also estimated based on the acquired data of altered rock distribution (alunite zone, kaolinite zone and silicified zone, etc.).

(3) Structural Analysis for Fault/Lineaments

This analysis is aiming to identify the main faults/lineaments firmly related to regional fluid migration. In fields where the exploratory wells have been drilled, the detailed structural elements are picked up to the extent to the local faults/lineaments. While in fields with short of sufficient data, the estimated structure will be described as much as possible from data of the geophysical survey. Through these structural elements such as fault trends and fracture

distributions, fluid passage and reservoir extension will be considered.

In addition, in a view to clarify the presence of the recent volcanic rocks and the intrusive rocks and to date the volcanic/hydrothermal activity, rock sampling was done in fields.

Items and number of rock samples are as follow:

- ✓ Microscopic observation
  - Preparation of thin sections ……21 pieces
  - Petrographic observation ……10 pieces
- ✓ Rock chemical composition analysis
  - X-ray analysis ……20 pieces
  - ICP-MS analysis ……11 pieces
- ✓ Rock dating analysis
  - Thermo-Luminescence method ……18 pieces
  - K-Ar method ……5 pieces

With regard to rock dating, the suitable method to each sample was applied in consideration of the forecasted time range from the existing information and the result of field survey.

4.2.2 Result

(1) Result of Field Survey

The results of survey analyses and interpretation will be referred to the Essential Elements of the Geothermal Structure Models (shown to App.4.5.2-1 and App.4.5.2-2) for each field with including the existing data, which will be mentioned in Chapter 3. Newly obtained knowledge and notable facts provided by execution of this geological survey are as follows;

The geothermal fields in Sumatra are broadly distributed along the Great Sumatra Fault Zone in all over the island. Except some fields (Muara Labuh and Sungai), each reservoir is formed as a heat source of remnant magma derived from the Quaternary active volcanism. In Tambang Sawah, B. Gedung Hulu Lais, Muara Labuh and Sungai Penuh, the graben typed reservoir are developed and consisting of a pull-apart basin with huge exploitable potential.

The geothermal fields in Java and Bali occur widely in E-W direction in parallel to the border of the tectonic plates and the volcanic belt. Other than Cisolok-Cisukarame, almost

all of fields are recognized to relate to the quaternary volcanism. The geothermal reservoirs formed by caldera and/or dome structure are dominant and hot fluids are reserved along subordinate N-S, NE-SW or NW-SE trending faults derived from the regional structure.

The geothermal fields in North Sulawesi is situated the southern end of volcanic belt extended from Mindanao island, Phillippinnes. NE-SW trending regional faults occur in this field and promising geothermal prospects exist surrounding Tondano caldera and the Ambang volcano. In Kotamobagu field, a part of caldera structure was collapsed by regional faults and a graven typed geothermal system is generated in Kopandakan and Bakan district. Hot springs are shown in Suwawa, Gorontalo, but unknown to the relation to the young volcanic events.

Although the reservoir potential of each geothermal field in Flores Island is relatively small, many promising prospects with a type of caldera and dome structure exist close to the young volcanoes.

(2) Results of Rock Sample Analysis

In the fields, each rock sample seemed to be a fresh rock faces on the naked observation, but was clarified to replace the consisting minerals to slightly altered minerals under the petrographic observation utilizing the polarized microscope.

Observation results by each analysis are shown in Apps.4.2.2-2 to 4.2.2-6.

Petrographic observation of microscopic observation

X-ray analysis

ICP-MS analysis

Thermo-Luminescence method

K-Ar method

The results of rock sample analyses and interpretation will be referred to the Essential Elements of the Geothermal Structure Models (shown to Apps. 4.5.2-1 and 4.5.2-2) for each field with including the existing data, which will be mentioned in Chapter 3. Newly obtained knowledge and notable facts provided by execution of this analysis are as follows;

From the microscopic observation, the basement rock underlied the geothermal reservoir sequence in Pusuku Bukit-Danau Toba field was recognized to be a limestone with a part of fossil fragments

In Sungai Penuh field, the Great Sumatra Fault zone was estimated to extend widely at the

west side of regional graven structure by the granitic rock petrographic observation, which shows the strongly sheared deformation structure on thin section.

From the result of thermo-luminescence dating analysis to each sample, thermal activity age from 1.7 Ka to 2, 400 Ka was estimated in the fields.

Slightly alted andesite rock was recognized at the southern portion of hot springs area in the Cisolok geothermal field from a petrographic observation by polarized microscope.

4.3 Geochemical Survey

In the geochemical survey, in order to assess or improve the inferences on the reservoir fluid characteristics (origin, heating process, sub-surface temperature, mixing, flow patern, etc.), water and gas sampling for chemical and isotopic analysis of surface thermal manifestations was conducted in the fields where sufficient chemical data for hydro-geochemical study had been lacking.

4.3.1 Survey Procedure

Fluid sampling from hot springs and fumaroles was conducted at the each field and its surrounding area, and the collected samples were analyzed for chemical and isotopic constituents in a laboratory in Japan. The sampling locations were selected based on the field condition of the each manifestation as well as the number, sampling locations and analyzed chemical parameters of the existing data for the survey field.

Thermal spring water samples were collected in plastic bottles with volumes from 0.5 to 4 liter. To prevent precipitation of dissolved ions, one of the samples was acidified by adding HCl solution at the field. Water discharge temperature and atmospheric temperature were measured at the sampling. The pH and electric conductivity (EC) of water sample were also measured by portable pH and EC meters.

Gas and steam condensate from fumaroles were sampled in an evacuated glass bottle containing alkali (NaOH) solution, which is known as “Giggenbach’s method”. The gas and steam sample was collected through a silicon tube attached to a stainless funnel being placed upside-down over the fumaroles.

The collected water and gas samples were sent to Japan and analyzed for chemical and isotopic constituents in a laboratory. Analytical methods are listed in App. 4.3.1-1. Analyzed species and numbers of the samples are as below. For the water analyses, the water samples being likely to contain deep geothermal reservoir water from its properties of high discharge temperature, neutral-pH and high salinity (high EC) were selected.

- Hot spring water

  pH, EC, T-SiO2, δ D(H2O), δ 18O(H2O) …… 18 samples

  Cl …… 19 samples

  Na, K, Ca, Mg, Fe, NH4, SO4, HCO3, B …… 10 samples

- Fumarolic gas

  NCG content, CO2, H2S, HCl, H2, N2, CH4, O2, Ar …… 10 samples

  δ D(H2O), δ 18O(H2O) (steam condensate) …… 9 samples

The number of fields where the water samples were collected and analyzed in this survey is 16 among the 23 fields where the field reconnaissance was carried out.

4.3.2 Results of Analyses

Results of chemical and isotopic analyses of hot spring waters and fumarolic gases, and geochemical temperatures and chemical ratios calculated from the results are shown in Apps.4.3.2-1 to 4.3.2-3.

The analyses of water samples revealed that most of the waters have high Cl ion and T-SiO_2 concentrations which suggest the contribution of deep reservoir water. The highest concentrations of Cl ion and of T-SiO_2 were recognized in the waters from Rajabasa (6,830 mg/L) and from Sungai Penuh (402 mg/L) repectively.

The results of gas chemical analyses show that all the samples had contained O_2 believed to be derived from the air possibly contaminated at the sampling or during shipping of samples. Thus, for data analyses and interpretations, the data were corrected into air-free composition (App.4.3.2-3 bottom) (however, the data for Muaralabuh exhibits 'excess O_2' so that the air-free correction is impossible for this data). Significantly high non-condensable gas (NCG) contents over 15 mole% were recognized in the data for four fields including Simbolon-Samosir, B. Gedung Hulu Lais, Ungaran and Wilis/Ngebel. Since the discharge temperature of fumaroles in these fields is lower than the boiling point, the high NCG contents may be caused by steam condensation near the surface. A major component in NCG is CO_2, and minor H_2S is contained with the highest concentration of 14.8 mole% (G. Skencau). HCl gas, which is contained in high temperature gases directly derived from magma, is not contained with concentration less than 0.1 mole%.

4.3.3 Data Analysis and Interpretation

Using the chemical and isotopic data of hot spring waters and fumarolic gases that obtained

in this survey, data processing and interpretation were conducted as listed below;

- origin of thermal fluid (meteoric, seawater, etc.):
  hydrogen and oxygen isotopic composition (App.4.3.3-1)
- water classification and heating process of thermal water:
  major anion composition (App.4.3.3-2), Cl/SO4 － pH cross plot (App.4.3.3-3)
- origin and host rock of thermal fluid: B－Cl cross plot (App.4.3.3-4)
- estimation of subsurface fluid temperature from water chemistry:
  geothermometries (App.4.3.3-3)
  T-SiO2－Cl cross plot (App.4.3.3-5)
  Na-K-Mg ternary plot (App.4.3.3-6)
  comparison of geochemical temperatures (App.4.3.3-7)
- origin of fumarolic steam (meteoric, magmatic, etc.):
  hydrogen and oxygen isotopic composition (App.4.3.3-8)
- estimation of subsurface fluid temperature from gas chemistry:
  geothermometries (App.4.3.2-3), gas chemical temperature cross plot (App.4.3.3-9)

The hydrogen and oxygen isotopic data for the plots in App.4.3.3-1 and App.4.3.3-8 include the unpublished data of cold surface waters in northern Sumatra which are provided by Dr. M. Takahashi of National Institute of Advanced Industrial Science and Technology (AIST). The geothermometers adopted in this study are as follows;

Silica geothermometer

T SiO_2: quartz, chalcedony, α -cristobalite (Fournier, 1977)

Cation geothermometer

T Na/K(T): (Truesdell, 1976)

T NaKCa: (Fournier and Truesdell, 1973)

T dMg = T NaKCa-dMg: (Fournier and Potter, 1979)

T K/Mg: (Giggenbach, 1988)

Gas geothermometer

T D&P = T CO_2-H_2S-H_2-CH_4 (D'Amor and Panichi, 1980)

T CO_2/Ar: (Giggenbach, 1991)

The results of data analyses and interpretation will be referred for the geothermal resource evaluation for each field with using the existing data, which will be mentioned in Chapter 3. Newly obtained knowledge and notable facts provided by execution of this geochemical survey are as follows;

Newly obtained isotopic data elucidate origin of thermal fluids in several fields. It is ascertained that the fluids in G. Sekincau, Ungaran and Wilis/Ngebel contain magma-derived water.

Oxygen isotopic shift, which is resulted from water-rock interaction and recognized for typical deep hot reservoir waters, is observed for hot spring waters in several fields including Muaralabuh, Sungai Penuh, Suoh Antatai and Tompaso. This implies extremely high possibility of occurrence of hot reservoir water in these fields.

Newly additional geothermometries with using the chemical data of hot spring waters and fumarolic gases can contribute to improvement of estimation accuracy of subsurface fluid temperature. The geothermometries using chemical data obtained by this survey suggest that hot fluid with a temperature around 200^{o}C or higher occurs in Muaralabuh, Sungai Penuh, B. Gedung Hulu Lais, Suoh Antatai, G. Sekincau, Rajabasa, Cisolok-Cisukarame, Ungaran and Wilis/Ngebel.

4.4 Supplemental Geophysical Survey

4.4.1 Selection of TDEM/MT Survey Areas

The geophysical survey areas were decided at the Counterpart Meeting held between the JICA study team and several Indonesian authorities on October 17, 2006.

In this meeting, firstly the JICA study team explained the 34 candidate fields to be judged from the points of reservoir temperature, potentials and fluid chemistry through the result of the supplemental field survey (23 fields) and existing survey reports in other fields (refer to Table 4.4.1-1).

Secondly, the Center for Geo-Resource (CGR in Bandung) introduced the following adequate fields for MT survey in the government-public area, namely Sokoria-Mutubusa in East Nusa Tenggarah and Muala Labuh in West Sumatra.

Subsequently, PERTAMINA introduced the suitable places for MT survey in their

concessions (Kotamobagu in North Sulawesi and Sungai Penuh in Jambi)

After the discussion of resource potentials, social-environmental aspects and the future development plans among DGMCG, CGR and PERTAMINA, the following two fields were finally selected:

1) Sokoria-Mutubusa in East Nusa Tenggarah

2) Kotamobagu in North Sulawesi

4.4.2 Methodology

The objective of the supplemental geophysical survey (Magnetotelluric method and Time Domain Electromagnetic method) was to detect promising zones for geothermal development by studying the detailed subsurface resistivity distribution obtained from the MT/TDEM survey results. In particular, delineating the locations of the fracture systems by studying resistivity discontinuities, and the cap rock zones of geothermal reservoirs by studying low resistivity zones at relatively shallow depths, are important in selecting future drilling targets.

In the survey, the Magnetotelluric (MT) method was applied to estimate deep subsurface resistivity structures. And the Time Domain Electromagnetic (TDEM) method was applied to estimate the shallow resistivity structure and to correct the MT information at shallow depths. With the MT data corrected using TDEM results, the detailed resistivity structure was estimated from shallow zone to deep zone in the two selected prospective geothermal fields.

Measuring stations were placed in a grid configuration of station-separations from 600m to 1250m in order to detect fault systems, which often provide passages for geothermal fluids. The total number of stations in each survey was planned to be 35 (for a total of 70 stations in two different fields).

Based on our experiences in many geothermal fields, the depth of the geothermal reservoirs economically viable as drilling targets is expected to be between 1000m and 2500m approximately. Therefore, to obtain the resistivity information from this depth and from deeper levels, more than 30 frequencies in the range from 360Hz to 0.001Hz were utilized for the MT data acquisition. With this frequency range, the investigation depth was considered to reach levels deeper than 2.5km even in a conductive environment.

In addition, shallow resistivity information was obtained by the TDEM method and the shallow resistivity information was used for MT data correction (static-shift correction). Moreover, two-dimensional resistivity inversions with smoothness constraint were

conducted to estimate the detailed subsurface resistivity structure.

(1) Contents of the Survey

(a) Survey Method

Remote-reference Magnetotelluric (MT) survey and Time-domain electromagnetic (TDEM) survey

(b) Survey Area

1) Sokoria field: Approximately 9.0km^2

2) Kotamobagu field: Approximately 37.5km^2

(c) Number of Measured Stations

1) Sokoria field: 35 stations

2) Kotamobagu field: 35 stations

(d) Acquired Electromagnetic Signals

1) MT: 3 components of magnetic signal (*Hx*, *Hy*, *Hz*) and 2 components of electric signal (*Ex*, *Ey*)

2) TDEM: time varying vertical magnetic signal (Hz) after shutting off the applied current

(e) Frequencies to be Used for the Surveys

1) MT : 360Hz ～ 0.00041Hz
(Apparent resistivity value and phase values at 80 frequencies which range from 360Hz to 0.00041Hz were calculated)

2) TDEM: 2.5Hz (applied current)

(2) MT Survey Field Procedure

(a) Survey Area and Station Configuration

The station location maps for the MT/TDEM surveys in the Sokoria geothermal field and

the Kotamobagu geothermal field are shown in Fig. 4.4.2-1 and Fig. 4.4.2-2 respectively. As shown in these maps, measuring stations were basically placed in a grid configuration in order to delineate the detailed subsurface resistivity structures. The intervals between measuring stations are approximately 600m in the Sokoria field and are approximately 1,250m in the Kotamobagu field. The total number of measuring stations was 35 both in the Sokoria field and in the Kotamobagu field, and the location of each station was determined by GPS readings conducted prior to the actual MT and TDEM measurements (The locations of the MT/TDEM stations in the Sokoria and Kotamobagu fields are listed in Table 4.4.2-1). The data acquisition in the fields and logistic coordination were carried out by PT. ELNUSA GEOSAINS of Jakarta, Indonesia and the field geophysical services were provided by West JEC. CGR was in charge of acquiring the permission for field work and assisted the field work in the Sokoria field, and PT. PERTAMINA was in charge of acquiring the permission for field work and assisted the field work in the Kotamobagu field.

(b) Remote Reference Site (MT survey)

The remote reference site should be located in a quiet place free of noise or of low noise level. The ideal site must be free from pipelines, running water, free of or with a low level of local micro-seismic activity, free of power lines and far from human activity. A site roughly 20km east of the Sokoria survey area was selected as the remote reference site during the Sokoria survey period. For the Kotamobagu field, a site roughly 70km northeast of the Kotamobagu survey area was selected as the remote reference site during the Kotamobagu survey period.

(c) Data Acquisition

To assure data quality, the MT surveys were carried out in the Sokoria field and the Kotamobagu field using the remote reference method. Daily, two or three (occasionally one, including the fixed remote station) arrays were deployed for data acquisition. Time series corresponding to two components of the electric field (*Ex, Ey*) and three component magnetic signals (*Hx, Hy, Hz*) were recorded. Similar data series were simultaneously recorded at the remote station except for the vertical magnetic component (*Hz*). The spacing between electrodes for measuring *Ex* and *Ey* is basically 70～100m both for the Sokoria survey and the Kotamobagu survey.

The time series data were recorded during the night from 16:00P.M. to 8:00A.M. of the following day, since artificial noise during the night is supposed to be less than that during the daytime. The frequency of measured data ranged from 360Hz to 0.00041Hz. From this frequency range, MT parameters at 80 frequencies were calculated. Time series of the field data were acquired at the local and at the remote station simultaneously. The time series data were saved on a compact flash memory card of 256MB and/or 512MB capacity. Measured data at each station were transferred to a portable computer using a Compact

Flash memory and were archived on an external hard disk drive in the field residence.

The Time Domain Electromagnetic (TDEM) method is an active method that involves inducing eddy currents within subsurface conductors using pulsed electromagnetic (EM) energy transmitted from a square loop of wire located on the ground. The decaying secondary EM signal induced by these eddy currents is measured over a series of time domain windows immediately after the transmitted signal is shut off using the transmitter loop, or more commonly, a smaller second receiver coil located at the center of the transmitter loop. TDEM soundings are capable of providing information on the conductivity of different layers within the subsurface to depths of between 10-500m. The method is very effective for correcting the static shift problem in the MT method.

The MT and TDEM layout sketches are shown in Fig. 4.4.2-3.

(d) Data Processing in the Field to Control Data Quality

Data processing using the remote reference technique was done on the time series acquired from the remote site and on those from the measuring stations. After the data processing, the following MT parameters were calculated basically.

1) Apparent resistivity versus frequencies

2) Impedance phase versus frequencies

3) Coherencies for Ex-Hy, Ey-Hx, Ex-Hx and Ey-Hy

4) Tipper Magnitude values

With reference to these parameters on the display, cross power data were edited from noise to reduce the standard deviation and enhance resistivity continuity. After this editing, data quality was evaluated. The standard deviation of the fair data is not small at low frequencies, but it is still possible to trace apparent resistivity changes. In a situation like this, the sounding curve passes quality control. When data quality was not good enough for data analysis, re-acquisition of data was carried out at the same station or in the worst case the station was moved to a new site (adjacent site).

Cross-power data at each frequency, consisting of 20 time segments (entire measurement time is divided by 20) was created after the remote reference data processing. Some segments could be rather noisier than others for various reasons such as signal strength, wind noise, artificial electromagnetic noise and so on, so cross-power editing was carried out to improve the data quality by selecting good time segments. This work was carried out every night in the base-camp after the daytime fieldwork.

(3) Data Analysis

The final objective of the data analysis is to obtain the horizontal and vertical resistivity distributions over the explored areas. These distributions will assist interpretation from the standpoint of electrical resistivity structure.

(a) Basic Theory

1) Cagniard Equation

The apparent resistivity is calculated from the ratio of the magnitudes of the electric and magnetic fields and using the well-known Cagniard equation (Cagniard, 1953). This equation is obtained from Maxwell's equations assuming a plane wave.

$$\rho_a = \frac{0.2}{f}\left|\frac{E}{H}\right|^2 \qquad (1)$$

Where,

ρ_a : apparent resistivity in Ohm-m

f : frequency in Hz

E : Electric field magnitude in mV/km

H : Magnetic field magnitude in nT

2) Penetration Depth

The effective depth of MT exploration is dependent upon the resistivity of the rock and the frequencies being measured. The effective depth of penetration can be determined from the following equation:

$$\delta = 355 \times (\rho / f)^{1/2} \qquad (2)$$

Where,

δ : effective penetration depth in meters

ρ : apparent resistivity in Ohm-m

f : frequency in Hz

When the resistivity changes with depth, the apparent resistivity varies with frequency. The penetration of the electromagnetic wave into the earth medium will depend on its frequency. Deep penetration is made with low frequencies

whereas the contrary is true with high frequencies. This means that the resistivity structure from the shallow zone to the deep zone can be analyzed with data from higher to lower frequencies.

3) Impedance Tensor

In general, apparent resistivity at each frequency varies with respect to the orientation of the measurements. The electric field *Ex* is partly induced by *Hy*, but also partly produced by currents induced by *Hx*, which have been affected by the structure underground. The same is true for *Ey*, thus the mathematical relations can be written as follows:

$$\left.\begin{aligned} Ex &= ZxxHx + ZxyHy \\ Ey &= ZyxHx + ZyyHy \end{aligned}\right\} \qquad (3)$$

Where,

Ex: component of *E* in the *x* direction (mV/km)

Ey: component of *E* in the *y* direction (mV/km)

Hx: component of *H* in the *x* direction (gamma)

Hy: component of *H* in the *y* direction (gamma)

Z : impedance tensor elements relating *Ei* to *Hj* (ohm-m)

And the relation between the vertical magnetic field *Hz* and the horizontal electric fields *Hx, Hy* is as follows:

$$Hz = A \cdot Hx + B \cdot Hy \qquad (4)$$

Where,

A, B : constant values

The impedance tensor elements *Zij* are parameters, which contain resistivity information. Apparent resistivity values can be calculated from the impedance tensor elements by using the Cagniard equation.

4) Remote Reference Data Processing

In the Sokoria and Kotamobagu surveys, the remote reference technique was employed to reduce non-coherent noise in the time series data. In this technique, measuring time and band numbers written in the time series data during data acquisition are referenced to synchronize the data at the measuring station and that at the remote reference site. For the Sokoria and Kotamobagu cases, 20 cross-power data were created from remote reference processing and the impedance tensor elements were calculated by the following equations:

$$
\begin{aligned}
Zxx &= (< ExHxr^* >< HyHyr^* > - < ExHyr^* >< HyHxr^* >) \\
&\quad / (< HyHxr^* >< HxHyr^* > - < HyHyr^* >< HxHxr^* >) \\
Zxy &= (< ExHxr^* >< HxHyr^* > - < ExHyr^* >< HxHxr^* >) \\
&\quad / (< HyHxr^* >< HxHyr^* > - < HyHyr^* >< HxHxr^* >) \\
Zyx &= (< EyHxr^* >< HyHyr^* > - < EyHyr^* >< HyHxr^* >) \\
&\quad / (< HyHxr^* >< HxHyr^* > - < HyHyr^* >< HxHxr^* >) \\
Zyy &= (< EyHxr^* >< HxHyr^* > - < EyHyr^* >< HxHxr^* >) \\
&\quad / (< HyHxr^* >< HxHyr^* > - < HyHyr^* >< HxHxr^* >)
\end{aligned}
\qquad (5)
$$

Where,

Ex : component of *E* at station in the x direction (mV/km)

Ey : component of *E* at station in the y direction (mV/km)

Hx : component of *H* at station in the x direction (gamma)

Hy : component of *H* at station in the y direction (gamma)

Hxr: component of *H* at remote site in the x direction (gamma)

Hyr: component of *H* at remote site in the y direction (gamma)

* : conjugate Complex

Apparent resistivity values (ρxy, ρyx) and phase values (ϕxy, ϕyx) were calculated by the following equations.

$$
\left.
\begin{aligned}
\rho xy &= (1/5f)\left|Zxy\right|^2 \\
\rho yx &= (1/5f)\left|Zyx\right|^2 \\
\phi_{xy} &= \tan^{-1}(\mathrm{Im}(Z_{xy})/(\mathrm{Re}(Z_{xy})) \\
\phi_{yx} &= \tan^{-1}(\mathrm{Im}(Z_{yx})/(\mathrm{Re}(Z_{yx}))
\end{aligned}
\right\} \qquad (6)
$$

5) Static Shift Correction for MT

Very small-scale inhomogeneities (that is, with dimensions much less than the skin depth at the highest recorded frequency) can produce a shift of the MT apparent resistivity sounding curve, moving it parallel to the undistorted curve on a log-scale apparent resistivity versus log-scale frequency plot. This parallel shift is commonly referred to as a static shift. Removing this effect from the data is important in interpreting the subsurface resistivity structure. As the static shift is caused by very small-scale inhomogeneities just below the ground surface, high frequency apparent resistivity data at a station located over a very small-scale inhomogeneity is very different from those at adjacent stations.

On the other hand, the TDEM method is suitable for acquiring relatively shallow resistivity information and the data of TDEM is much less affected by the static

shift effects mentioned above. Therefore, TDEM data acquisition at the same stations used for the MT survey was performed and the TDEM data was used to remove the static shift effect.

The following method was employed to remove the static shift effect in the data processing.

i) TDEM data was acquired at the MT measuring stations.

ii) One-dimensional inversions were performed with the acquired TDEM data at every station.

iii) Based on the one-dimensional inversion results obtained in process b), MT responses (apparent resistivity values at high frequencies) were calculated.

iv) The observed MT apparent resistivity curves were shifted up or shifted down to match the predicted MT apparent resistivity curves derived from the results of the TDEM one-dimensional inversions, and then the static shift correction factor at each station was estimated.

Apparent resistivity data corrected using the static shift correction factors was used for the two-dimensional resistivity inversion analysis. The static shift correction factors are listed in Table 4.4.2-2.

6) Two Dimensional resistivity modeling

i) Concept of Two-dimensional Modeling

In two-dimensional modeling, a two-dimensional resistivity structure whose resistivity distribution varies in the x (horizontal) direction and the z (vertical) direction, as shown in Fig. 4.4.2-4, is assumed. Resistivity values of each element of the 2-D model are determined by iterating the calculation to minimize the value of Σ(log(observed apparent resistivity values) – log(calculated apparent resistivity values))^2 + Σ(observed phase values — calculated phase values)^2. This analysis is expected to lead to a more accurate subsurface resistivity model than that derived from 1-D analysis.

ii) Basic Theory in Two-dimensional Modeling

The electromagnetic field can be explained by Maxwell's equations shown below.

$$\nabla \times E = i\omega\mu H \qquad (7)$$

$$\nabla \times H = \sigma E \tag{8}$$

Where,

ω : angular frequency

μ : magnetic permeability

σ : electric conductivity

The displacement current is ignored because it is very small.

From equations (7) and (8), the following equations are derived.

$$\nabla \times (\nabla \times H) = \nabla \times \sigma E = \sigma \times \nabla \times E = k^2 H \tag{9}$$

$$\nabla \times (\nabla \times E) = \nabla \times i\omega\mu H = i\omega\mu \times \nabla \times H = k^2 E \tag{10}$$

Where,

$$k^2 = i\omega\mu\sigma$$

After introducing the orthogonal coordinate system, (9) and (10) lead to equations (11) and (12) respectively.

$$\left.\begin{aligned} &\partial^2 Hx/\partial y^2 + \partial^2 Hx/\partial z^2 - k^2 Hy/\partial x\partial y - \partial^2 Hz/\partial x\partial z - k^2 Hx = 0 \\ &\partial^2 Hy/\partial x^2 + \partial^2 Hy/\partial z^2 - k^2 Hx/\partial y\partial x - \partial^2 Hz/\partial y\partial z - k^2 Hy = 0 \end{aligned}\right\}$$

(11)

$$\partial^2 Hz/\partial x^2 + \partial^2 Hz/\partial y^2 - k^2 Hx/\partial z\partial x - \partial^2 Hz/\partial z\partial y - k^2 Hz = 0$$

$$\left.\begin{aligned} &\partial^2 Ex/\partial y^2 + \partial^2 Ex/\partial z^2 - k^2 Ey/\partial x\partial y - \partial^2 Ez/\partial x\partial z - k^2 Ex = 0 \\ &\partial^2 Ey/\partial x^2 + \partial^2 Ey/\partial z^2 - k^2 Ex/\partial y\partial x - \partial^2 Ez/\partial y\partial z - k^2 Ey = 0 \end{aligned}\right\}$$

(12)

$$\partial^2 Ez/\partial x^2 + \partial^2 Ez/\partial y^2 - k^2 Ex/\partial z\partial x - \partial^2 Ez/\partial z\partial y - k^2 Ez = 0$$

Assuming that the subsurface resistivity structure is two-dimensional, equation (11) is simplified to the following equation for the TM mode.

$$\partial^2 Hy/\partial x^2 + \partial^2 Hy/\partial z^2 - k^2 Hy = 0 \tag{13}$$

Equation (13) can be solved for *Hy* by the finite elements method and *Ex* is derived from the equation $Ex = 1/\sigma \cdot (\partial Hy / \partial z)$. Finally, apparent resistivity and phase for TM mode can be calculated in the following equations:

$$\begin{aligned} \rho xy &= 1/i\omega\mu \cdot |Ex/Hy| \\ \phi xy &= \arg(Ex/Hy) \end{aligned} \tag{14}$$

For TE mode, the following equation is derived from equation (12)

$$\partial^2 Ey/\partial x^2 + \partial^2 Ey/\partial z^2 - k^2 Ey = 0 \tag{15}$$

Equation (15) can be solved for *Ey* by the finite elements method and *Hx* is derived from the equation $Hx = -1/i\omega\mu(\partial Ey/\partial z)$. Finally, apparent resistivity and phase for TE mode can be calculated in the following equations:

$$\begin{aligned} \rho yx &= 1/i\omega\mu \cdot |Ey/Hx| \\ \phi yx &= \arg(Ey/Hx) \end{aligned} \tag{16}$$

iii) Two-dimensional Forward Modeling with the Finite Element Method

First, we divide the 2-D resistivity section into many small triangular elements. It is assumed that the electric field in a triangular element is derived from the following equation:

$$Hy = \sum NiEyi = N1Ey1 + N2Ey2 + N3Ey3 \tag{17}$$

In Galerkin's theorem, the integral of each weighted residual is set to zero. Therefore the following equation (18) is derived.

$$\iint Ni(\partial^2 Hy/\partial x^2 + \partial^2 Hy/\partial Z^2 - k^2 Hy)ds = 0 \tag{18}$$

By using Green's theorem, equation (18) can be divided into a surface integral term and a curvilinear integral term. The curvilinear integral term can be ignored on the condition that the nodal point of the triangular element is not located on the model edge. Then, equation (15) can be transformed into the following equation.

$$\iint(\partial^2 Hy\partial Ni/\partial x\partial x - \partial Hy\partial Ni/\partial_z\partial_z - k^2 Hy)dxdz = 0 \tag{19}$$

Substituting equation (17) for equation (19), equation (20) can be derived.

$$\int\int(\sum Hyj \cdot \partial Nj/\partial_x \cdot \partial Ni/\partial x + \sum Hyj \cdot \partial Nj/\partial_z \cdot \partial Ni/\partial_z)$$

$$-k^2 \sum NiEyiNi)dxdz = 0(j = 1,2,3...n) \qquad (20)$$

Equation (20) can be solved to get the apparent resistivity and phase values for TM mode with boundary conditions. Also, the apparent resistivity and phase values for TE mode can be obtained from a procedure similar to that described above.

In solving equation (20), the following boundary conditions are applied for TM mode and TE mode.

(TM mode)

Hy = 0	at the bottom edge of the 2-D model
∂Hy/∂x = 0	at the side edges of the 2-D model
Hy = 1	at the ground surface

(TE mode)

Ey = 0	at the bottom edge of the 2-D model
∂Ey/∂x = 0	at the side edges of the 2-D model
Ey = 1	at 100km above the ground surface

iv) Two-dimensional Inversion Scheme

The scheme used in the two-dimensional resistivity inversion is based on linearized least-squares inversion with a smoothness constraint. For this method, we minimize the following function *U*,

$$U = (W\Delta d - WA\Delta m)^T (W\Delta d - WA\Delta m) + \alpha (C\Delta m)^T (C\Delta m) \qquad (21)$$

Where *W* is a weighting matrix, Δd is a vector of differences between modeled responses and observed data, Δm is the correction vector to the model parameter, *A* is the Jacobian matrix, α is a smoothing factor and *C* is a roughening matrix.

The first term on the right hand side of the equation (21) shows the data misfit and the second term shows the 2-D resistivity model roughness. The correction vector to the model parameter, Δm, which minimizes the function *U* can be obtained by solving equation (22). Since the relation between model parameters and model response is non-linear, equation (22) is solved iteratively so as to obtain the final 2-D resistivity model.

$$\{\{(WA)^T (WA) + \alpha C^T C\}\Delta m_{K+1} = (WA)^T \Delta d \qquad (22)$$

Where Δm_{k+1} is the correction vector to the model parameter at the $(k+1)$th iteration and A is a Jacobian matrix consisting of partial derivatives of the MT responses with respect to the model parameters.

The final 2-D model parameters (resistivity values in the 2-D model blocks) can be obtained to solve equation (22) repeatedly. A finite element model adjusted for the topography was applied in the 2-D resistivity inversion.

4.4.3 Results of the Survey in the Sokoria Field

(1) Data Analysis

(a) Apparent Resistivity

As described in 4.4.2, (3), (a), 2), frequencies are related to penetration depths in MT theory. Namely, the apparent resistivity at high frequencies reflects the resistivity structure in the shallow zone and that at low frequencies reflects the resistivity structure in the deep zone. Thus, apparent resistivity contour maps at 100Hz, 1Hz and 0.01Hz are shown in Fig. 4.4.3-1, 4.4.3-2 and 4.4.3-3 respectively. Apparent resistivity values of determinant mode are used in these maps, since determinant mode apparent resistivity values are average values of TE mode and TM mode apparent resistivity values.

1) Apparent Resistivity Map (determinant mode, 100Hz)

The apparent resistivity map (determinant mode, 100Hz) is shown in Fig. 4.4.3-1. The apparent resistivities at 100 Hz range from 2.5ohm-m to 70ohm-m approximately. The resistivity information is from surface to the penetration depth, which is roughly in the range of 55m to 300m.

A low resistivity zone of less than 10ohm-m is widely distributed in the central portion of the survey area including the Mutubusa fumaroles. The low resistivity zone is likely to reflect a hydrothermally altered zone present in shallow depths, because some alteration zones and Mutubusa hot spring are present in this area.

On the other hand, a relatively high apparent resistivity zone of greater than 32ohm-m is distributed in the northwestern portion of the survey area. Resistivity discontinuity Rs1 can be seen in between the low apparent resistivity zone situated in the central portion and the high apparent resistivity zone situated in the northwestern portion of the survey area.

2) Apparent Resistivity Map (determinant mode, 1Hz)

The apparent resistivity map (determinant mode, 1 Hz) is shown in Fig. 4.4.3-2.

The apparent resistivity values at 1Hz range from 2.5ohm-m to 50ohm-m approximately. The resistivity information is from surface to the penetration depth, which is roughly in the range of 560m to 2500m. The distribution pattern of the apparent resistivity at 1Hz quite differs from that at 100Hz. A low resistivity zone of less than 4ohm-m is widely recognized in the western portion of the survey area. No indication of resistivity discontinuity Rs1 can be seen in the map.

On the other hand, a relatively high apparent resistivity zone of greater than 32ohm-m is distributed broadly in the eastern portion of the survey area as Fig. 4.4.3-2 indicates.

3) Apparent Resistivity Map (determinant mode, 0.01Hz)

The apparent resistivity map (determinant mode, 0.01Hz) is shown in Fig. 4.4.3-3. The apparent resistivity values at 0.01Hz range from 20ohm-m to 350ohm-m approximately. The resistivity information is from surface to the penetration depth, which is greater than 15000m.

The apparent resistivity values in this map are slightly higher than those at 1Hz. A relatively high apparent resistivity zone aligned in a NE-SW direction is clearly recognized in the eastern portion of the survey area, but low apparent resistivity zones of less than 10ohm-m cannot be recognized in this apparent resistivity map.

(b) Two-dimensional Resistivity Modeling Analysis

Two dimensional resistivity inversions with smoothness constraints were conducted for the sections along line-AA, BB, CC, DD, EE and FF, and are presented in Fig. 4.4.4-4. The data used for the 2-D inversion were determinant mode apparent resistivity and phase values, which are rotationally invariant, in a frequency range between 251Hz and 0.01Hz.

On the basis of the results obtained from the two-dimensional resistivity inversions, resistivity maps at different depths, namely 200m, 500m, 750m, 1000m, 1500m, 2000m and 2500m were drawn. These maps are shown in Figs. 4.4.3-5 to 4.4.3-11.

Resistivity sections along line-AA, BB, CC, DD, EE and FF were prepared and these resistivity sections are shown in Figs. 4.4.3-12 to 4.4.3-17.

The resistivity model derived from the two-dimensional resistivity inversions roughly reveals three layers: a very shallow high resistivity layer of about 10 to 30ohm-m, an intermediate low resistivity layer of less than 10ohm-m underlying the upper high resistivity layer, and a deep high resistivity layer with values roughly greater than 20ohm-m underlying the low resistivity layer.

1) Resistivity map at a depth of 200m

The resistivity map at a depth of 200m is shown in Fig. 4.4.4-5. The resistivity values at a depth of 200m range roughly from 3ohm-m to 40ohm-m and the resistivity values at this depth roughly show minimum values.

In the map, a low resistivity zone of less than 5ohm-m is distributed in the central portion of the survey area and it has a tendency to extend in a NNE-SSW direction. Based on the resistivity distribution pattern in the resistivity map, resistivity discontinuity Rs1, which runs in the northwestern portion of the survey area in a NE-SW direction, can be detected.

In many geothermal fields, because of the abundance of conductive clay such as smectite and zeolite, low resistivity zones are generally distributed on the top of the geothermal reservoir where the temperature conditions range approximately from 70^{o}C to 200^{o}C. Therefore, this widely distributed low resistivity zone probably reflects an area where conductive clay products such as smectite and zeolite are abundant.

2) Resistivity maps at depths of 500m, 750m and 1000m

The resistivity map at a depth of 500m, that at a depth of 750m and that at a depth of 1000m are shown in Figs. 4.4.3-6, 4.4.3-7 and 4.4.3-8 respectively. The resistivity values at a depth of 500m range roughly from 2 to 70 ohm-m, those at 750m range roughly from 4 to 90ohm-m and those at 1000m range roughly from 8ohm-m to 100ohm-m. Although the resistivity values become higher with increasing depth, the resistivity distribution patterns at depths of 500m, 750m and 1000m are similar.

In the resistivity map at a depth of 1000m, a relatively high resistivity zone of greater than 32ohm-m can be seen from the northeastern portion of the survey area to the south portion of the survey area. This relatively high resistivity zone has a tendency to extend in a NNE-SSW direction. On the other hand, a relatively low resistivity zone of less than 20ohm-m is widely distributed in the northwestern and western portions of the survey area.

In between the relatively high resistivity zone and the relatively low resistivity zone mentioned above, resistivity discontinuity Rs2 can be detected as shown in Fig. 4.4.3-7. In addition, resistivity discontinuity Rs3 can be also detected at the eastern edge of the relatively high resistivity zone.

Resistivity discontinuity Rs2 is highly likely to reflect a fault structure, because an estimated fault based on the geological study is situated close to the resistivity discontinuity. However, the features of resistivity discontinuity Rs1 detected in the resistivity map at a depth of 200m cannot be recognized at this depth.

At a depth of 1000m, the area along resistivity discontinuity Rs2 shows resistivity values greater than 25ohm-m, despite the existence of the low resistivity zone in the same area at a depth of 200m. A relatively high resistivity zone laid sequentially below the low resistivity zone often indicates a zone where chlorite and/or illite are formed at shallower depth than surrounding areas, since relatively high-temperature alteration products such as chloritic clays, illitic clays and epidote are considered to be relatively high in resistivity compared to low-temperature alteration products such as smectite and zeolite. Therefore, the relatively high resistivity zone along resistivity discontinuity Rs2 underlying the distributed low resistivity zone perhaps reflects a relatively high temperature zone where geothermal fluids may circulate.

3) Resistivity maps at depths of 1500m, 2000m and 2500m

The resistivity maps at a depth of 1500m, at a depth of 2000m and at a depth of 2500m are shown in Figs. 4.4.3-9, 4.4.3-10 and 4.4.3-11 respectively. The resistivity values at a depth of 1500m range roughly from 20 to 180ohm-m, those at 2000m range roughly from 30 to 250ohm-m and those at 2500m range roughly from 50ohm-m to 350ohm-m. Although the resistivity values become higher with increasing depth at these depths, the resistivity distribution patterns at depths of 1500m, 2000m and 2500m are similar to each other.

No low resistivity zones of less than 10ohm-m are detected, but a widely distributed high resistivity zone around stations 27, 33 and 34 is clearly recognized in the resistivity maps at depths of 1500m, 2000m and 2500m.

Above the high resistivity zone situated in the eastern portion of the survey area (around stations 27, 33 and 34), low resistivity zones of less than 10ohm-m cannot be detected at shallower depths. Therefore, hydrothermal activities are likely to be weak in the zone around stations 27, 33 and 34.

4) Resistivity Sections

Resistivity sections along line-AA, BB, CC, DD, EE and FF, which run E-W, are shown in Figs. 4.4.3-12 to 4.4.3-17. Locations of all the sections are presented in Fig. 4.4.3-4.

Low resistivity zones of less than 5ohm-m are recognized in all the section maps, so a low temperature hydrothermally altered zone formed with smectite and/or zeolite is likely to be distributed broadly in the survey area.

The eastern portion of the sections along line-BB, line-CC and line-DD at depth, clearly shows relatively high resistivity of greater than 80ohm-m. On the other hand, the western portion of these sections shows relatively low resistivity values. In between the relatively high resistivity zone and the low resistivity zone,

resistivity discontinuity Rs2 is clearly detected. In addition, resistivity discontinuity Rs3 is recognized in the sections along line-DD, line-EE and line-FF, and resistivity discontinuity Rs1 is recognized in the section along line-AA though the tendencies of the discontinuities are less clear than that of discontinuity Rs2.

(2) General Resistivity Structure of Geothermal Fields in Volcanic Areas

(a) The Low Resistivity Zone

In most geothermal fields in the world where electrical or electromagnetic methods have been applied, low resistivity zones of less than 10ohm-m can be detected. There are two viewpoints regarding the nature of these low resistivity zones. One is that the low resistivity zone reflects the geothermal reservoir itself, which contains hot water with lots of dissolved chemicals (Fig. 4.4.3-18, model A). The other is that the low resistivity zone does not represent the geothermal reservoir itself, but reflects hydrothermally altered zones formed over the geothermal reservoir due to the upward movement of geothermal water (Fig. 4.4.3-18, model B).

Considering that most geothermal reservoirs in volcanic areas are of the fractured type and are controlled by fault systems, the low resistivity zone located around the fault systems obtained from resistivity surveys can be regarded as reflecting the conductive clay such as smectite and zeolite generally formed over the geothermal reservoir with temperature conditions ranging approximately between 70^{o}C and 200^{o}C. This conductive clay zone functions as a cap rock of the reservoir in many geothermal fields.

Therefore, when the drilling target is considered on the basis of the resistivity structure, the target must be decided not only on the basis of information concerning the low resistivity zones, but also considering the geothermal structure, such as fault systems, and other geological and hydrological information.

(b) General Resistivity Structure of Geothermal Fields

Based on the ideas regarding to the nature of the low resistivity zone of geothermal fields in volcanic areas, the general resistivity structure of a geothermal field can be depicted as shown in Fig. 4.4.3-19. The resistivity structure can be basically divided into three zones, namely resistive overburden, low resistivity zone and resistive zone at depth.

The resistive overburden is a resistive zone near the ground surface which is composed of resistive rocks such as volcanic ash, alluvium, unaltered volcanic rocks and so on. Information concerning this shallow zone is not important in studying the geothermal structure as compared with the other two zones, which have the following characteristics:

The low resistivity zone is the zone which is very conductive, and the resistive zone at depth is the zone which is laid sequentially below the low resistivity zone and is relatively resistive compared to the low resistivity zone.

These two zones are usually difficult to correlate with the geological sections because the resistivity of rocks in geothermal areas is strongly affected by the degree of alteration, porosity, electrolytes and temperature rather than rock types generally. However, the low resistivity zone usually reflects hydrothermally altered products such as smectite and zeolite and it works as a cap rock of the geothermal reservoir in many cases. On the other hand, the relatively resistive zone distributed sequentially below the low resistivity zone often reflects high-temperature alteration products such as chlorite, illite and epidote. The geoelectrical features shown by the low resistivity zone and the resistive zone at depth in and around a geothermal reservoir are as follows:

1) A remarkable resistivity discontinuity can be continuously mapped from station to neighboring station. An uplifted structure is clearly recognized along the resistivity discontinuity. The resistivity discontinuity usually reflects the fracture system along the fault.

2) Resistivity values for the low resistivity zone along the resistivity discontinuity are smaller than those in the surrounding area and the low resistivity zone (smectite and/or zeolite) and usually indicate cap rock of the reservoir in geothermal fields. Such a zone is marked ρ_a in Fig. 4.4.3-19.

3) The hotter parts of geothermal systems are characterized by higher resistivity than is seen in the overlying conductive zone. The higher resistivity is due to the fact that the rock matrix is much less conductive than the saturating fluids because low conductivity alteration products dominate mineralisation in this zone. High temperature alteration processes may increase the resistivity of some rocks by converting smectite clays to illite or chlorite clays.

(3) Considerations Arising from MT/TDEM Survey Results

Based on the Data Analysis described in 4.4.3, (1) and the General Resistivity Structure of Geothermal Fields in Volcanic Areas described in 4.4.3, (2), considerations were made on the resistivity structure in and around the Sokoria geothermal filed. For the following description, refer to Fig. 4.4.3-20.

(a) Resistivity Discontinuities in the Sokoria field

In the Sokoria geothermal field, resistivity discontinuities Rs1, Rs2 and Rs3 are recognized based on the survey results.

1) Resistivity Discontinuity Rs1

Resistivity discontinuity Rs1 runs from the area beside station 22 to the area slightly north of station 9 roughly in a NE-SW direction.

Resistivity discontinuity Rs1 is recognized in the apparent resistivity map at 100Hz and resistivity distribution at shallow depths (at a depth of 200m) obtained from 2D inversion results. This Rs1 resistivity discontinuity is likely to be a caldera rim, because a caldera rim estimated from the geological study is situated close to resistivity discontinuity Rs1. However, the tendency of the discontinuity cannot be recognized in the resistivity distribution at depth. Therefore, this resistivity discontinuity probably controls the geothermal fluids only at shallow depths.

2) Resistivity Discontinuity Rs2

Resistivity discontinuity Rs2 runs from the area between the station 24 and 35 to the area between the station 16 and 19 roughly in a NNE-SSW direction. Resistivity discontinuity Rs2 can be recognized in the resistivity distributions (at depths of 500m, 750m, 1000m and 1500m) obtained from 2D inversion results.

This Rs2 resistivity discontinuity is likely to reflect a fault structure, because a fault estimated from the geological study is located close to resistivity discontinuity Rs2.

In addition, a remarkably low resistivity anomaly zone is clearly recognized around and to the west of resistivity discontinuity Rs2. Therefore, the resistivity discontinuity Rs2 probably indicates a fracture system which controls geothermal fluid at depth.

3) Resistivity Discontinuity Rs3

Resistivity discontinuity Rs3 runs from the area between station 32 and 33 to the area between station 18 and 25 roughly in a NE-SW direction. Resistivity discontinuity Rs3 is recognized in the apparent resistivity maps (at 1Hz and 0.1Hz) and the resistivity maps at depths of 500m, 750m and 1000m.

A relatively low resistivity zone of less than 10ohm-m is also recognized to the east of this resistivity discontinuity. However, this resistivity discontinuity is situated on the southeastern edge of the survey area and the tendency of the discontinuity is weak compared to that of discontinuity Rs2. Therefore, further information will be required to define this resistivity discontinuity.

(b) Resistivity Structure in the Sokoria Field

Based on the results of the Sokoria survey described previously, the MT/TDEM results for the Sokoria geothermal field suggest the following:

A remarkably low resistivity zone is widely distributed in the northwestern, western and central portions of the Sokoria geothermal field roughly around depths between 200m and 500m. This low resistivity zone probably reflects low-temperature hydrothermal-alteration clay minerals (smectite, zeolite, etc.) which often form the cap-rock of the geothermal reservoir with temperature conditions between 70^{o}C and 200^{o}C.

On the other hand, a relatively high resistivity zone is recognized in the eastern and northeastern portions relatively deep (at depths of 1000m, 1500, 2000m and 2500m). The zone around stations 27, 33 and 34 shows relatively high resistivity values greater than 100ohm-m at depths of 1500m, 2000m and 2500m. However, there is no low resistivity zone overlaying the high resistivity zone in this area. So, hydrothermal activities in this area are considered to be relatively weak compared to the central, western and northwestern portions of the survey area.

Based on the resistivity distribution derived from the 2D inversion results, three resistivity discontinuities (Rs1, Rs2 and Rs3) were detected. Considering the geological study results, resistivity discontinuity Rs1 probably reflects a Caldera rim and resistivity discontinuity Rs2 is likely to reflect a fault structure. The central portion along the resistivity discontinuity Rs2 shows resistivity values greater than 30ohm-m relatively deep (at depths of 1500m, 2000, and 2500m), despite the existence of the low resistivity zone of less than 5ohm-m in the same area at a depth of 200m. The area along resistivity discontinuity Rs2 indicating resistivity values of greater than 30ohm-m distributed at depth underlying the low resistivity zone of less than 5oh-m probably reflects high temperature alteration products such as illite and/or chlorite. Hence the area along resistivity discontinuity Rs2 at depth is possibly indicative of a higher temperature zone at depth. Therefore it is highly probable that the central portion of resistivity discontinuity Rs2 reflects a part of the fault-like structure where geothermal fluid may circulate at depth in the Sokoria geothermal field. Based on these facts, the zone along resistivity discontinuity Rs2 is likely to be a promising zone for geothermal development in the Sokoria geothermal field.

The resistivity discontinuity Rs1, extending approximately NE-SW, can be detected in the northwestern portion. The resistivity values of the area around and to the east of this resistivity discontinuity show less than 10ohm-m at relatively shallow depths and so it is likely to indicate low temperature hydrothermal alteration products such as semctite. However, the resistivity values of the area along resistivity discontinuity Rs1 show relatively low resistivity values at depth compared to those for the area along resistivity discontinuity Rs2. This fact suggests that the transition zone from smectite to

illite/chrolide along resistivity discontinuity Rs1 (approximately 150°C – 200°C) is situated deeper than that along resistivity discontinuity Rs2. Hence the temperature of the area along resistivity discontinuity Rs2 is probably higher than that of the area along resistivity discontinuity Rs1.

In the southeastern portion of the survey area, resistivity discontinuity Rs3 can be detected and a low resistivity zone of less than 10ohm-m is distributed at a depth of 200m in the southeast portion of resistivity discontinuity Rs3. However, since this feature is situated at the southeast edge of the survey area, and no geothermal indications are recognized based on the geological study, further information will be required to define the resistivity structure there.

4.4.4 Results of the Survey in the Kotamobagu

(1) Data Analysis

(a) Apparent Resistivity

As described previously, frequencies are related to penetration depths in MT theory. Namely, the apparent resistivity at high frequencies reflects the resistivity structure in the shallow zone and that at low frequencies reflects the resistivity structure in the deep zone. Thus, apparent resistivity contour maps at 100Hz, 1Hz and 0.01Hz are shown in Figs. 4.4.4-1, 4.4.4-2 and 4.4.4-3 respectively. Apparent resistivity values of determinant mode, which are average values of two polarizations of apparent revistivity values, are used in these maps.

1) Apparent Resistivity Map (determinant mode, 100Hz)

The apparent resistivity map (determinant mode, 100Hz) is shown in Fig. 4.4.4-1. The apparent resistivities at 100Hz range from 20ohm-m to 100ohm-m approximately. The resistivity information is from surface to the penetration depth, which is roughly in the range of 150m to 350m.

Low resistivity zones of less than 10ohm-m which often indicate hydrothermal altered zones are not recognized in the map. Thus, most of the shallow zones of the survey area seem to be less affected by hydrothermal alteration activities.

In addition, no significant features related to geological structures such as faults and Caldera rims can be seen in the map.

2) Apparent Resistivity Map (Invariant mode, 1Hz)

The apparent resistivity map (determinant mode, 1 Hz) is shown in Fig. 4.4.4-2. The apparent resistivity values at 1Hz range from 4ohm-m to 200ohm-m

approximately. The resistivity information is from surface to the penetration depth, which is roughly in the range of 700m to 5000m. The apparent resistivity values in this map are smaller than those at 100Hz. A low resistivity zone of less than 6.3ohm-m is widely distributed in the central-northern portion of the survey area (around stations 11, 19, 20, 21 and 22). The low resistivity zone is likely to reflect a hydrothermal altered zone (mostly smectite) present in the survey area. A resistivity discontinuity, Rk1, can be seen in the southwestern portion of the survey area and a relatively high apparent resistivity zone is distributed in the south of the resistivity discontinuity Rk1 as Fig. 4.4.4-2 indicates.

3) Apparent Resistivity Map (determinant mode, 0.01Hz)

The apparent resistivity map (determinant mode, 0.01Hz) is shown in Fig. 4.4.4-3. The apparent resistivity values at 0.01Hz range from 5ohm-m to 350ohm-m approximately. The resistivity information is from surface to the penetration depth, which is greater than 8000m.

The pattern of apparent resistivity distribution in this map is similar to that at 1Hz, while the apparent resistivity values are slightly higher than those at 1Hz. Also in this map, a low apparent resistivity zone is recognized in the central-northern portion of the survey area (around stations 11, 19, 20, 21 and 22) and a high apparent resistivity zone is recognized in the southwestern portion of the survey area.

(b) Two-dimensional Resistivity Modeling Analysis

Two dimensional resistivity inversions with smoothness constraints were conducted for the sections along line-A, B, C, D, E, F and G, and are presented in Fig. 4.4.4-4. The data used for the 2-D inversion were determinant mode apparent resistivity and phase values, which are rotationally invariant, in a frequency range between 251Hz and 0.01Hz.

On the basis of the results obtained from the two-dimensional resistivity inversions, resistivity maps at different depths, namely 200m, 500m, 750, 1000m, 1500m 2000m and 2500m were drawn. These maps are shown in Figs 4.4.4-5 to 4.4.4-11.

Resistivity sections along line-A, B, C, D, E, F and G were also prepared and these resistivity sections are shown in figures 4.4.4-12 to 4.4.4-18.

The resistivity model derived from the two-dimensional resistivity inversions roughly reveals three layers: a very shallow high resistivity layer of about 10 to 30ohm-m, an intermediate low resistivity layer of less than 10ohm-m underlying the upper high resistivity layer, and a deep high resistivity layer with values roughly greater than 30ohm-m

underlying the low resistivity layer.

1) Resistivity map at a depth of 200m

The resistivity map at a depth of 200m is shown in Fig. 4.4.4-5. The resistivity values at a depth of 200m range roughly from 5ohm-m to 250ohm-m.

The resistivity pattern in this map is similar to the apparent resistivity pattern at 100Hz. The resistivity distribution pattern is somehow distorted and no significant tendencies are observed, so the resistivity pattern is thought to reflect basically a resistivity distribution of unaltered rocks and/or weakly altered rocks situated above the cap rock of the geothermal reservoir.

2) Resistivity maps at depths of 500m and 750m

The resistivity maps at a depth of 500m and at a depth of 750m are shown in Fig. 4.4.4-6 and Fig. 4.4.4-7 respectively. The resistivity values at a depth of 500m range roughly from 1.5 to 250ohm-m and those at 750m range roughly from 2 to 350ohm-m.

The resistivity values at these depths roughly show minimum values and the pattern of the resistivity distributions are similar to each other.

In these maps, a low resistivity zone of less than 5ohm-m is widely distributed from the northern portion around stations, 11, 20 and 21 to the southeastern portion around stations 35 roughly in a NW-SW direction. On the other hand, a relatively high resistivity zone showing greater than 20ohm-m is distributed in the southwestern portion of the survey area. Based on the resistivity distribution pattern in the resistivity map at a depth of 500m, resistivity discontinuity Rk1, which runs in the southeastern portion of the survey area in a E-W direction can be detected.

In many geothermal fields, because of the abundance of conductive clay such as smectite and zeolite, low resistivity zones are generally distributed on the top of the geothermal reservoir where the temperature conditions range approximately from 70^{o}C to 200^{o}C. Therefore, this widely distributed low resistivity zone probably reflects an area where conductive clay products such as smectite and zeolite are abundant.

3) Resistivity maps at depths of 1000m and 1500m

The resistivity map at a depth of 1000m and that at a depth of 1500m are shown in Fig. 4.4.4-8 and Fig. 4.4.4-9 respectively. The resistivity values at a depth of 1000m range roughly from 3 to 800ohm-m and those at 1500m range roughly from 6 to 800ohm-m. Although the resistivity values become higher with

increasing depth between the depths from 750m to 1500m, the resistivity distribution patterns at depths of 1000m and 1500m are similar to those at a depth of 750m.

In these maps, a relatively low resistivity zone is also recognized in the area from the northern portion around stations, 11, 20 and 21 to the southeastern portion around station 35 roughly in a NW-SW direction.

Based on the resistivity distribution pattern in the resistivity map at a depth of 1500m, resistivity discontinuity Rk2, which runs from the area between station 22 and 24 to the area beside station 8 roughly in a NE-SW direction, can be detected.

4) Resistivity maps at depths of 2000m and 2500m

The resistivity map at a depth of 2000m, and that at a depth of 2500m are shown in Fig. 4.4.4-10 and Fig. 4.4.4-11 respectively. The resistivity values at a depth of 2000m range roughly from 8 to 800 ohm-m and those at 2500m range roughly from 8 to 1000ohm-m.

In the resistivity map at a depth of 2000m, a relatively low resistivity zone of less than 20ohm-m can be seen from the north-central portion of the survey area to the southeastern portion of the survey area. In addition, a relatively high resistivity zone of greater than 30ohm-m is widely seen in the western portion of the survey area and is also seen in the northeastern portion of the survey area. Based on the resistivity distribution pattern at a depth of 2000m, resistivity discontinuity Rk3, which runs in the central portion of the survey area in a NNW-SSE direction can be detected. Also, in the resistivity map at a depth of 2000m, the area around stations 9, 10, 12, 13 indicates relatively high resistivity values greater than 30ohm-m, despite the existence of the low resistivity zone in the same area at a depth of 500m. This fact suggests that the relatively high resistivity zone laid sequentially below the low resistivity zone is a zone where chlorite and/or illite are formed at shallower depth than surrounding areas, since relatively high-temperature alteration products such as chloritic clays, illitic clays and epidote are considered to be relatively high in resistivity compared to low-temperature alteration products such as smectite and zeolite. Therefore, the relatively high resistivity zone underlying the widely distributed low resistivity zone perhaps reflects a relatively high temperature zone where geothermal fluids may circulate.

5) Resistivity Sections

Resistivity sections along line-A, B, C, D, E, F and G, which run NNW-SSE, are shown in Figs 4.4.4-12 to 4.4.4-18. Locations of all the sections are presented

in Fig. 4.4.4-8.

Low resistivity zones of less than 10ohm-m are recognized in all the section maps, so a low temperature hydrothermally altered zone formed with smectite and/or zeolite is likely to be distributed broadly in the survey area.

The southern portions of the sections along line-A, B, C and D show relatively high resistivity greater than 20ohm-m and do not show any low resistvity zones of less than 10ohm-m. Therefore, there seem to be no hydrothermal alteration zones in these areas. This suggests that this high resistivity area is out of the geothermal system.

On the other hand, low resistivity zones of less than 5ohm-m are widely distributed along line-C, D and E. As described above, it is highly probable that this low anomaly indicates low temperature hydrothermal alteration products such as smectite and/or zeolite.

Resistivity discontinuity Rk1 is recognized clearly in the resistivity sections along line-A, B, C and D, and resistivity discontinuity Rk2 is recognized in the resistivity sections along line-C, D and E. In addition, resistivity discontinuity Rk3, which is detected in the resistivity maps at depths of 1500m and 2000m, can be seen in the resistivity sections along line-D and E.

(2) Considerations Arising from MT/TDEM Survey Results

Based on the Data Analysis described in 4.4.4, (1) and the General Resistivity Structure of Geothermal Fields in Volcanic Areas described in 4.4.3, (2), considerations were made on the resistivity structure in and around the Kotamobagu geothermal filed. For the following description, refer to Fig. 4.4.4-19.

(a) Resistivity Discontinuities in the Kotamobagu Field

The resistivity discontinuity is a structure which exhibits a big change in resistivity and/or apparent resistivity laterally. If such structures are distributed continuously along a line, a fault system and/or fracture system is expected to be located along the resistivity discontinuity structures. In general, geothermal fluid is trapped in and around the fault/fracture system, so detecting the resistivity discontinuities is important in studying the geothermal structure in the survey area. In the Kotamobagu geothermal field, resistivity discontinuities Rk1, Rk2 and Rk3 are recognized based on the survey results.

1) Resistivity Discontinuity Rk1

Resistivity discontinuity Rk1 runs from the area beside station 3 to the area beside station 17 roughly in an E-W direction.

Discontinuity Rk1 is recognized clearly in the apparent resistivity maps (at 10Hz, 1Hz and 0.1Hz) and resistivity distributions (at depths of 500m, 750m and 1000m) obtained from 2D inversion results. Because there are no low resistivity zones south of the resistivity discontinuity Rk1, this resistivity discontinuity is likely to be a boundary of the geothermal system.

2) Resistivity Discontinuity Rk2

Resistivity discontinuity Rk2 runs from the area beside station 30 to the area beside the station 8 roughly in a NE-SW direction.

Discontinuity Rk2 can be recognized in the resistivity distributions (at depths of 1500m and 2000m) obtained from 2D inversion results.

In addition, a remarkably low resistivity anomaly zone is clearly recognized around the center of resistivity discontinuity Rk2. Therefore, resistivity discontinuity Rk2 probably indicates a fracture system which controls geothermal fluid.

3) Resistivity Discontinuity Rk3

Resistivity discontinuity Rk3 runs from the area beside station 11 to the area between station 25 and 26 roughly in a NW-SE direction. Discontinuity Rk3 is recognized in the apparent resistivity maps (at 0.1Hz and 0.01Hz) and the resistivity maps at depths of 1000m, 1500m and 2000m.

In addition, a remarkably low resistivity anomaly zone is clearly recognized around the northern portion of resistivity discontinuity Rk3. Therefore, resistivity discontinuity Rk3 probably indicates a fracture system which controls geothermal fluid.

(b) Resistivity Structure in the Kotamobagu Field

Based on the results of the Kotamobagu survey described previously, the MT/TDEM results for the Kotamobagu geothermal field suggest the following:

A remarkably low resistivity zone is widely distributed in the northewestern, central and southeastern portions of the Kotamobagu geothermal field roughly around depths of 500m and 750m. This low resistivity zone probably reflects low-temperature hydrothermal-alteration clay minerals (smectite, zeolite, etc.) which often form the cap-rock of the geothermal reservoir with temperature conditions between 70^{o}C and 200^{o}C.

On the other hand, a relatively high resistivity zone is recognized in the eastern, southeastern and northeastern portions relatively deep (at depths of 2000m and 2500m). In

particular, the zone around stations, 9, 10, 12 and 13 at depth shows relatively high resistivity values greater than 30ohm-m, despite the existence of the low resistivity zone of less than 5ohm-m in the same area at shallow depths (at depths of 500m and 750m).

This relatively high resistivity zone around stations, 9, 10, 12 and 13 distributed at depth underlying the remarkably low resistivity zone probably reflects high temperature alteration products such as illite and/or chlorite. Hence the relatively high resistivity zone around stations, 9, 10, 12 and 13 at depth is possibly indicative of a higher temperature zone at depth compared to the surrounding areas. In addition, at the eastern edge of the relatively high resistivity zone, resistivity discontinuity Rk3 is clearly detected and an uplifted structure of the resistive zone at depth is also recognized along and to the west of discontinuity Rk3. Therefore it is highly probable that the northern portion of the resistivity discontinuity Rk3 reflects one of the fault-like structures where geothermal fluid may circulate at depth in the Kotamobagu geothermal field.

Moreover, resistivity discontinuity Rk2, which runs approximately NE-SW, can be detected at the southern edge of the above-mentioned relatively high resistivity zone at depths of 1500m and 2000m. Along this resistivity discontinuity, a remarkably low resistivity zone probably reflecting smectite and/or zeolite is widely distributed at relatively shallow depths (500m and 750m). Therefore, the western portion of this resistivity discontinuity Rk2 probably reflects a fault-like structure where geothermal fluids circulate at depth.

Based on these facts, the zone around stations 9, 10, 12 and 13 including the intersection of resistivity discontinuities Rk2 and Rk3, is likely to be a promising zone for geothermal development in the Kotamobagu geothermal field.

In the central and eastern portion of the survey area, a low resistivity zone of less than 10ohm-m is widely distributed at depths of 500m, 750m and 1000m. However, the area still indicates relatively low resistivity values, showing less than 20ohm-m at relatively great depths of 2000m and 2500m. Therefore, high temperature alteration products such as illite and/or chlorite are probably less developed in this area at depths of 2000m and 2500m. This suggests that hydrothermal activities in this area are less intense compared to the hydrothermal activities in the area around stations, 9, 10, 12 and 13. However, further geo-scientific information will be required to understand this low resistivity zone at depth.

In the southwestern portion of the survey area, the other resistivity discontinuity, Rk1, is detected at relatively shallow depths such as 500m and 750m. However, no low resistivity zone is detected around this resistivity discontinuity at any depth from 200m down to 2500m. Hence, there seems to be no hydrothermal alteration zones (smectite, zeolite etc) around Rk3 and to the south of Rk3. Therefore resistivity discontinuity Rk3 possibly indicates a boundary of the geothermal area and the area south of Rk3 seems to be less promising for geothermal development.

4.5 Geothermal Conceptual Model

4.5.1 Methodology

In order to construct the geothermal conceptual model, data and information of three essential components, such as reservoir structure (underground geological structure), heat source (geothermal/volcanic activity history), and water availability (extent of reservoir & chemical property), were collected, analyzed and integrated.

(1) Reservoir Structure (underground geological structure)

Based on the map of regional geology, and tectonic structure, rock distribution, geological setting and sequence, local geological structure, basement formation, and young volcanic intrusive were identified in 23 supplemental survey fields. In 11 MT/TDEM candidate fields, information regarding trend of faults and distribution of permeable formation and structure controlled the hydrogeology were taken noted.

Regarding analysis of fault/fracture/lineaments, all information with close relation to the regional fluid flow was collected. In the survey with detailed well data, information from the well logging was collected as much as possible. In the fields of insufficient data and information of geological structure, faults and fractures were estimated from the geophysical data (gravity, air-photo), the distribution of surface alteration and alignment/trend of hot springs/fumaroles.

(2) Heat Source

Aiming to clarify the history of volcanic activity and thermal activity and to recognize the center of recent volcanic activities, various data related to heat source of the geothermal system were collected and integrated from the distribution of regional volcanic rocks and rock dating. Since the heat source in geothermal system is usually evaluated through geologic ages and the depth, volume and type of residual magma reservoir, the most suitable dating method to each rock sample was selected.

Thermal manifestation on surface is supposed to be connected with up flow zone of geothermal fluid (discharge zone). In addition, distribution and linear arrangement of hot springs and fumaroles are often close to geological structure. Based on the structural information and mineralogical classification information (arenite zone, kaolinate zone, siliceous zone, and so on), the subsurface volcanic activity and the heat derived from the magma reservoir were evaluated.

(3) Reservoir Fluid

Interpretation and evaluation of characteristics and behavior of reservoir fluids in each field were conducted based mainly on the results of geochemical data analyses and locality of the surface thermal manifestations.

The geochemical diagrams constructed by using the chemical and isotopic data of hot spring waters and fumarolic gases obtained in this survey in addition to the existing data were shown from Apps.4.5.1-1 to 15. The existing data includes chemical and isotopic data newly provided by PERTAMINA and additionally obtained data through data collection at CGR during the JICA team's activity in Indonesia from August to October 2006. In addition, the hydrogen and oxygen isotopic data include the unpublished data of hot spring waters that are provided by Dr. M. Takahashi of AIST.

For evaluation of reservoir fluid characteristics and behavior, the following articles listed below were discussed with data and the diagrams.

- origin of geothermal fluid based on hydrogen and oxygen isotopic composition: contribution of meteoric, seawater and magmatic water
- existence of typical geothermal reservoir: occurrence of neutral-pH chloride water, oxygen isotope shift due to water-rock interaction, equilibrium condition based on Na-K-Mg composition, etc.
- reservoir extension and fluid flow pattern: locality and distribution of hot springs and fumaroles exhibiting high discharge and geochemical temperature
- estimation of reservoir fluid temperature: water and gas geothermometries
- fluid appropriateness for power generation: existence of corrosive fluid, non-condensable gas concentration

Hydro-geochemical parameters derived from the results of data analyses and interpretations are tabulated in App.4.5.1 -1. From the data obtained at present, based on existence of neutral-pH chloride spring water and high geochemical temperatures, occurrence of exploitable hot thermal fluid is almost certainly expected in Muaralabuh, Lempur/Kerinci, Sungai Penuh, B.Gedung Hulu Lais, Suoh Antatai, G.Sekincau, Kotamobagu and Tompaso from geochemical viewpoints. Incidentally, the estimated reservoir fluid temperatures based on the geothermometries were adopted into the reservoir temperatures assumed for stored-heat volumetric calculations for resource capacity estimation.

(4) Extent of Reservoir

Extent of geothermal reservoir is one of parameters to calculate the geothermal potential by the stored heat method, which is stipulated in Chapter 4. In this study, reservoir extent in each field was estimated in the under-mentioned way.

The extent of reservoir in the developed field was comprehended accurately with sufficient scientific data and well drilling data. However, only surface surveys without well drilling in most of the target fields in this study have been done. In order to secure the underground information, fault and fracture structures (trend of faults and discontinuity lines estimated from gravity survey, electric survey and magnetic survey) related to the fluid flow, subsurface resistivity distribution as a feature of up flow zone of geothermal fluid, anomaly of soil gas content, and geochemical data of hot springs/fumaroles were utilized for estimation of reservoir extent in consideration of modeling of each geothermal structure.

In the developed fields where geothermal models had been already prepared by PERTAMINA or CGR, reservoir extent data in the models were used for the evaluation..

4.5.2 Geothermal Conceptual Models

Following the above-mentioned methodology, reservoir structure (underground geological structure), heat source (geothermal/volcanic activity history), water availability (fluid characteristics and behavior) and extent of reservoir in the selected 34 fields were integrated in Apps.4.5.2-1 and 4.5.2-2.

App. 4.5.2-2 describes concisely the contents of the three essential components, such as reservoir structure (underground geological structure), heat source (geothermal/volcanic activity history), and water availability (extent of reservoir & chemical property) in the selected 34 fields.

4.6 Geothermal Resource Database

4.6.1 Construction and Expansion of Geothermal Resource Database

The geothermal resource database was constructed by utilizing the existing database prepared by CGR. The examples of several input windows of the newly updated database are shown to the Figs. 4.6.2-1 to 6.

4.6.2 Update of Geothermal Resource Database

In collaboration with CGR, the database was updated, with “characteristics of geothermal reservoir and reservoir evaluation” and “wellproduction data ” newly added to the database.

Iinformation concerning geology, geochemistry, geophysics, well study and resource potential which had been collected and analyzed during the study, was incorporated into the data base. Those examples of windows are referred to Figs. 4.6.2-7 and 4.6.2-8.

Compiled and classified geoscientific data for each geothermal field incorporated in the geothermal resource database are utilized for the evaluation of geothermal fields which have a high potential for electricity development.

4.7 Calculation of Resource Potential and Simplified Economical Evaluation

4.7.1 Calculation of Resource Potential by Stored Heat Method

After the completion of the supplemental field survey, the geothermal resource potential was calculated by means of the Stored Heat Method at the stage of preliminary evaluation was re-evaluated owing to provision of additional information. The resource potential of 38 fields among the 73 prospective fields was evaluated because these fields yielded enough data to calculate the resource potential. The results of evaluation are shown in Table 4.7.1-1, and the results of Monte Carlo Analysis of each field are attached in Appendix. Methodology is described in chapter 4.1.

The fields under development were excluded from resource potential evaluation using the Stored Heat Method, and their planned power outputs, which had been decided through detailed evaluations such as reservoir simulation study, were adopted as their resource potentials for this study.

4.7.2 Simplified Economy Evaluation

After the completion of the supplemental field survey, simplified economic evaluation was conducted for 49 fields, those are the above 38 fields mentioned above and 11developed fields. The relationship between reservoir depth or temperature and predicted production rate of a well is shown in Table 4.7.2-1. In the simplified economy evaluation, the initial capital investment per kW, which is the cost per kW required for constructing a geothermal power plant, was roughly estimated. Methodology and pre-condition of evaluation are described in chapter 4.1. The initial capital investments per kW of the 49 fields are shown in Table 4.7.2-2. The results of the calculation indicate that the initial capital investment per kW has a range from about 1,500 US$/kW to 2,300 US$/kW. Properly speaking, the initial capital investment should be actually more costly than the estimate in this study, because the construction costs of access roads, pipelines, and transmission lines were not included in the estimate of the initial capital investment. However, the value of the initial capital investment was not used for the project planning but for understanding relative economy of geothermal development project of each field. The calculated values of economy of the projects were used as one of criteria for considering development priority of the geothermal

fields.

4.8 Prospective Geothermal Fields from the Viewpoints of Geothermal Resources

To devise an adequate plan to promote the utilization of geothermal resources in Indonesia, it is necessary to understand the present situation with respect to geothermal capacity of each field. Through the construction of a database geothermal resource in Indonesia, various kinds of information concerning each field were compiled with the aim of identifying, assessing and characterizing geothermal reservoirs. Taking into consideration reservoir potentials, chemical features and development stages, possible fields worth exploiting were evaluated for future development. The selected fields are recommendedfor development in consideration of the present status of power development

4.8.1 Methodologies

(1) Present Status of Geothermal Resource Development

Confirmation of the present status of geothermal power development in each field was conducted and the results are summarized in Table 4.8.1-1 using the following brevity code:

1) RE: unexplored or regional reconnaissance only.

2) S1: local surface exploration done - this may include geology and geochemistry, but still lack of sub-surface information (underground structure and resistivity distribution).

3) S2: detailed surface exploration done - this comprises activities of geology, geochemistry, geophysics (gravity, resistivity and/or othersurveys) and /or temperature gradient drilling

4) F1: pre-feasibility studies done – it is confirmed or disproved that a commercially exploitable reservoir is likely to exist by deep drilling well(s) and/or some reasonable information.

5) F2: feasibility studies done – this comprises several well drilling and testing with sufficient outcome to confirm commercially viable development of some specific MW.

6) OP: power plant in operation.

(2) Results

The results of evaluation and classification of geothermal resource in each field are described in Tables 4.8.2-1 to 4.8.2-3. This table contains the items of resource sizes by reservoir volume, temperature, surface water type and reservoir potential. for example, B. Gedung Hulu Lais in Bengkulu, Seulawah Agam in Aceh, S. Merapi-Sampuraga in North Sumatra, Muaralabuh in West Sumatra, G. Karaha in West Jawa, Suoh Antatai in Lampung, Lumut Balai in South Sumatra, and Sungai Penuh in Jambi (100 x $10^9 m^3$ over) are picked up as the fields with the largest reservoir volume. However, all of these fields except G. Karaha are not well explored and bear the burden of very uncertain reservoir extent until further exploration by resistivity survey and exploratory well drilling.

(a) Sumatra

- Iboih-Jaboi (Aceh)
- Seulawah Agam (Aceh)
- Lau Debuk-Debuk/Sibayak (North Sumatra)
- Sarulla (North Sumatra)
- Sibual Buali (North Sumatra)
- S. Merapi-Sampuraga (North Sumatra)
- Muaralabuh (West Sumatra)
- Lempur/Kerinci (Jambi)
- Sungai Penuh (Jambi)
- B. Gedung Hulu Lais (Bengkulu)
- Tambang Sawah (Bengkulu)
- Marga Bayur (South Sumatra)
- Lumut Balai (South Sumatra)
- Ulubelu (Lampung)
- Suoh Antatai (Lampung)
- G. Sekincau (Lampung)
- Rajabasa (Lampung)
- Wai Ratai (Lampung)

Sumatra is the richest island in geothermal resources in Indonesia. However, geothermal developments in Sumatra Island are retarded, in comparison with those in Jawa Island.

Although construction and operation of the geothermal power plant in Sibayak was started from October 2000, the other geothermal power developments have not been conducted for a long time. Since the reservoir in this field seems to be moderately positioned (about 1,500m – 2,200m) and high in temperature (270°C in geothermometry), further exploitation with relatively low development risk should be carried out. Reservoir potential estimated in this study is 170 MW and proven and possible potentials of this field were reported to be 39 MW and 131 MW respectively in the previous works, which were conducted by PERTAMINA. These capacities are larger than the output of the existing power plant. It can be said that additional power development should be carried out in order to maintain the power output of the existing plant and future power plant construction.

The following advanced field in Sumatra is Sarulla. A feasibility study (of resource development) has been roughly completed and, depth, temperature and characteristics of the reservoir in this field were revealed; therefore rapid progress of geothermal power development of this field is expected. Existence of reservoirs was confirmed by deep well drilling and physical and chemical characteristics of the deep reservoirs were considered to be adequate for power generation. 13 deep wells were drilled in the 1990s and power generation with 330 MW for 30 years was proven. Behind the economic crisis in 1997-1998, several IPP companies finally start to develop the power plant construction. In this field, there are four geothermal systems, such as Silangkitang, Namora-I-langit, Sibualbuali and Donotasik. Five wells were drilled in Silangkitang field, located in the Sarulla graben along the main trace of the Great Sumatra Fault. Two of the wells found a strong upflow zone with fluid temperatures in excess of 310^{o}C. Four wells drilled in the Namora-I-Langit in an area of extensive thermal activity. These wells are all highly productive, encountering a large, high permeability geothermal system with fluid temperature in excess of 260^{o}C. Three of the wells produced neutral Na-Cl brine, but the fourth produced a low-pH Na-Cl-SO_4 fluid. Four wells were drilled in the Sibualbuali, which is located on the extinct Sibualbuali andesitic stratovolcano. The wells are productive, finding a geothermal system with a maximum temperature of 267 ^{o}C. Strong lateral and vertical temperature gradients found in the system are attributed to channeling of fluids along strands of the reginal fault. Though undrilled in Donotasik, the permeability seems to be strongly controlled by the Great Sumatra Fault, as well as other three prospects.

To develop the other three fields listed previously, Ulubelu, Lumut Balai, B. Gedung Hulu Lais, detailed surface surveys and studies and exploratory well drillings are necessary. Construction of geothermal structure modeling and well drilling to increase the success rate of well drilling and to confirm the existence of geothermal resources should be carried out. After the confirmation and model construction, generation capacity should be clarified by using reservoir simulation techniques for a feasibility study and power plant construction. At present, depth, temperature, and characteristics (mainly chemical) of the reservoir are assumed from the data of a preliminary study (surface surveys and studies). Capacities estimated in this study are remarkably large (580-1,220 MW) and, temperatures

(250-290°C) and chemical characteristics (mostly neutral Cl type) of reservoir fluids assumed from the surface data are adequate for power generation.

Eight geothermal fields given top priority for power development in Sumatra are regarded to have high temperature (240-270°C) and characteristics (neutral or weakly alkaline Cl type) of deep geothermal fluid in a reservoir to a relatively large extent (Muaralabuh, Sungai Penuh, Tambang Sawah, Rajabasa, Suoh Antatai, G. Sekincau, and Wai Ratai). It is strongly anticipated to accrete power development of these fields and to contribute to power supply through the Sumatra transmission networks by PLN in the near future.

In addition to these fields, geothermal resources in Seulawah Agam and S. Merapi-Sampuraga seem to be promising for geothermal development, because of the high temperature (>230°C) estimated by geochemical method and good indication of fluid chemistry. These resources were considered to have huge potential (640-900MW), but still uncertain permeability of the reservoir.

Other two fields (Iboih-Jaboi and Marga Bayur) were given to 2nd rank in development possibility. These fields are also necessary to conduct the study by exploratory well drilling after the detailed surface exploration.

Generation capacity of geothermal resources in Sumatra is regarded to be larger than 7,500 MW. Most geothermal fields in this region have large capacities (larger than 100 MW) of generation. Development of these fields is expected to contribute power supply to the north, the central and the south Sumatra electricity grid systems.

(b) Jawa-Bali

- Kamojang (West Jawa)
- G. Salak (West Jawa)
- Darajat (West Jawa)
- Cisolok-Cisukarame (West Jawa)
- G. Patuha (West Jawa)
- G. Wayang-Windu (West Jawa)
- G. Karaha (West Jawa)
- G. Telagabodas (West Jawa)
- Dieng (Central Jawa)
- Ungaran (Central Jawa)
- Wilis-Ngebel (East Jawa)

- Bedugul (Bali)

In Jawa and Bali islands, there are many promising geothermal fields adequate for power development. The Kamojang, Salak, Darajat, Wayang Windu and Dieng fields had been developed and power plants were constructed and have been operated. Generation capacities of the fields estimated in this study are larger than the present and planned ones. The power development of these fields, which contributes power supply to the Jawa-Bali region through the transmission line network, will be carried out with certainty, if the geothermal reservoirs in the fields are evaluated using resource data of additionally conducted study and field operation in detailed.

Additional power development can be conducted in the Kamojang and Dieng fields by PERTAMINA and GEODIPA. For example, in the Kamojang fields where a feasibility study was conducted by JETRO support, 40 – 60 MW can be generated in addition to the present 140 MW by the existing power plants and the planned 60 MW (Kamojgang IV). The Dieng field has been also operated from 1998 with 60MW and planned another 240 MW on Road Map 2025.

A high potential of the geothermal resources seems to exist in the Patuha, G. Karaha, G. Telagabodas and Bedugul fields (G. Karaha and G. Telagabodas seems to belong the same concession). High temperatures (245-285^{o}C) were measured and estimated and significant reservoirs (200-600MW) have been shown by integrated geoscientific studies. In spite of confirmation of geothermal reservoir, these fields have not yet been commissioned to construct the power plant. It is necessary to conduct prompt development by the investigated companies, contracted with PERTAMINA and PLN, through the governmental instruction.

Regarding the remaining three fields, Cisolok-Cisukarame, Ungaran and Wilis-Ngebel, it is worthwhile studying for future power development, because reservoir volume, measured or estimated temperatures, and chemical characteristics of the geothermal reservoir seem to be adequate for geothermal development. Geoscientific data for a feasibility study is not sufficient to identify resource existence and evaluate capacity. A resource study and development programs should be prepared for these field developments. Geothermal resources evaluated in this study are relatively large and development of these fields will contribute to power supply in Jawa-Bali region and activate local industries.

Generation capacity of geothermal resources in Jawa-Bali is regarded to be larger than 4,500 MW in this study. Since the selected fields have a considerably large generation capacity, systematic development plan, survey to well drilling and testing with relatively high technologies will be expected.

(3) Sulawesi and East Indonesia

- Hu'u Daha (West Nusa Tenggara)
- Wai Sano (East Nusa Tenggara)
- Ulumbu (East Nusa Tenggara)
- Bena-Mataloko (East Nusa Tenggara)
- Sokoria-Mutubusa (East Nusa Tenggara)
- Oka-Larantuka (East Nusa Tenggara)
- Atadei (East Nusa Tenggara)
- Lahendong (North Sulawesi)
- Kotamobagu (North Sulawesi)
- Tompaso (North Sulawesi)
-Tulehu (Maluku)
- Jailolo (North Maluku)

As the most promising fields of geothermal development in this region, Lahendong, Tompaso and Kotamobagu fields inSulawesi Island and Ulumbu, Bena-Mataloko and Sokoria-Mutubusa fields in Flores Island are selected.

Of these fields, Lahendong has been under development by PERTAMINA since 1984. Unit I (20MW) commenced the commercial operation in August 2002. Unit II and III (each, 20 MW) are currently under construction by PLN in anticipation of continuing electricity demand growth in North Sulawesi. More than 16 deep wells have been drilled with a proven generating capacity of 80MW from PERTAMINA calculation. Even in this study, 175 MW of resource potential is estimated in this prospect. Since abundant active surface manifestations exist at the surrounding field of the existing and developing areas, further expansion will be probably expected in Lahendong concession.

Other two fields in North Sulawesi listed previously, Tompaso and Kotamobagu, are necessary to do the detailed surface survey and studies and exploratory well drilling. At present, depth, temperature and characteristics (mainly chemical) of the reservoir are assumed from the data of the surface surveys and studies. Resource potentials estimated in this study are remarkably large (240-460MW) and temperatures (250-260^{o}C) of reservoir fluids assumed from the geothermometry are adequate for power generation. Construction of geothermal structure modeling, well drilling to increase the success rate of well drilling and confirmation of the existence of geothermal resources should be carried out through the integration of subsurface resistivity survey by PERTAMINA and JICA.

On the Island of Flores, PLN drilled three exploration holes at the Ulumbu field and CGR drilled two wells in Bena-Mataloko field. In addition, the magneto-telluric survey was done in Sokoria-Mutubusa field in this study. The reservoir temperature measured or estimated in these three fields is 230-250^{o}C and each chemical characteristic is among slightly acidic SO_4 type. A high potential of the geothermal resources seems to exist in these fields, but low population and an isolated island may limit the demand of electricity market. However, geothermal development in these fields is very effective and helpful for local industries, which use hot water and heat supplied from geothermal power plant.

Regarding the remaining six fields, Hu'u Daha, Wai Sano, Oka-Larantuka, Atadei, Tulehu and Jailolo, it is worthwhile studying for future power development. These fields show the adequate temperature (200^{o}C over) for geothermal generating and water from hot springs indicates neutral in pH. In spite of Shortage of field survey data, but surface manifestations show possibility of potential resource existence.

Generation capacity of geothermal resources in Sulawesi-East Indonesia is regarded to be larger than 2,000 MW in this study. Although most geothermal fields in this region have sufficient resource potential, small-medium scaled power development is recommended in consideration of local electricity demand.

Fig. 4.1.1-1(1) Study Area (Sumatra)

Fig. 4.1.1-1(2) Study Area (Java)

Fig. 4.1.1-1 (3) Study Area (Sulawesi & Maluku)

Fig. 4.1.1-1 (4) Study Area (Nusa Tenggara)

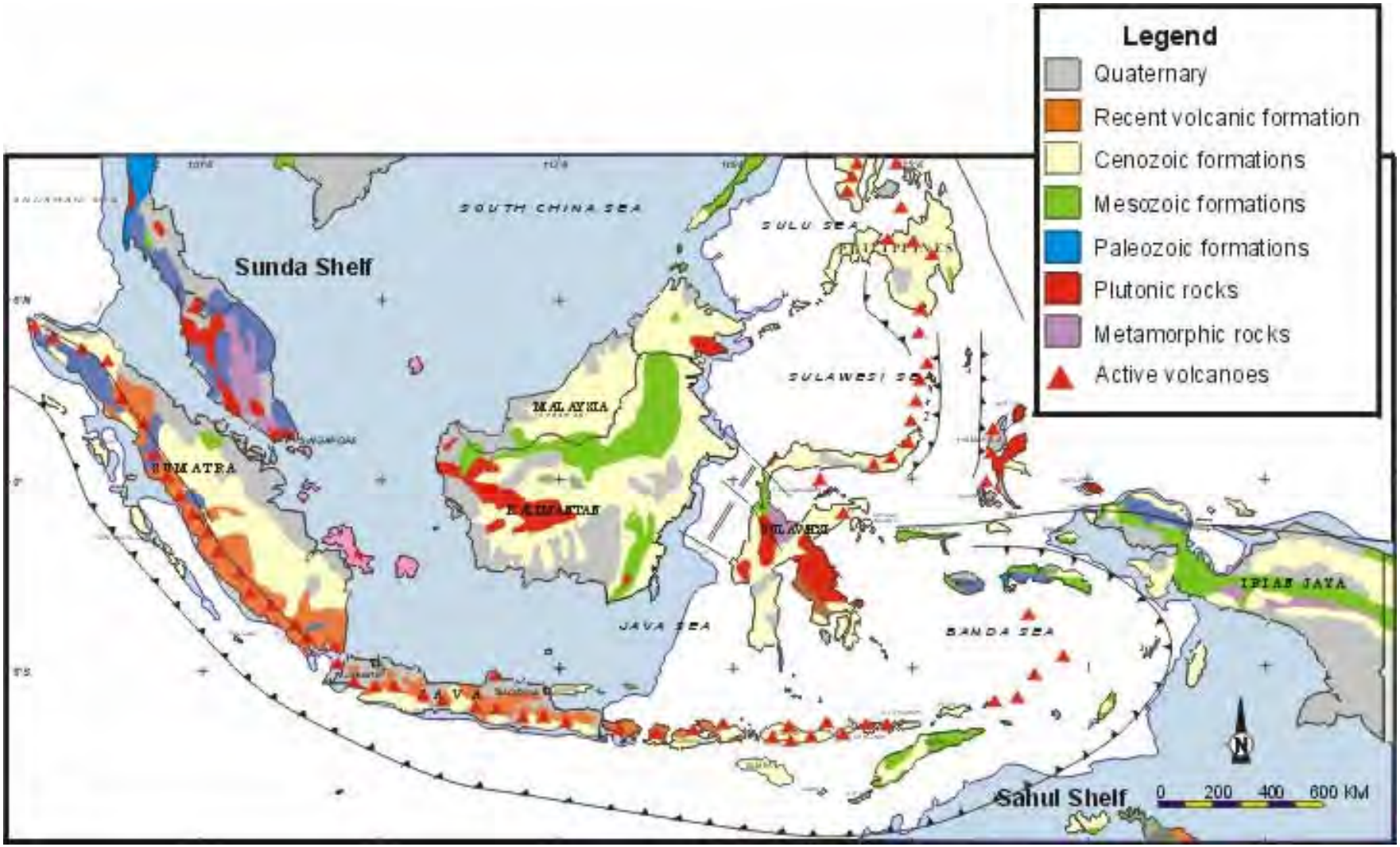

Fig. 4.1.1-2 Regional Geology of Indonesia

Table 4.1.1-1 Hydro-geochemical Parameters of the 73 Geothermal Fields.

Region	No	Names of the 73 fields in this Survey	Surface Tmax(℃)	Surface Water Type (Hot Spring)			Acid Sulfate Spring	Neutral Chloride Spring	Seawater Contribution	Water Chemical Temperature (℃)				Gas Chem. Temp.(℃)	
				pH	Major Anion	Cl max (ppm)				HS-TSiO$_2$	HS-Na/K	HS-dMg,K/Mg	Well-TSiO$_2$	Fumarole	Well
Nangroe Aceh Darussalam	1	IBOIH - JABOI	100	2.4-7.1	SO4, HCO3, Cl-HCO3	1353	present	present	possible	94-162	217-300	34-149	-	277-286	-
	2	LHO PRIA LAOT	101	6.5	Cl	5312		present	none	137-166	190-219	122-215	-	-	-
	3	SEULAWAH AGAM	89	7	Cl-SO4	2399		present	none?	-	178-209	101	-	-	-
	4	G. GEUREUDONG	69												
	5	G. KEMBAR	89	7.8	Cl-SO4	828		present	none	77-100	333-347	163-191	-	-	-
North Sumatera	6	G. SINABUNG													
	7	LAU DEBUK-DEBUK / SIBAYAK	116	6.7	HCO3	110				51-71	-	42-75	-	-	-
	8	SARULA	101	3.1-9.3	SO4, HCO3, Cl-HCO3, Cl-SO4	1310	present	present	none	99-228	140-280	132-271	-	275-300	-
	9	SIBUAL BUALI	72	7.5-7.9	HCO3, Cl-HCO3	288		present	none	95-138	156-230	90-160	-	250-310	-
	10	S. MERAPI - SAMPURAGA	99	2.5-7.4	SO4, Cl-HCO3	503	present	present	none	-	189-218	134-144	99-127	-	-
	11	PUSUK BUKIT - DANAU TOBA	90	2.5-3.4	SO4	394	present			-	-	-	-	237	-
	12	SIMBOLON - SAMOSIR	43	3.4	SO4	24	present			-	-	-	-	152	-
West Sumatera	13	MUARALABUH	104	6.75-8	SO4, Cl	1200		present	none	153-184	185-215	194-215	-	-	-
	14	G. TALANG	98	8.2	HCO3	10				-	-	-	-	-	-
Jambi	15	LEMPUR / KERINCI	97	2.8-7.2	SO4, HCO3	9	present			-	-	-	192-224	167-285	250-307
	16	SUNGAI TENANG	96	8.0	Cl-SO4	392		present	none	123-151	178-209	176	-	-	-
	17	SUNGAI PENUH	102	7.0		579		present	none	198-243	-	288	-	-	-
	18	SUNGAI BETUNG	30												
	19	AIR DIKIT	98	2.5	SO4	3	present			-	-	-	-	-	-
	20	G. KACA	41												
Bengkulu	21	B. GEDUNG HULU LAIS	95	2.1	SO4	3	present			-	-	-	-	272-292	-
	22	TAMBANG SAWAH	95	8.0	Cl	2557		present	none	108-134	191-219	167-203	-	-	-
	23	BUKIT DAUN	95	2.3	SO4	47	present			-	-	-	-	-	-
South Sumatera	24	MARGA BAYUR	96	6.7	SO4	5				176	-	-	-	-	-
	25	LUMUT BALAI	98	2.5	SO4	80	present			-	-	-	-	-	-
	26	RANTAU DADAP - SEGAMIT	96												
Lampung	27	ULUBELU	99	2-neutral		900									240-250
	28	SUOH ANTATAI	99	7.2	Cl	1326		present	none	215-228	249-264	-	-	-	-
	29	G. SEKINCAU	98	7.5	Cl	1370		present	none	251-257	236-254	228-240	-	-	-
	30	RAJABASA	99	6.0-6.5	HCO3, Cl	5570		present	none?	114-149	148-185	113-195	-	-	-
	31	WAI RATAI	92	7.4	Cl	1939		present	none?	207-221	189-218	114-134	-	-	-
West Java	32	KAMOJANG	96	2.9-8.2	SO4, HCO3	17	present			-	-	-	-	-	-
	33	G. SALAK											225		
	34	DARAJAT	77	3.0-5.0	SO4	14	present			-	-	-	-	-	-
	35	CISOLOK - CISUKARAME	98	7.9-8.7	Cl-HCO3, Cl-SO4	405		present	none	109-159	96-190	88-117	-	-	-
	36	G. PATUHA	89												
	37	G. WAYANG - WINDU	50										203-262		
	38	G. KARAHA	95	6.6	SO4	11				-	-	-	264	-	-
	39	G. TELAGABODAS	92												
	40	TANGKUBANPERAHU	96	2.5-7.4	SO4, HCO3, Cl-HCO3, Cl-SO4, Cl	879	present	present	none	127-165	124-222	65-169	-	-	-
Banten	41	BATUKUWUNG	52												
	42	CITAMAN - G. KARANG	94												
	43	G. ENDUT	84												
Central Java	44	DIENG	94												
	45	MANGUNAN	46												
	46	TELOMOYO													
	47	UNGARAN	86	6.0-8.0	HCO3, Cl-HCO3	870		present	none?	100-147	130-170	68-161	-	180-279	-
	48	G. SLAMET	51	7.9	HCO3	26				-	-	-	-	-	-
East Java	49	G. ARJUNO - WELIRANG	70	6.7	HCO3	334				102	-	88-135	-	-	-
	50	WILIS / NGEBEL	93	6.6	Cl	4627		present	none	74-97	191-219	115	122-150	-	-
	51	IJEN	57	6.5-8.3	HCO3	152				115	-	88-131	-	-	-
Bali	52	BEDUGUL	32												
West Nusa Tenggara	53	HU'U DAHA	86	2.2-6.7	SO4, HCO3, Cl-SO4	1555	present	present	possible	-	-	-	-	-	-
East Nusa Tenggara	54	WAI SANO	92	5.7-7.1	SO4, HCO3, Cl-HCO3, Cl	20000		present	none?	56-113	150-286	53-257	-	-	-
	55	ULUMBU	96	3.0-4.4	SO4	36	present			-	-	-	-	-	245-249
	56	BENA - MATALOKO	95	2.5-6.4	SO4	36	present			-	-	-	-	212-256	270-273
	57	SOKORIA - MUTUBUSA	97	1.9-8.0	SO4, HCO3, Cl-HCO3, Cl-SO4	1384	present	present	none	71-122	99-193	88-175	-	230-323	-
	58	OKA - LARANTUKA	90	2.6-8.6	SO4, HCO3, Cl-HCO3, Cl-SO4, Cl	4994	present	present	possible	92-156	177-246	70-243	-	-	-
	59	ILI LABALEKEN													
	60	ATADEI	97	8.1	HCO3	10				-	-	-	-	175	-
North Sulawesi	61	LAHENDONG	99	8.7	mixed	290				198-213	-	141	-	-	-
	62	KOTAMOBAGU	98	7.8	SO4	380				86-110	212-236	101-110	-	286	-
	63	TOMPASO	98												
Central Sulawesi	64	BORA	81												
	65	MARANA	90	6.8-8.8	HCO3, mixed, Cl-HCO3, Cl-SO4, Cl	3569		present	possible	75-129	86-222	48-126	-	-	-
South Sulawesi	66	BITUANG	98												
Southeast Sulawesi	67	LAINEA	85												
Maluku	68	TONGA WAYANA	60												
	69	TULEHU	92	6.5-7.7	HCO3, Cl-HCO3, Cl-SO4, Cl	14300		present	present	34-169	130-239	43-225	-	166	-
	70	JAILOLO	97	7.2-7.8	HCO3, Cl-HCO3, Cl-SO4, Cl	6954		present	possible	59-131	112-171	81-190	-	-	-
North Sumatera	71	SIPAHOLON-TARUTUNG	65	6.2-7.2	SO4, HCO3, mixed, Cl-HCO3	277		present	none	77-138	-	50-95	-	-	-
East Java	72	ARGOPURO	47	7.4	HCO3	26				-	-	-	-	-	-
Gorontalo	73	SUWAWA-GORONTALO	83	7.4-7.8	SO4, Cl-SO4	923		present	none?	50-122	130-170	44-126	-	-	-

Water/Gas Chemical Temperature : HS=Hot Spring Water, Well=Well Water/Gas

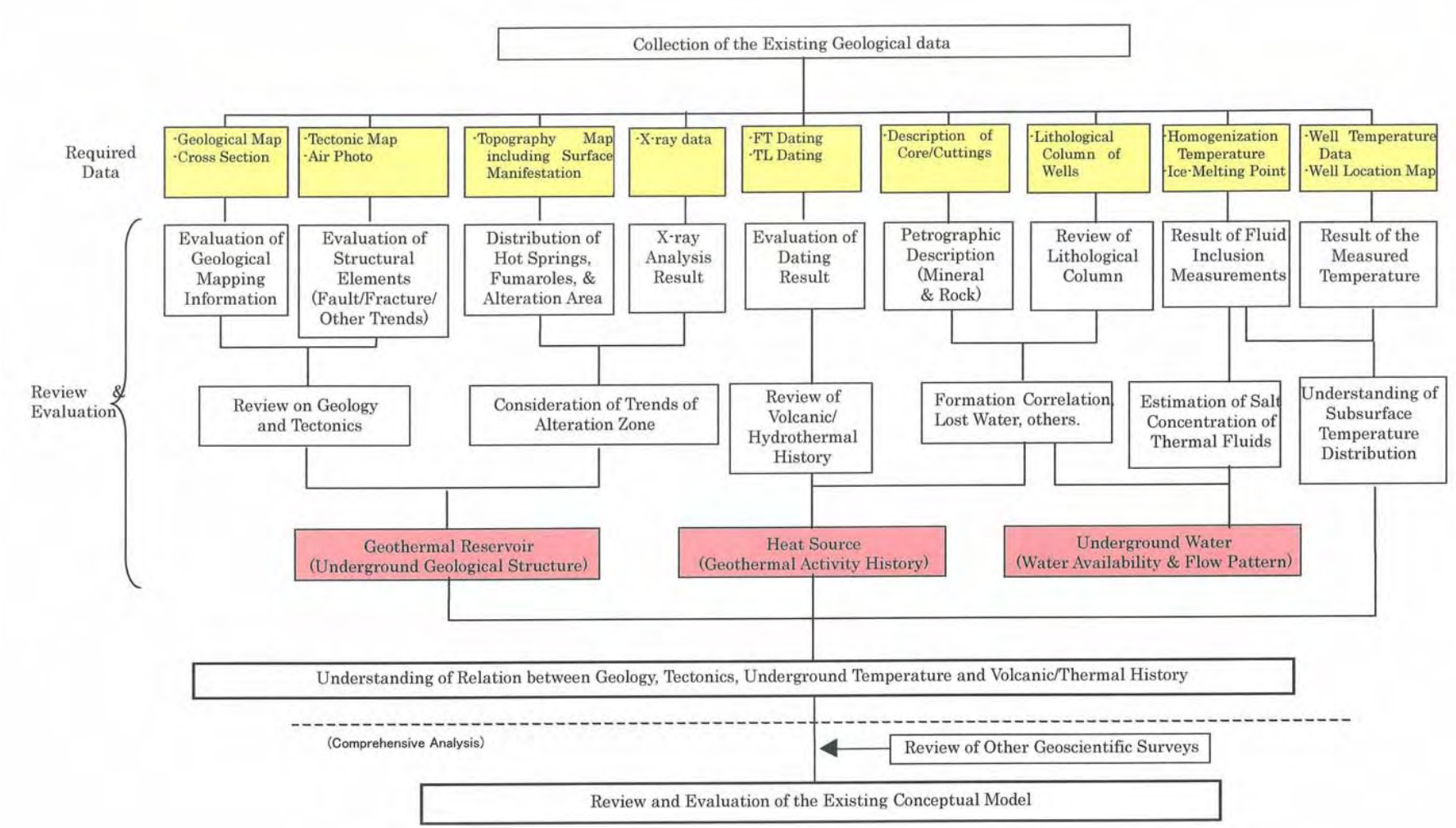

Fig. 4.1.1-3 Schematic Process for Conceptual Model Construction

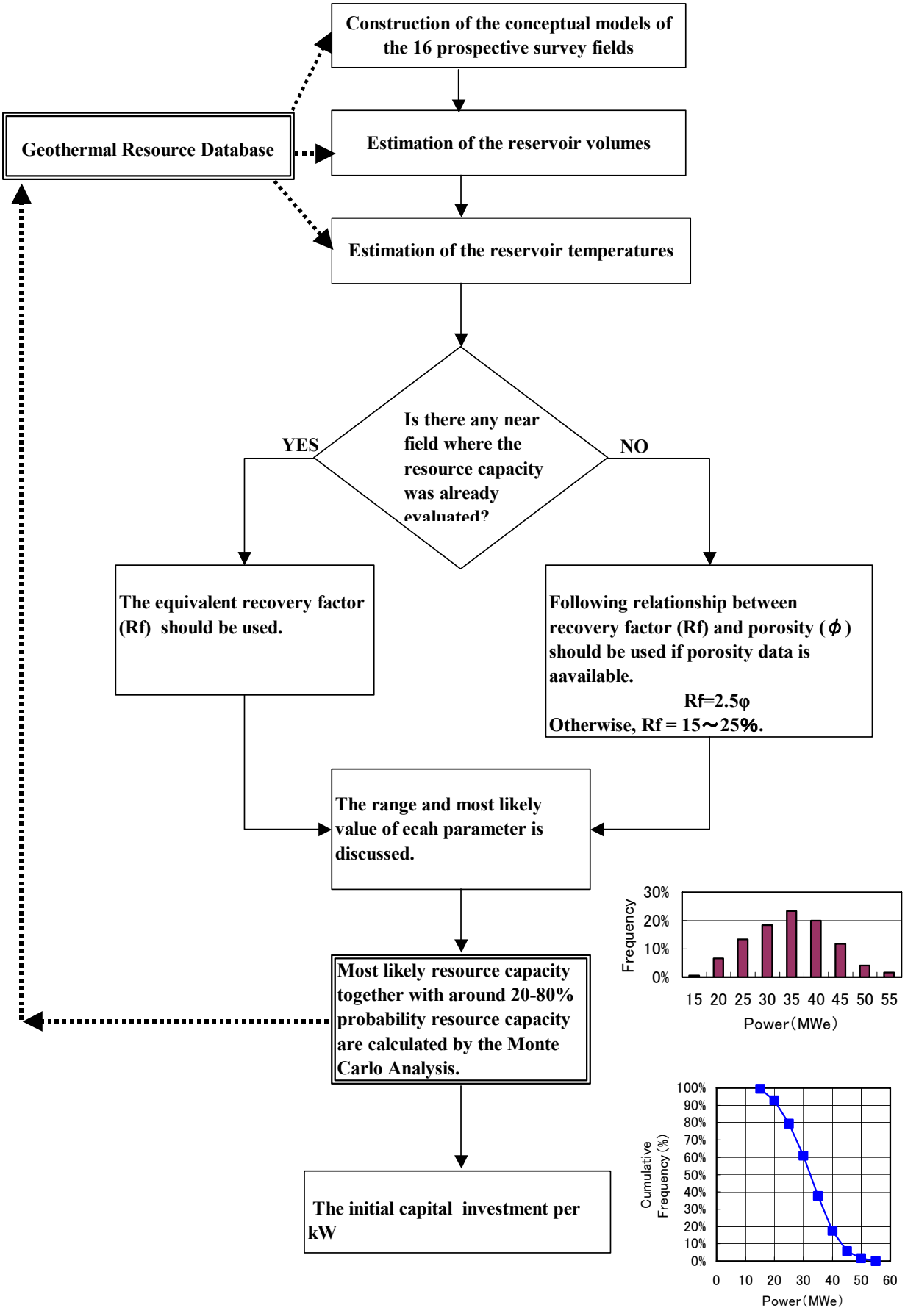

Fig. 4.1.1-4 Flow Chart of the Resource Evaluation

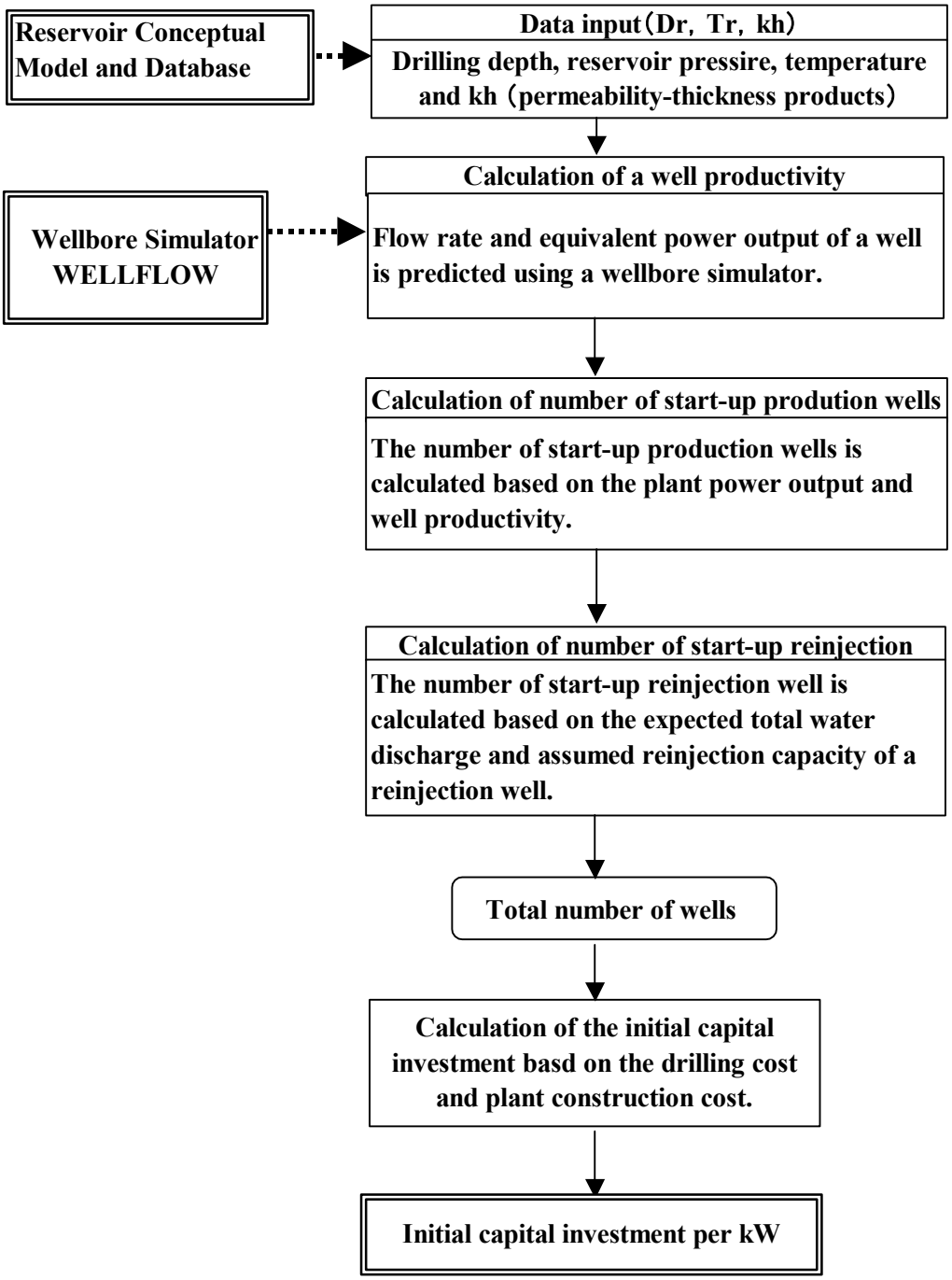

Fig. 4.1.1-5 Flow Chart of the Simplified Economical Evaluation

Table 4.1.2-1 Item for Evaluation of Each Geothermal Field

Evaluation Criteria	
① Economy	
Simplified Economic Evaluation:	Cost ranking on the simplified economic evaluation based on the initial investment cost per kW (US$/kW) and characteristics of each geothermal reservoir (drilling depth, productivity and reinjectivity)
② Security	
Safety Instruction :	Following to the safety instruction of Foreign Ministry of Japan, geothermal areas situated in the following provinces are prohibited to visit. – Nanggroe Aceh Darussalam – Central Sulawesi, West Timor of East Nusa Tenggara – Maruku, North Maruku, Papua
③ Development Stage	
Already Installed :	Areas already installed the generating facilities.
JOC :	Joint Operation Contract areas.
WKP :	Detailed-explored areas with the development plan (on the Road Map 2025).
Protection Area :	Areas with natural/social/environmental problems and the restriced areas on regulation
④ Purpose of Development	
Regional Electricity Gridding :	large-scale power plant connecting regional power grid
Isolated Gridding :	Independent power plants for rural electrification (small-scale power plant in multipurpose utilization)
⑤ Development Scheme	
ODA :	IPP by private investors
IPP :	Government developer financially supported by ODA (ex. Soft-Loan)
Small-scale Generating :	Government developer by public support and/or local government
⑥ Difficulty in Develoment	
Infrastructure/Accessibility/Regulation :	Necessity of supplemental field survey was finally considered on condition of infrastructure construction, power demand, access to the site, distance to the grid-line, development condition of surrounding areas, etc.

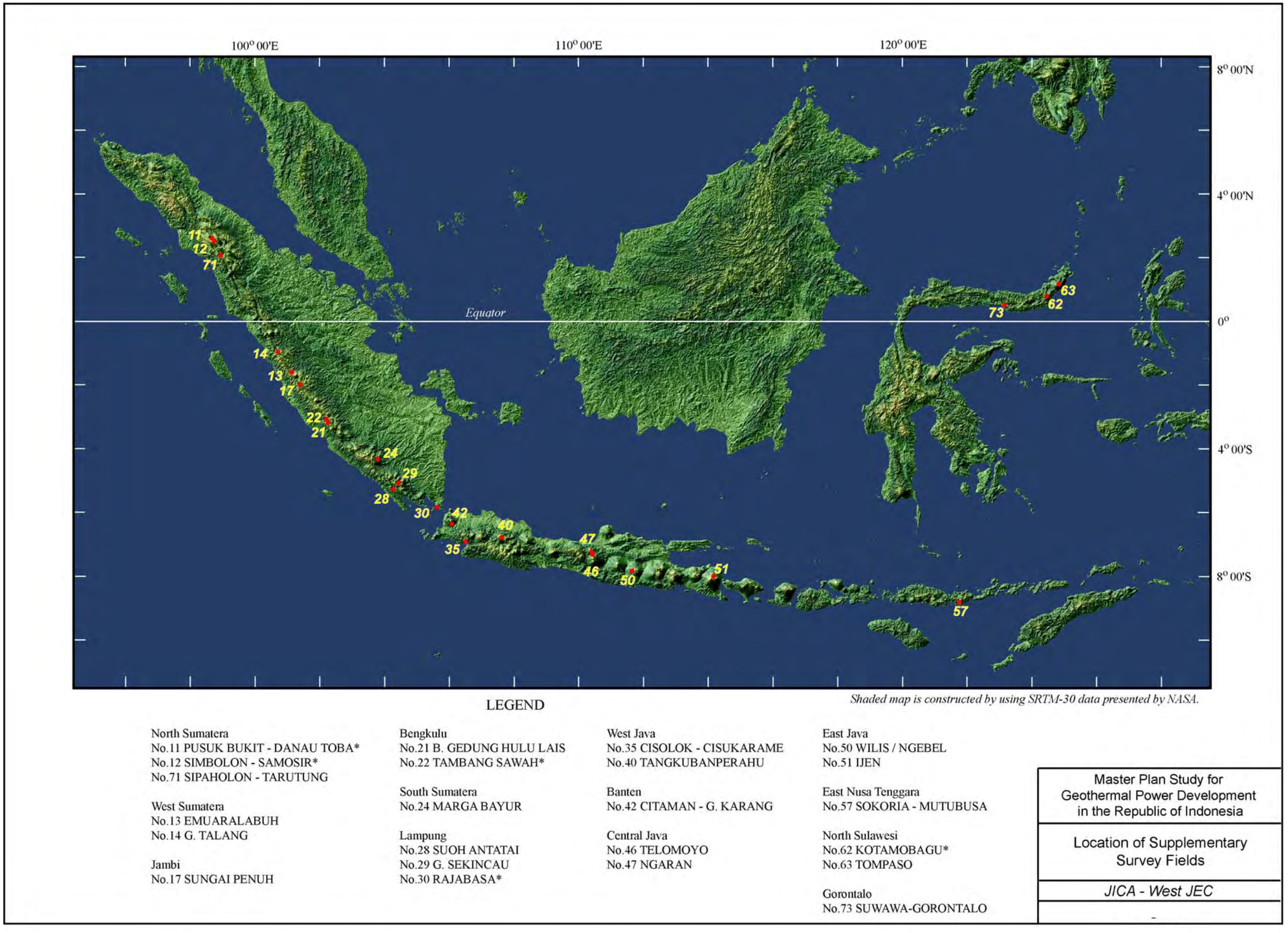

Fig. 4.1.2-1 Location of Supplementary Survey Fields

Table. 4.4.1-1 List of 34 Geothermal Fields

Region	Field
Aceh	IBOIH-JABOI (No.1) LHO PRIA LAOT (No.2) SEULAWAH AGAM (No.3) G. KEMBAR (No.5)
North Sumatera	S. MERAPI-SAMPURAGA (No.10) PUSUK BUKIT - DANAU TOBA (No.11) SIMBOLON – SAMOSIR (No.12) SIPAHOLON – TARUTUNG (No.71)
West Sumatera	MUARALABUH (No.13) G. TALANG (No.14)
Jambi	LEMPUR / KERINCI (No.15) SUNGAI PENUH (No.17) AIR DIKIT (No.19)
Bengkulu	B. GEDUNG HULU LAIS (No.21) TAMBANG SAWAH (No.22)
South Sumatera	MARGA BAYUR (No.24)
Lampung	SUOH ANTATAI (No.28) G. SEKINCAU (No.29) RAJABASA (No.30) WAI RATAI (No.31)
West Java	CISOLOK – CISUKARAME (No.35) TANGKUBANPERAHU (No.40)
Banten	CITAMAN - G. KARANG (No.42)
Central Java	TELOMOYO (No.46) UNGARAN (No.47)
East Java	WILIS / NGEBEL (No.50) IJEN (No.51)
East Nusa Tenggara	WAI SANO (No.54) BENA-MATALOKO (No.56) SOKORIA – MUTUBUSA (No.57)
North Sulawesi	KOTAMOBAGU (No.62) TOMPASO (No.63)
Maluku	TULEHU
Gorontalo	SUWAWA-GORONTALO (No.73)

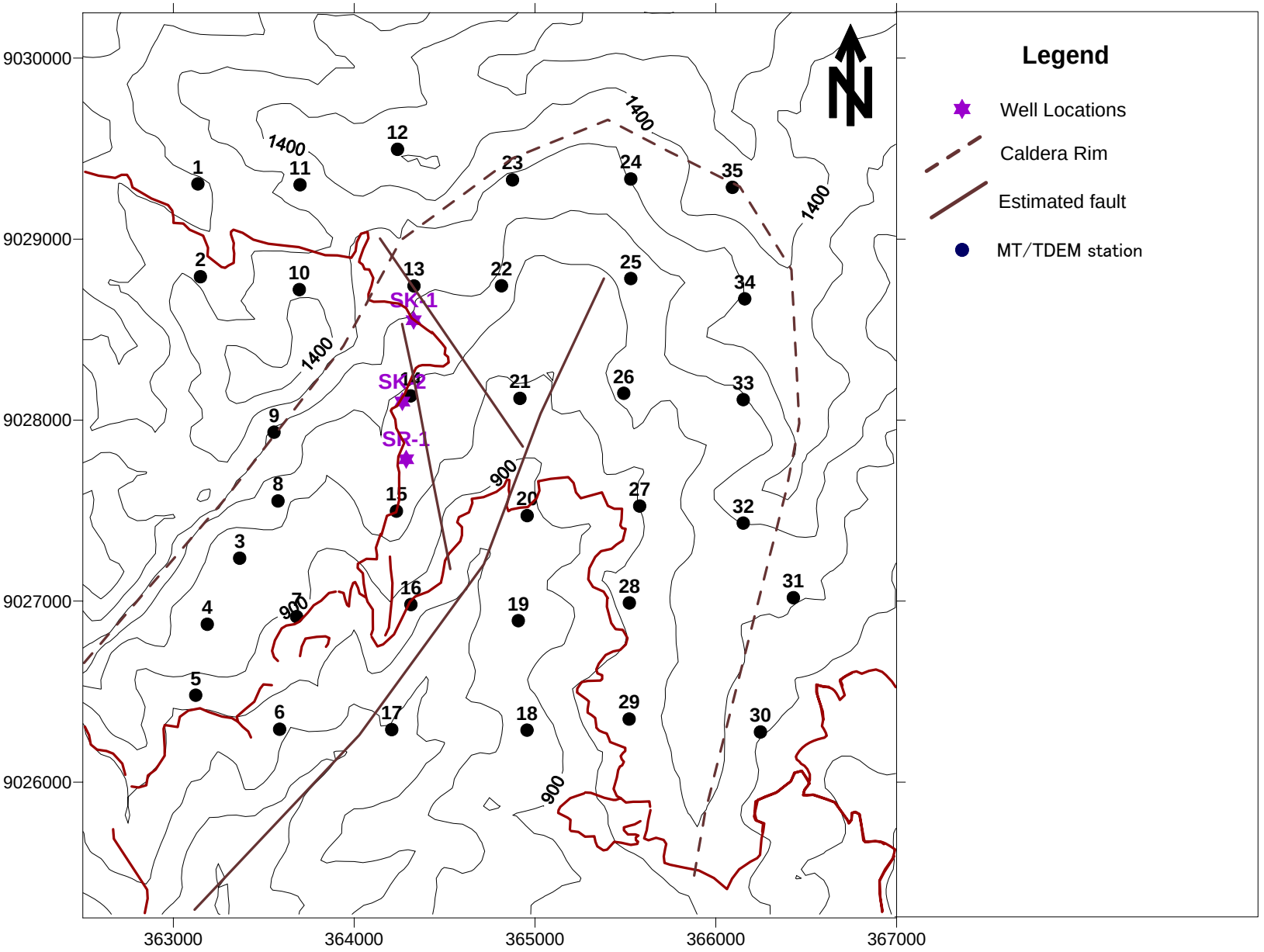

Fig. 4.4.2-1 Station Location Map (Sokoria MT/TDEM survey)

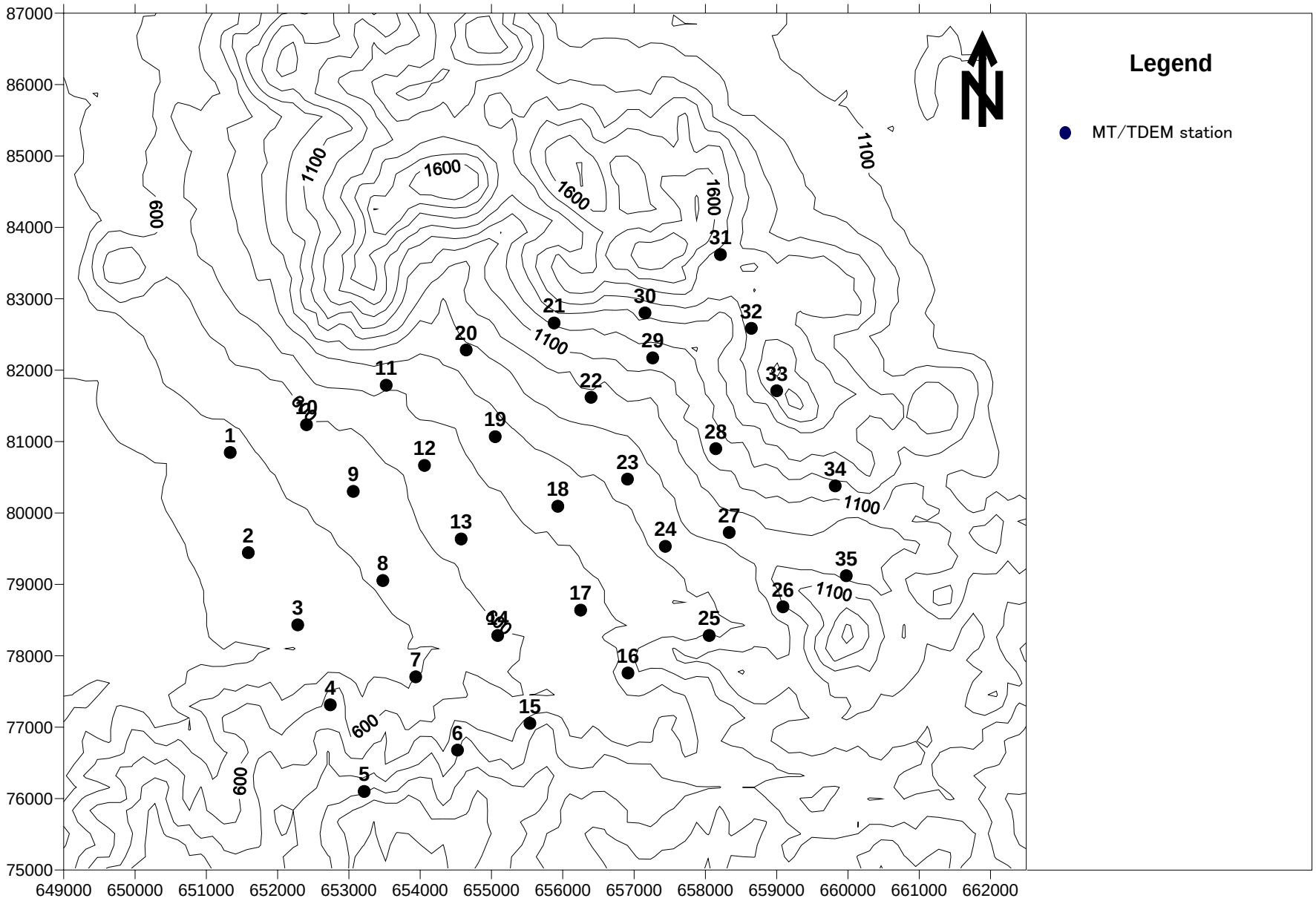

Fig. 4.4.2-2 Station Location Map (Kotamobagu MT/TDEM survey)

Table 4.4.2-1 Locations of MT/TDEM stations (Kotamobagu and Sokoria fields)

Coordinat Survey MT & TDEM				Coordinat Survey MT & TDEM			
Sokoria, East Nusa Tenggara				Kotamobagu, North Sulawesi			
MT Site	Long (m)	Lat (m)	Elev (m)	MT Site	Long (m)	Lat (m)	Elev (m)
MTSC01	363136	9029305	1196	MTKB01	651335	80847	483
MTSC02	363150	9028792	1317	MTKB02	651589	79444	454
MTSC03	363367	9027237	970	MTKB03	652282	78433	457
MTSC04	363188	9026872	950	MTKB04	652739	77313	609
MTSC05	363124	9026480	831	MTKB05	653214	76100	896
MTSC06	363588	9026292	775	MTKB06	654523	76679	760
MTSC07	363682	9026914	871	MTKB07	653937	77705	511
MTSC08	363579	9027553	1079	MTKB08	653476	79054	535
MTSC09	363557	9027933	1243	MTKB09	653061	80302	563
MTSC10	363697	9028721	1414	MTKB10	652405	81236	594
MTSC11	363701	9029300	1338	MTKB11	653523	81789	732
MTSC12	364240	9029496	1493	MTKB12	654060	80666	639
MTSC13	364331	9028741	1230	MTKB13	654574	79636	624
MTSC14	364313	9028134	1092	MTKB14	655087	78284	585
MTSC15	364234	9027497	1061	MTKB15	655539	77054	712
MTSC16	364314	9026981	895	MTKB16	656914	77759	718
MTSC17	364208	9026290	690	MTKB17	656250	78640	663
MTSC18	364956	9026287	826	MTKB18	655930	80094	736
MTSC19	364908	9026892	856	MTKB19	655052	81069	750
MTSC20	364957	9027472	872	MTKB20	654645	82283	916
MTSC21	364917	9028120	996	MTKB21	655879	82661	1201
MTSC22	364815	9028742	1197	MTKB22	656396	81620	956
MTSC23	364876	9029327	1307	MTKB23	656907	80474	824
MTSC24	365530	9029332	1256	MTKB24	657438	79533	810
MTSC25	365530	9028782	1113	MTKB25	658053	78284	789
MTSC26	365491	9028148	1102	MTKB26	659088	78686	973
MTSC27	365579	9027525	974	MTKB27	658334	79727	921
MTSC28	365522	9026990	1018	MTKB28	658146	80901	1150
MTSC29	365521	9026348	1067	MTKB29	657261	82172	1125
MTSC30	366247	9026277	1009	MTKB30	657153	82802	1344
MTSC31	366429	9027019	1138	MTKB31	658211	83619	1450
MTSC32	366152	9027431	1189	MTKB32	658734	82579	1439
MTSC33	366152	9028113	1196	MTKB33	659000	81712	1581
MTSC34	366160	9028670	1300	MTKB34	659821	80379	1171
MTSC35	366092	9029286	1407	MTKB35	659976	79121	972

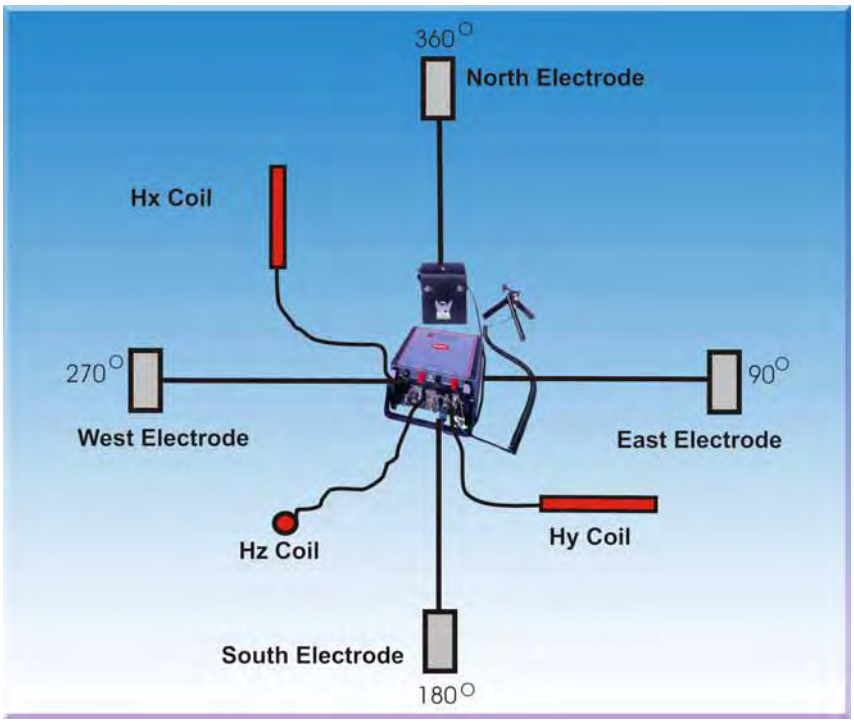

MT layout

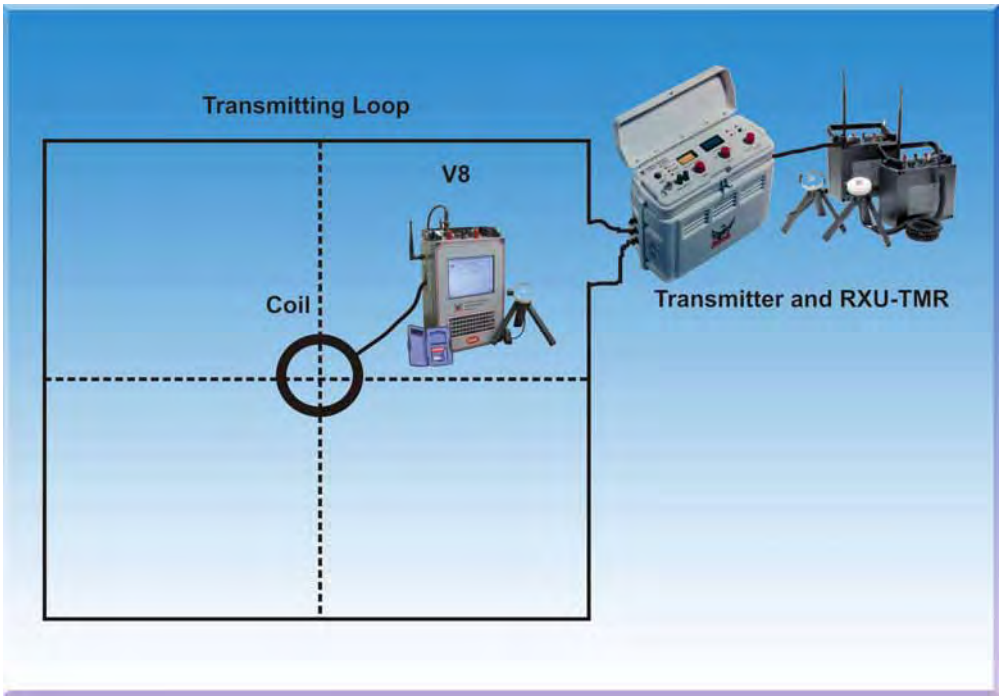

TDEM layout

Fig. 4.4.2-3 MT and TDEM layout Sketches

Table 4.4.2-2 Static Shift values for Kotamobagu and Sokoria MT surveys

Sokoria		
SITE	for Rhoxy	for Rhoyx
MTSC01	-0.066	0.066
MTSC02	0.459	1.029
MTSC03	-0.329	-0.236
MTSC04	-0.352	-0.287
MTSC05	-0.085	0.171
MTSC06	-0.168	-0.077
MTSC07	-0.224	-0.170
MTSC08	-0.473	-0.017
MTSC09	-0.602	-0.099
MTSC10	0.465	0.705
MTSC11	0.519	-0.450
MTSC12	1.084	0.218
MTSC13	-0.494	-0.305
MTSC14	-0.134	-0.119
MTSC15	0.098	0.549
MTSC16	-0.187	-0.061
MTSC17	-0.160	0.291
MTSC18	-0.133	0.053
MTSC19	-0.240	-0.077
MTSC20	-0.115	-0.132
MTSC21	0.042	0.012
MTSC22	0.687	0.585
MTSC23	0.293	0.106
MTSC24	0.496	0.185
MTSC25	-0.037	-0.126
MTSC26	0.459	0.122
MTSC27	0.007	-0.117
MTSC28	-0.079	-0.025
MTSC29	0.025	0.016
MTSC30	0.136	-0.065
MTSC31	0.082	0.336
MTSC32	-0.202	-0.147
MTSC33	0.170	0.197
MTSC34	0.385	0.438
MTSC35	0.670	0.037

Kotamobagu		
SITE	for Rhoxy	for Rhoyx
MTKB01	0.133	-0.026
MTKB02	-0.098	-0.050
MTKB03	0.075	0.000
MTKB04	0.634	0.623
MTKB05	0.008	0.614
MTKB06	-0.002	0.092
MTKB07	0.116	0.163
MTKB08	-0.156	-0.103
MTKB09	0.144	-0.034
MTKB10	-0.137	-0.085
MTKB11	-0.256	-0.159
MTKB12	-0.035	0.009
MTKB13	-0.011	-0.052
MTKB14	-0.064	-0.221
MTKB15	0.611	-0.138
MTKB16	-0.181	0.199
MTKB17	-0.074	-0.035
MTKB18	-0.077	0.068
MTKB19	-0.048	-0.002
MTKB20	0.013	-0.091
MTKB21	-0.035	-0.067
MTKB22	0.010	0.112
MTKB23	-0.269	0.124
MTKB24	-0.114	-0.192
MTKB25	-0.074	-0.093
MTKB26	0.047	-0.075
MTKB27	-0.231	-0.307
MTKB28	0.080	-0.183
MTKB29	-0.044	0.235
MTKB30	0.552	0.724
MTKB31	-0.155	-0.066
MTKB32	-0.104	-0.086
MTKB33	0.266	0.185
MTKB34	-0.135	0.103
MTKB35	-0.143	-0.124

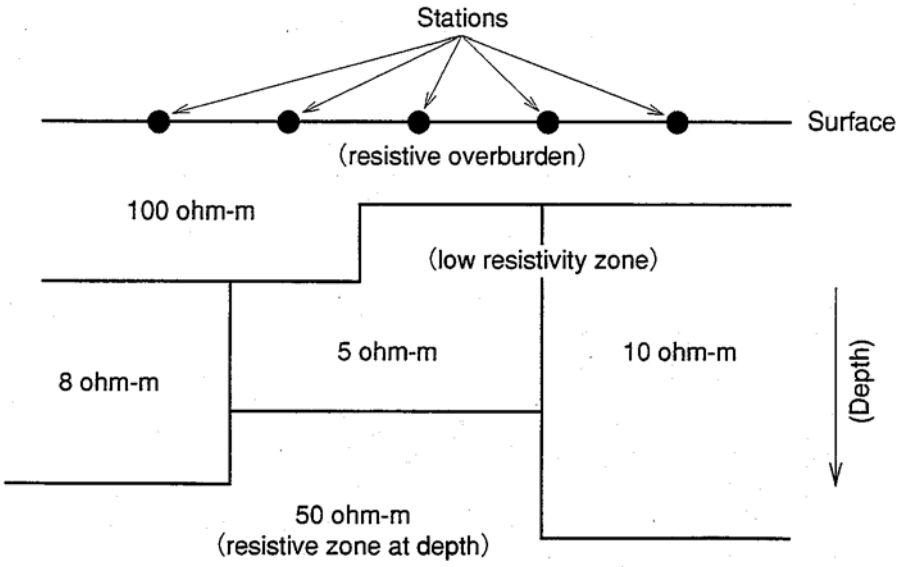

Assuming 2-dimensional resistivity structure.

2-dimensional inversion is carried out with data at several to several tens of stations.

Fig. 4.4.2-4 Conceptual Illustration of 2D Resistivity Modeling

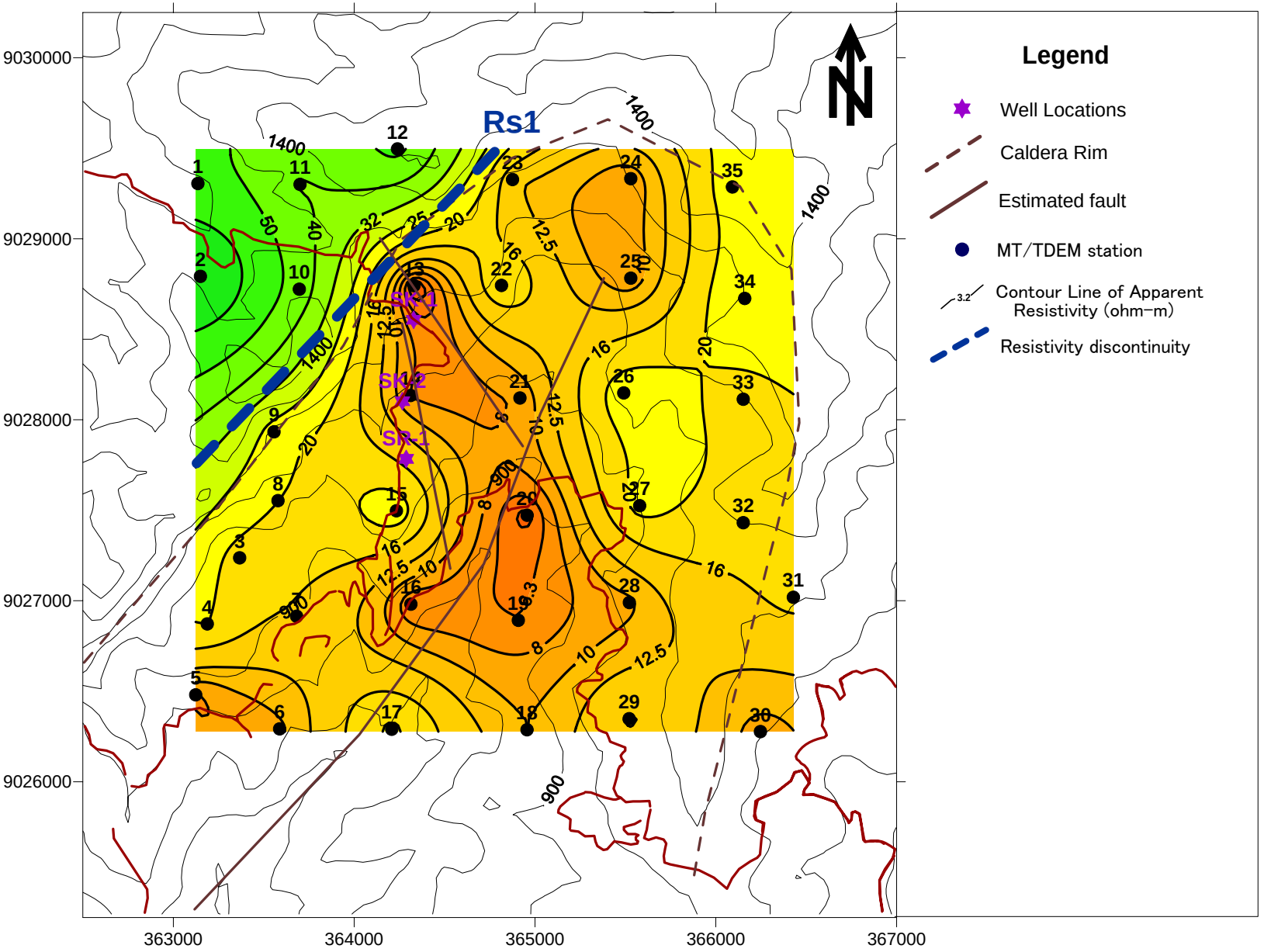

Fig. 4.4.3-1 Apparent Resistivity Map at 100Hz (Sokoria field)

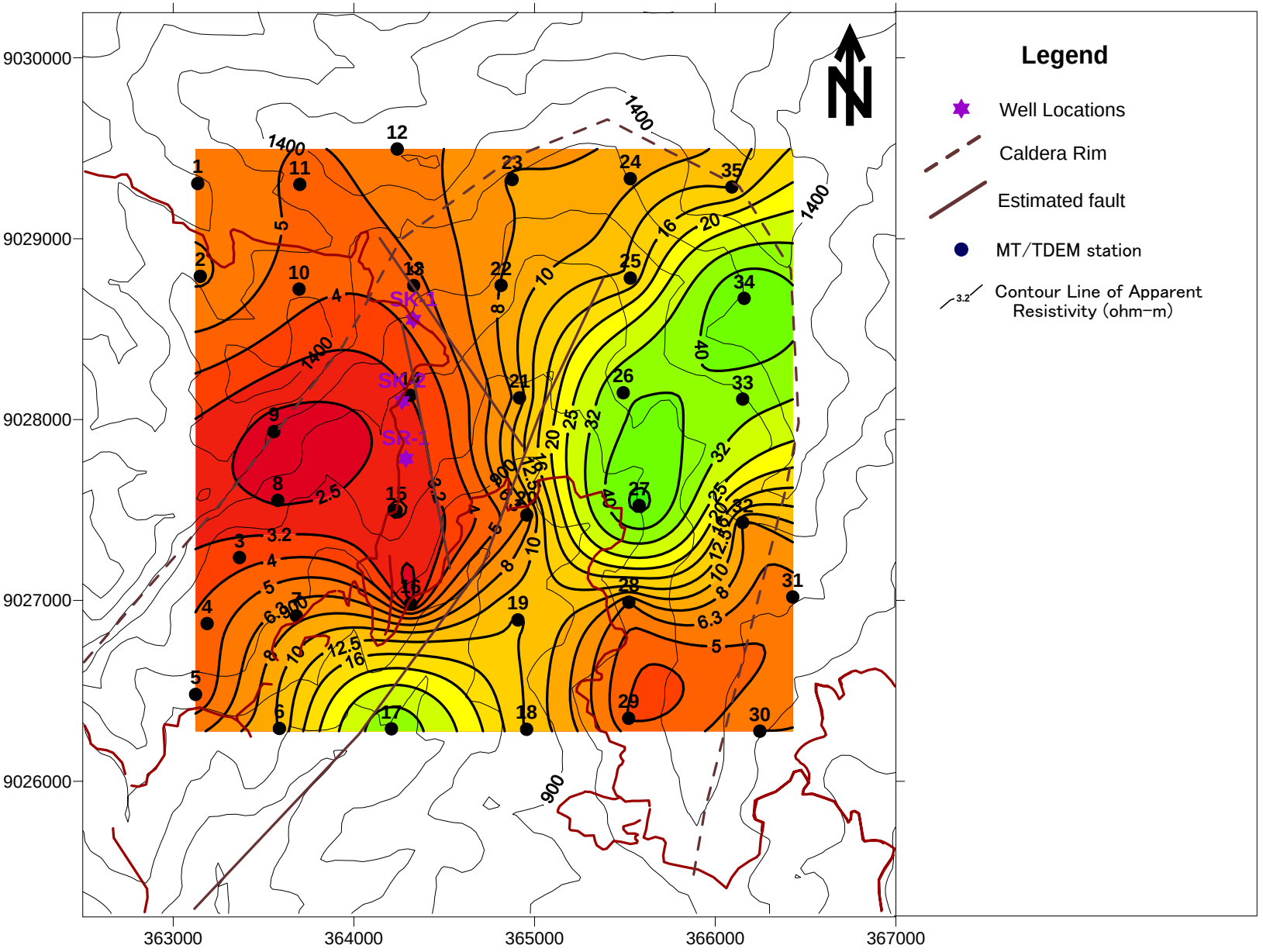

Fig. 4.4.3-2 Apparent Resistivity Map at 1Hz (Sokoria field)

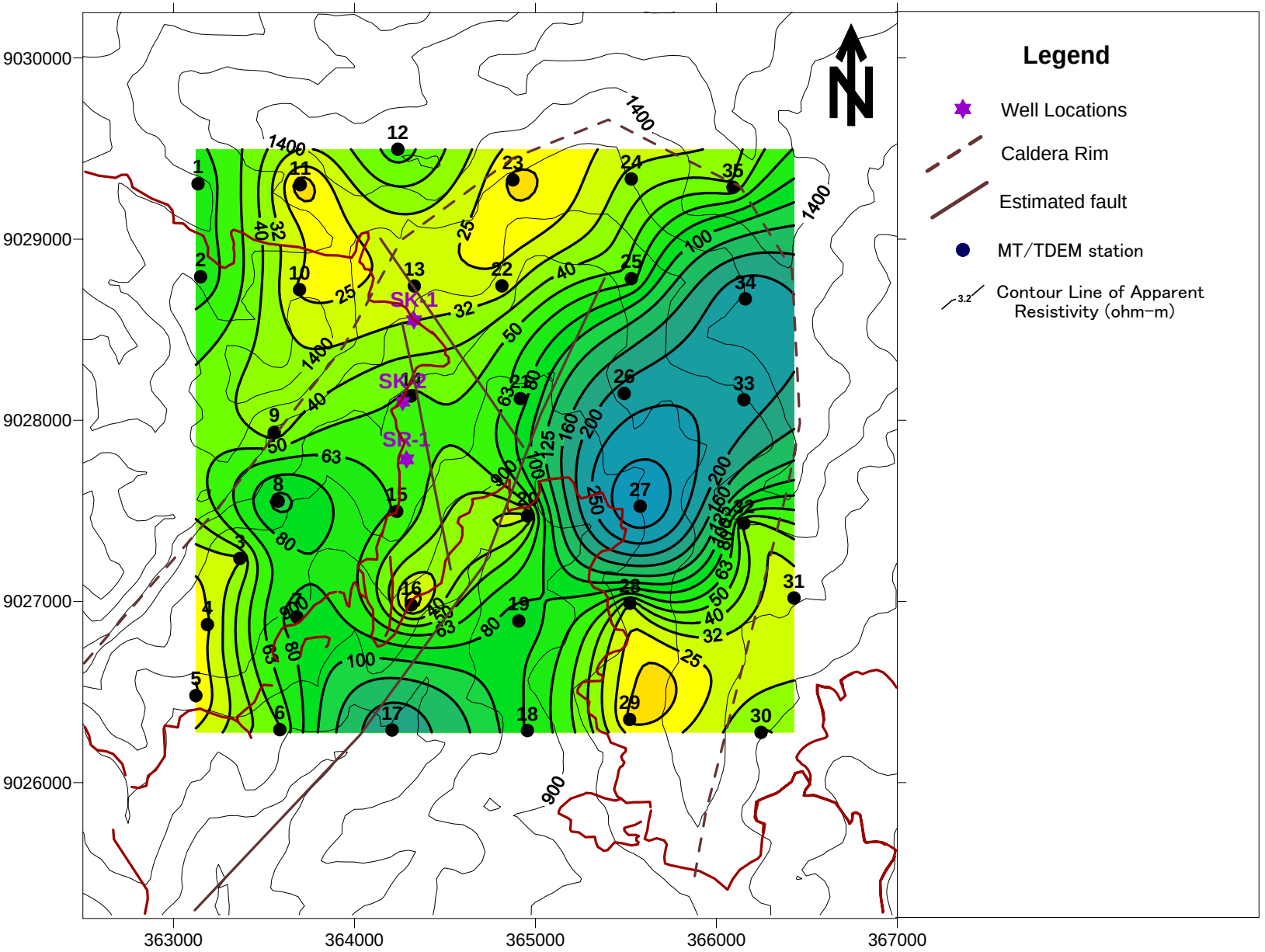

Fig. 4.4.3-3 Apparent Resistivity Map at 0.1Hz (Sokoria field)

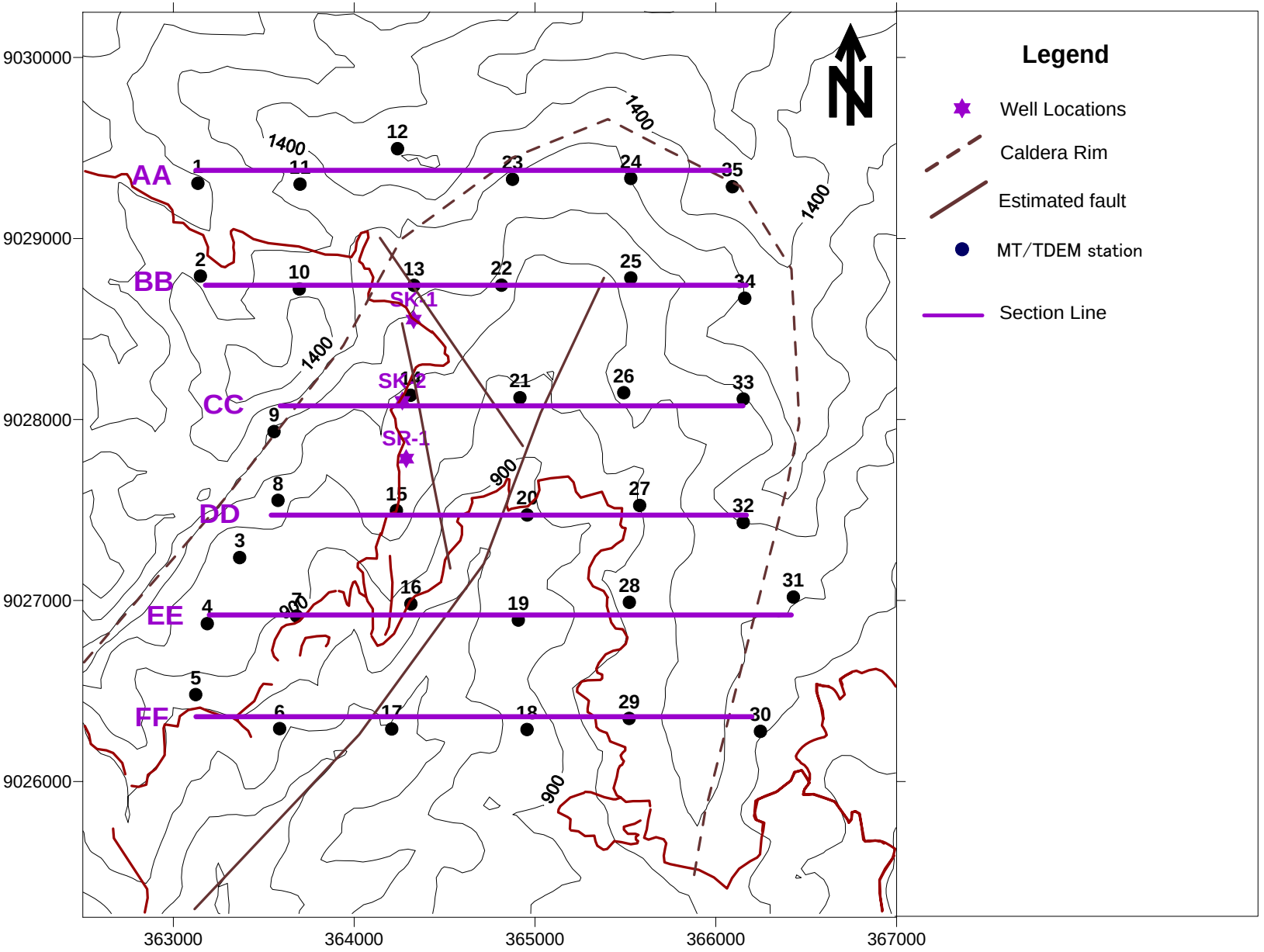

Fig. 4.4.3-4 Location of Section Lines (Sokoria field)

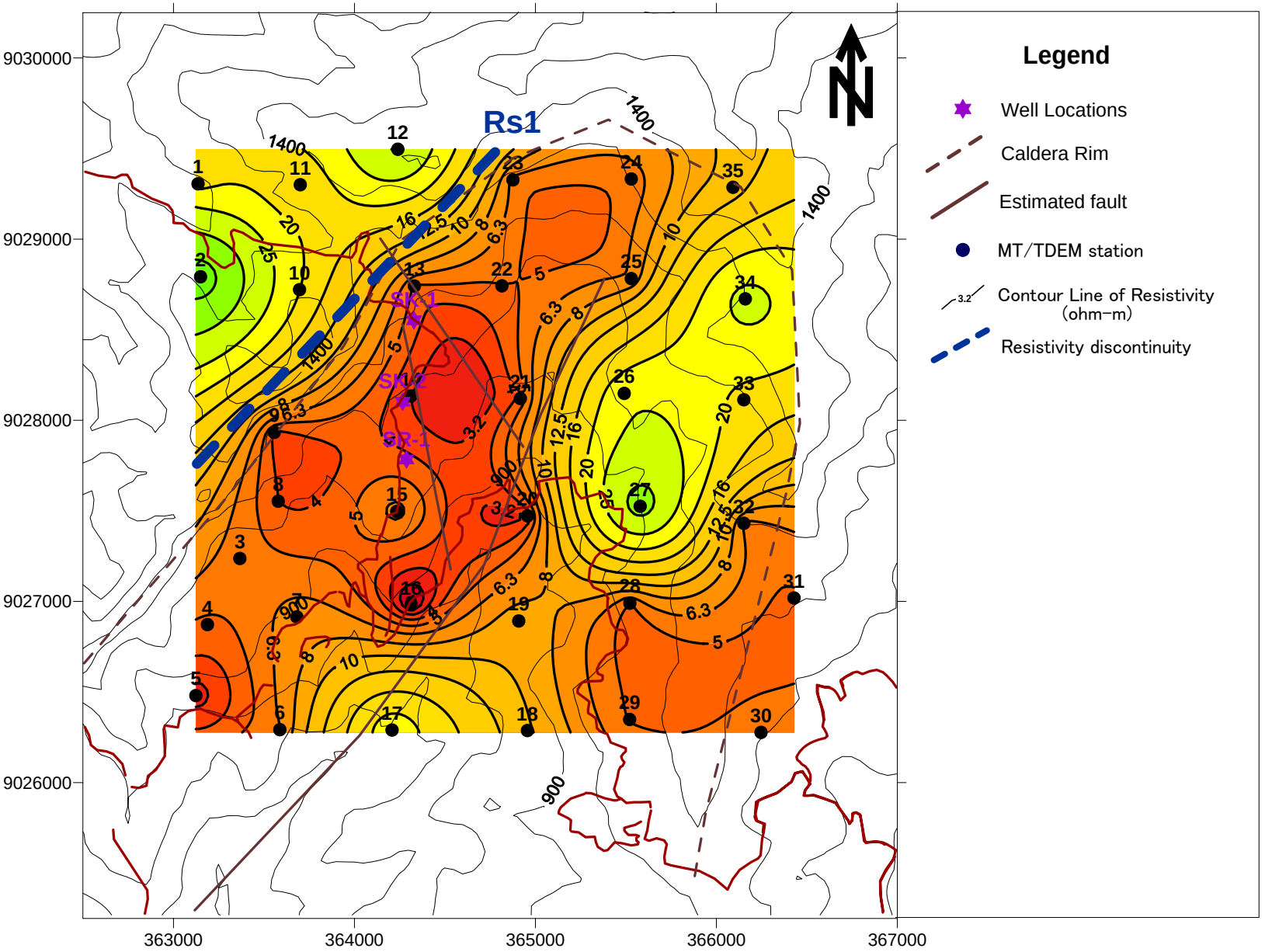

Fig. 4.4.3-5 Resistivity Map at a depth of 200m (Sokoria field)

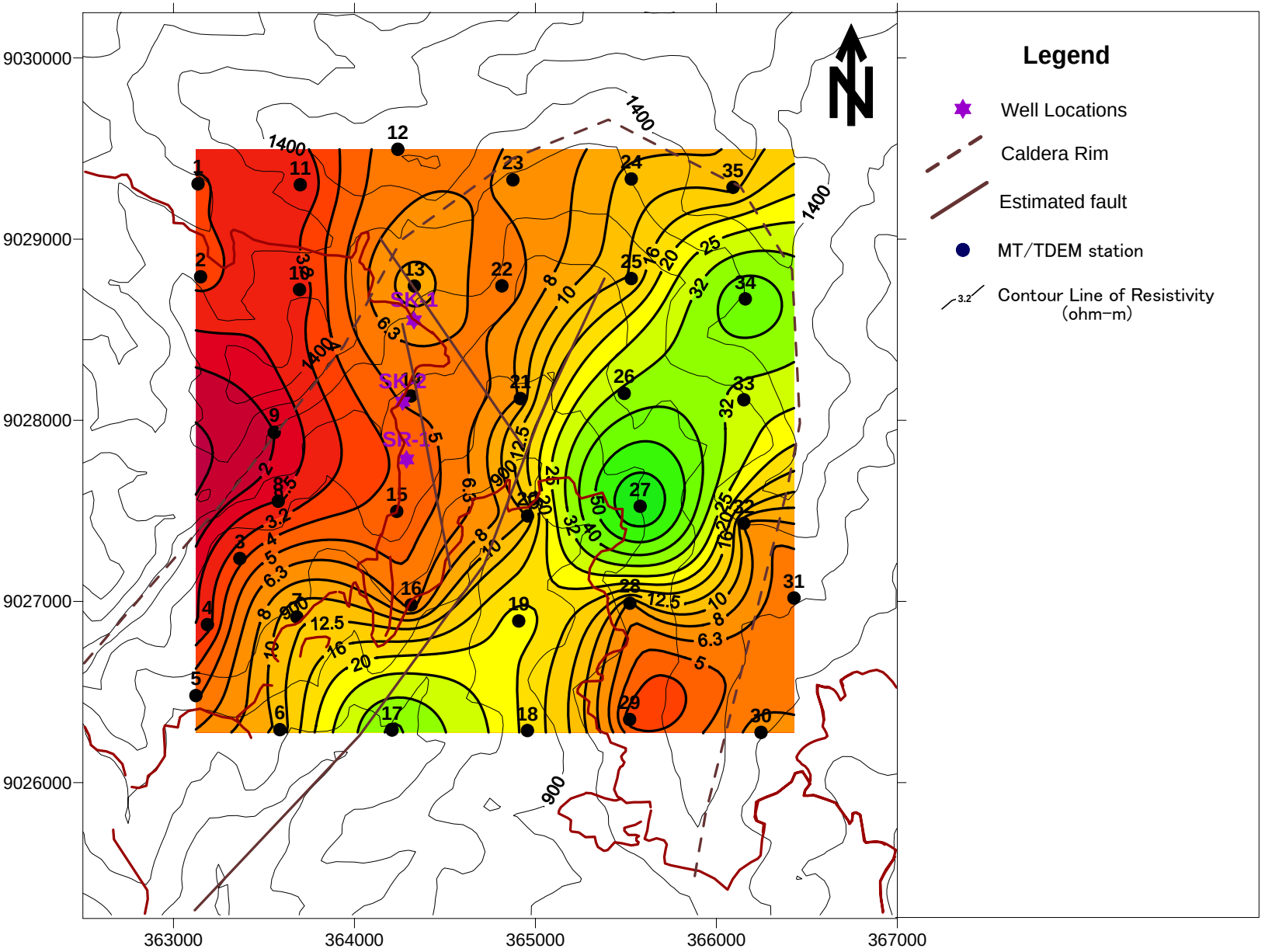

Fig. 4.4.3-6 Resistivity Map at a depth of 500m (Sokoria field)

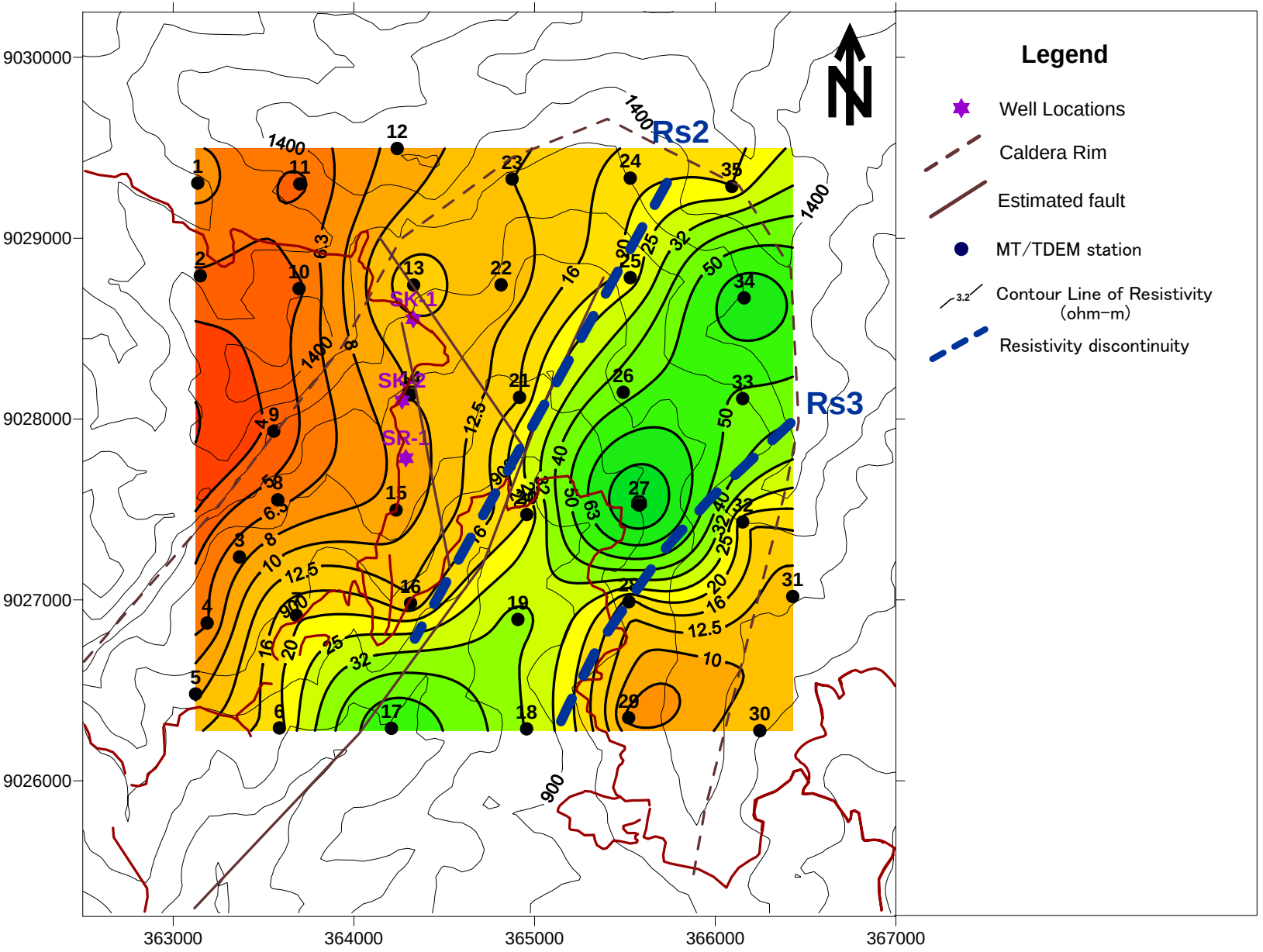

Fig. 4.4.3-7 Resistivity Map at a depth of 750m (Sokoria field)

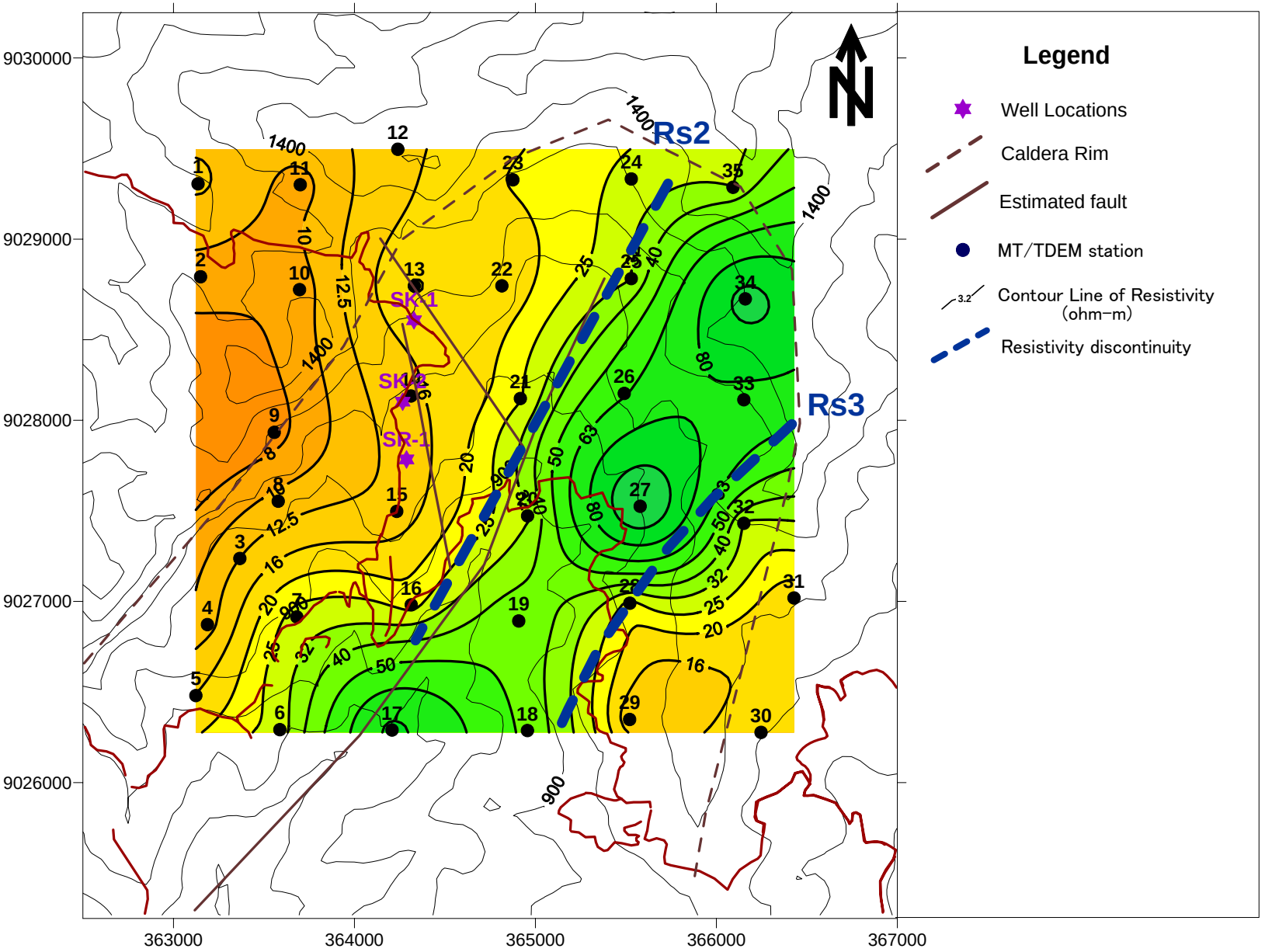

Fig. 4.4.3-8 Resistivity Map at a depth of 1000m (Sokoria field)

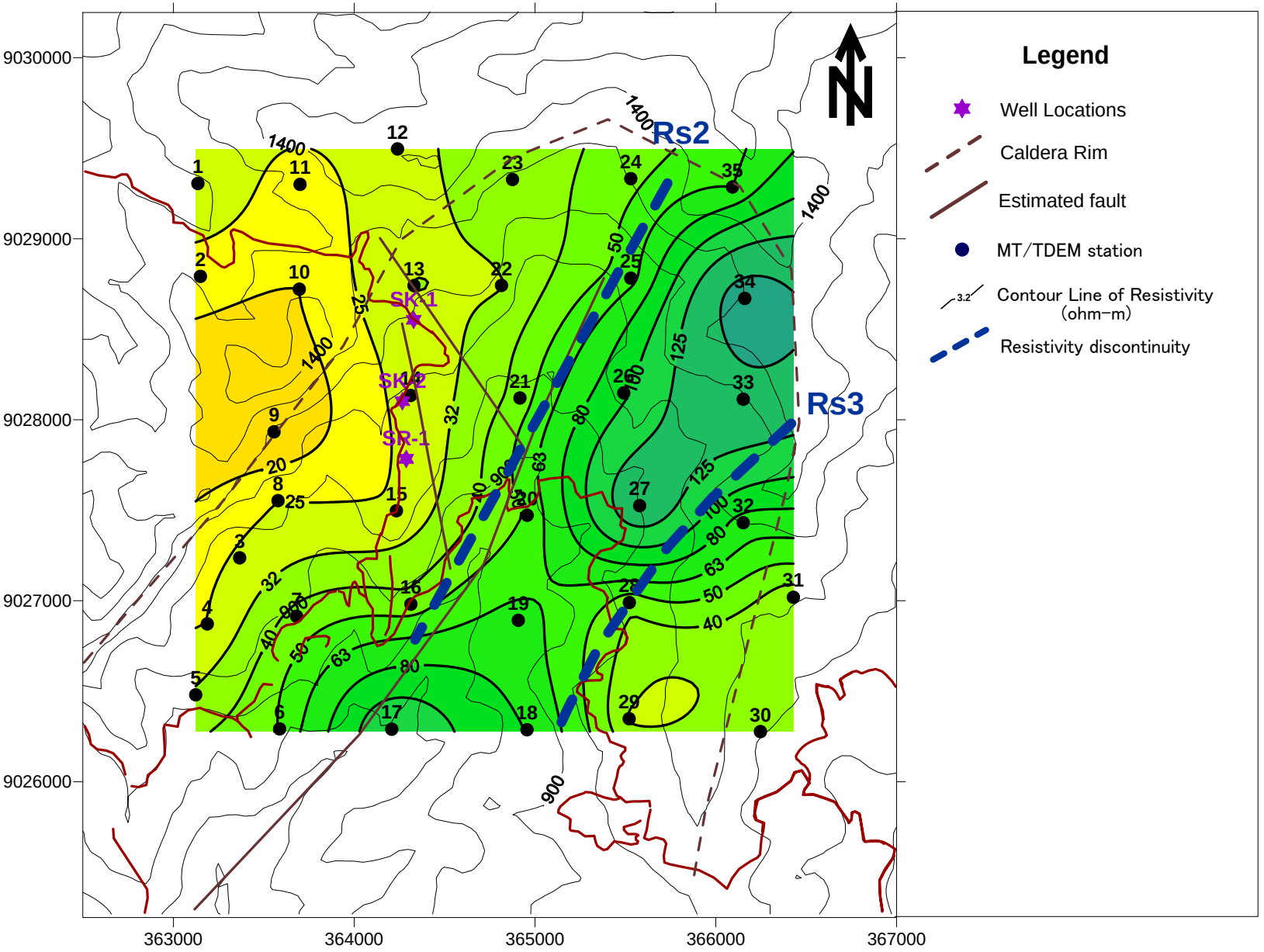

Fig. 4.4.3-9 Resistivity Map at a depth of 1500m (Sokoria field)

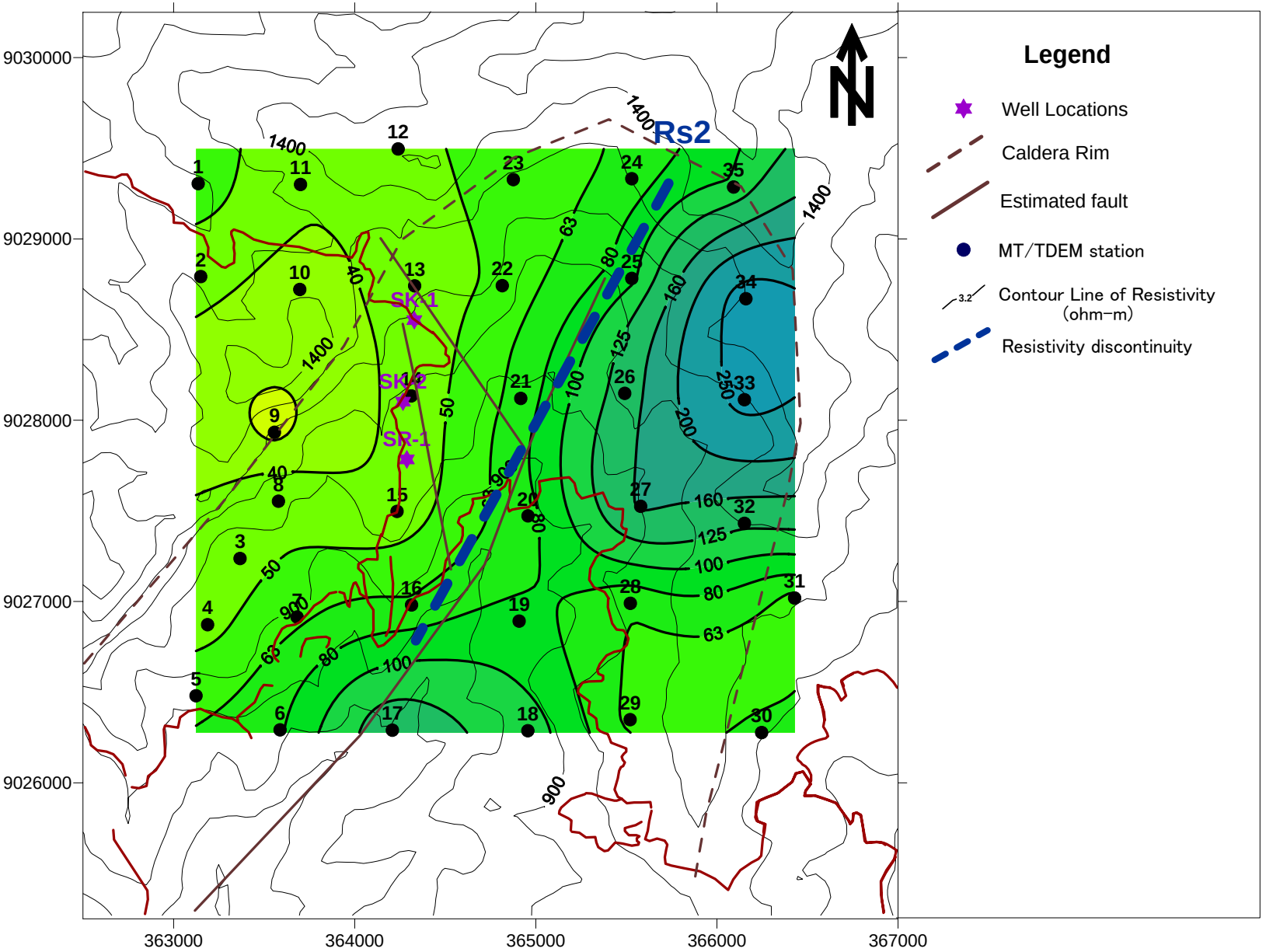

Fig. 4.4.3-10 Resistivity Map at a depth of 2000m (Sokoria field)

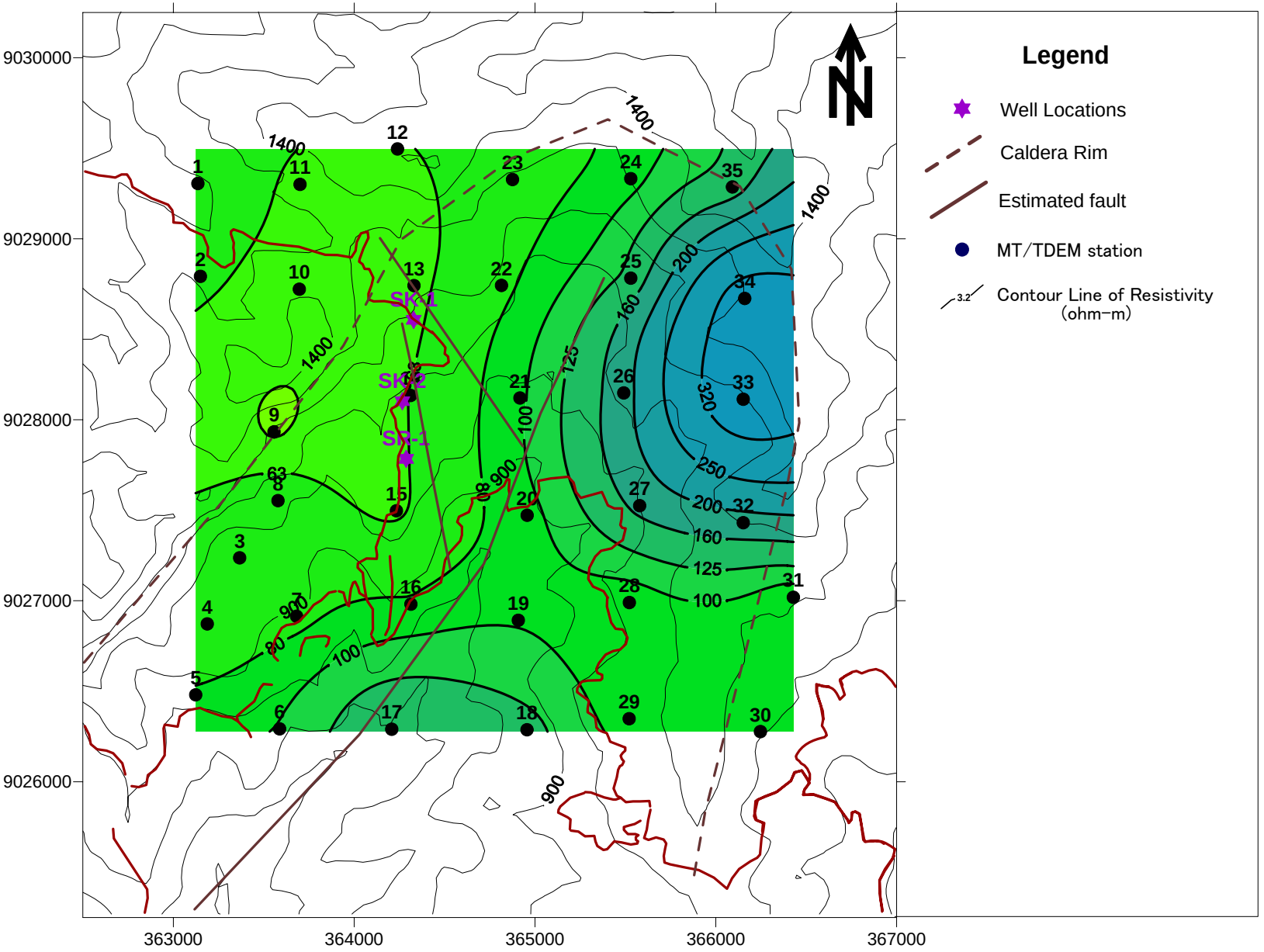

Fig. 4.4.3-11 Resistivity Map at a depth of 2500m (Sokoria field)

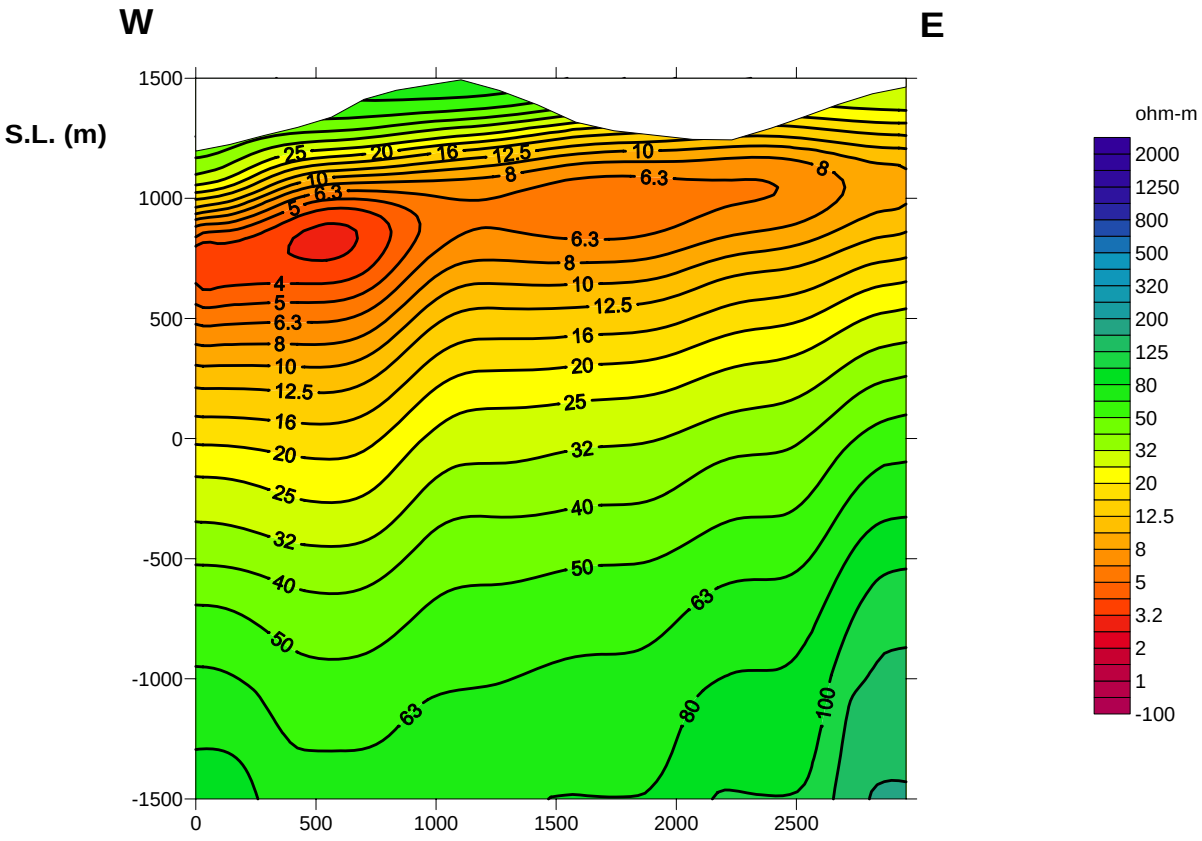

Fig. 4.4.3-12 Resistivity Section Map along line-AA (Sokoria field)

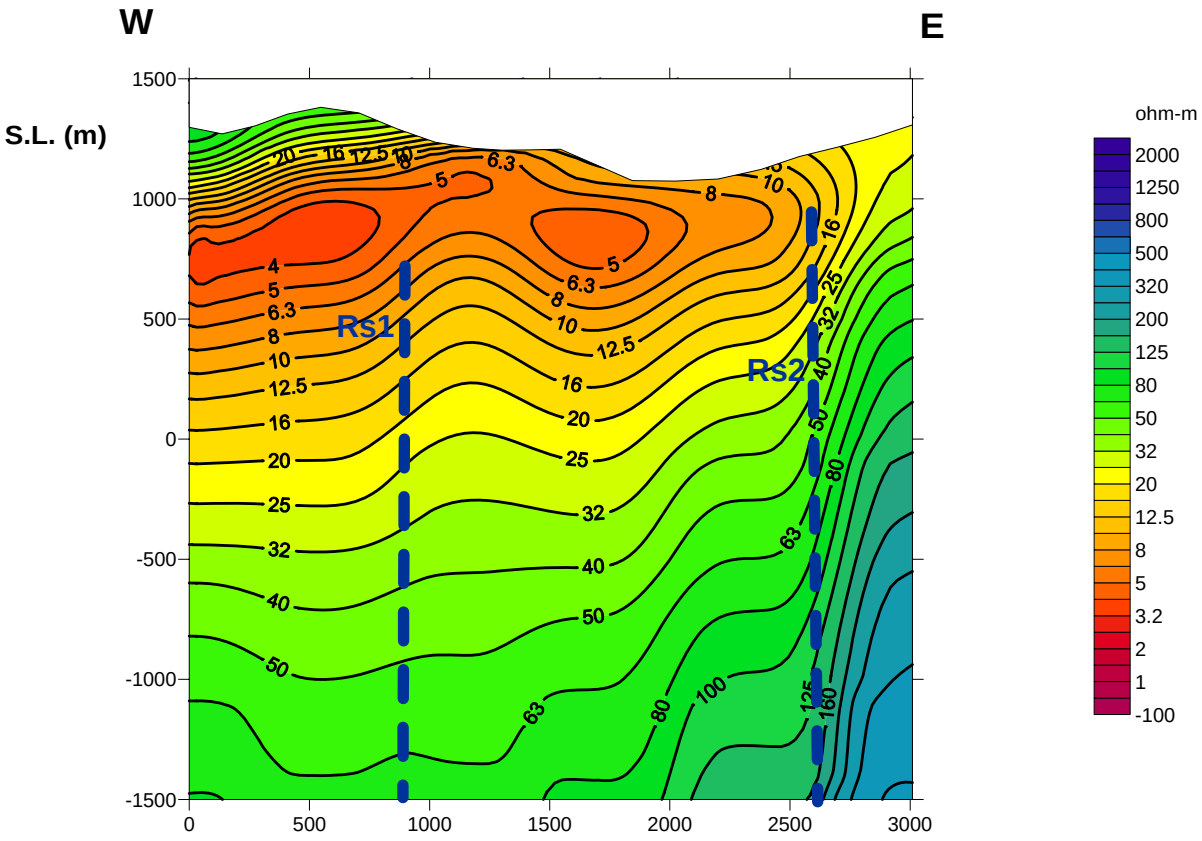

Fig. 4.4.3-13 Resistivity Section Map along line-BB (Sokoria field)

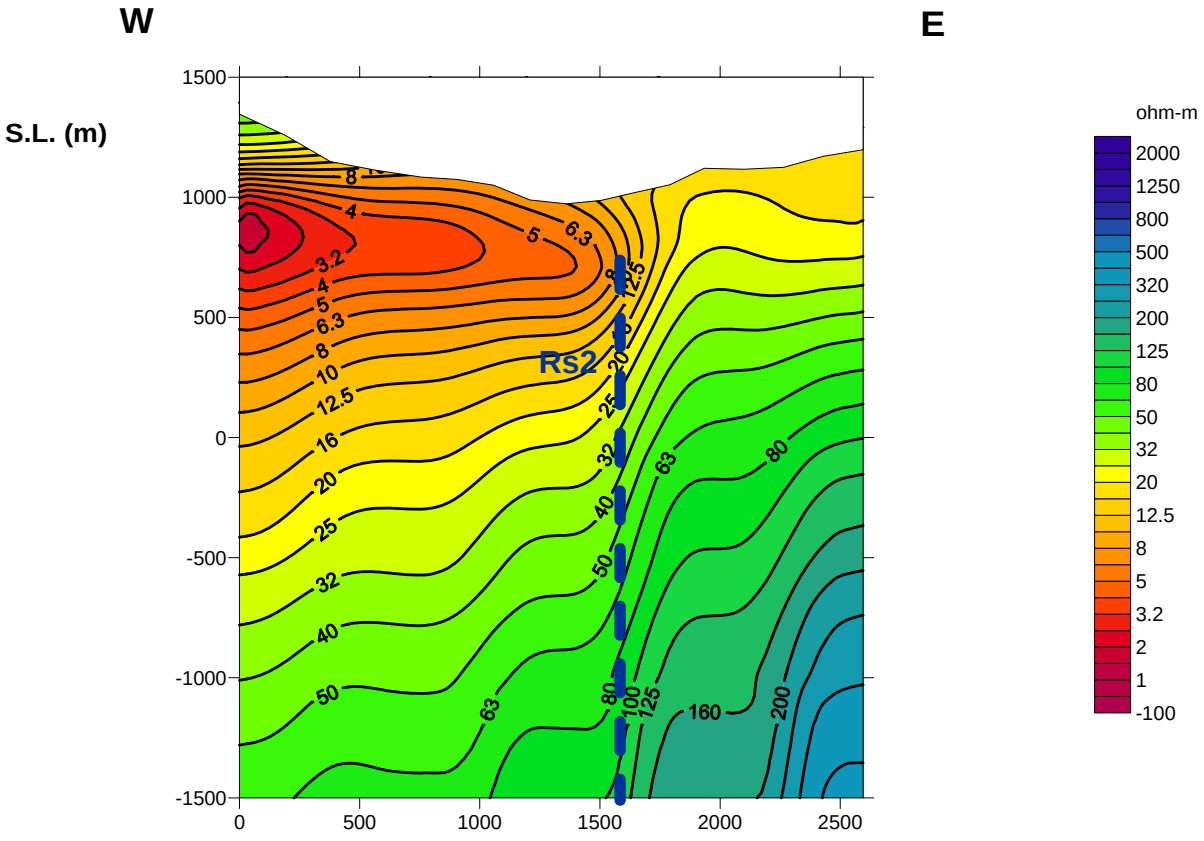

Fig. 4.4.3-14 Resistivity Section Map along line-CC (Sokoria field)

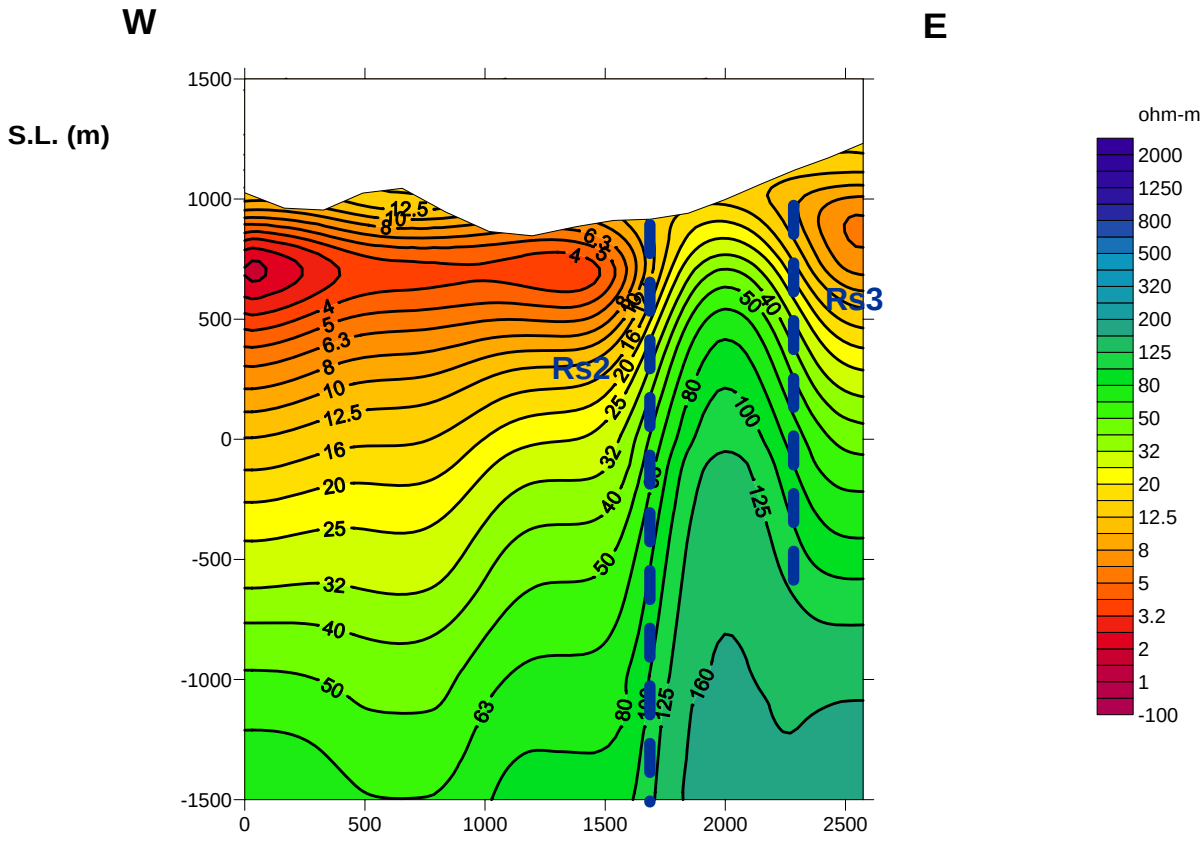

Fig. 4.4.3-15 Resistivity Section Map along line-DD (Sokoria field)

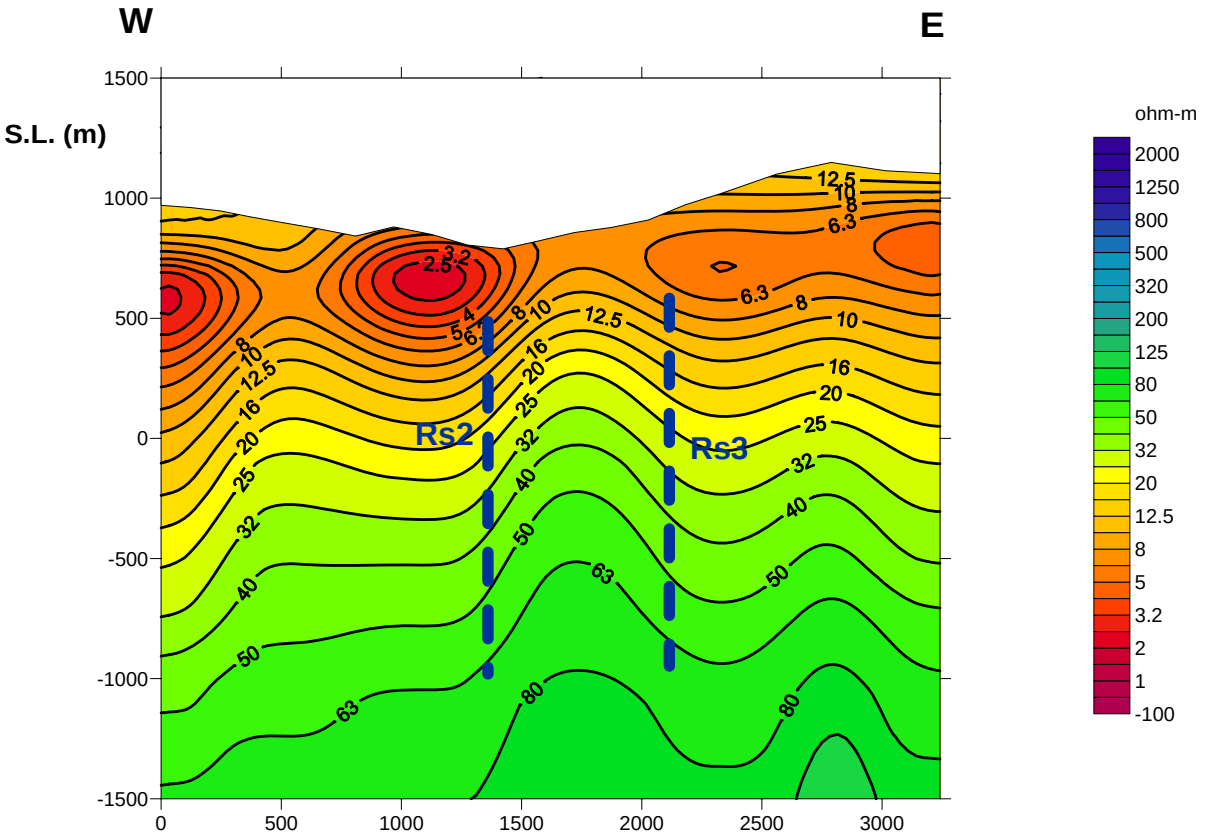

Fig. 4.4.3-16 Resistivity Section Map along line-EE (Sokoria field)

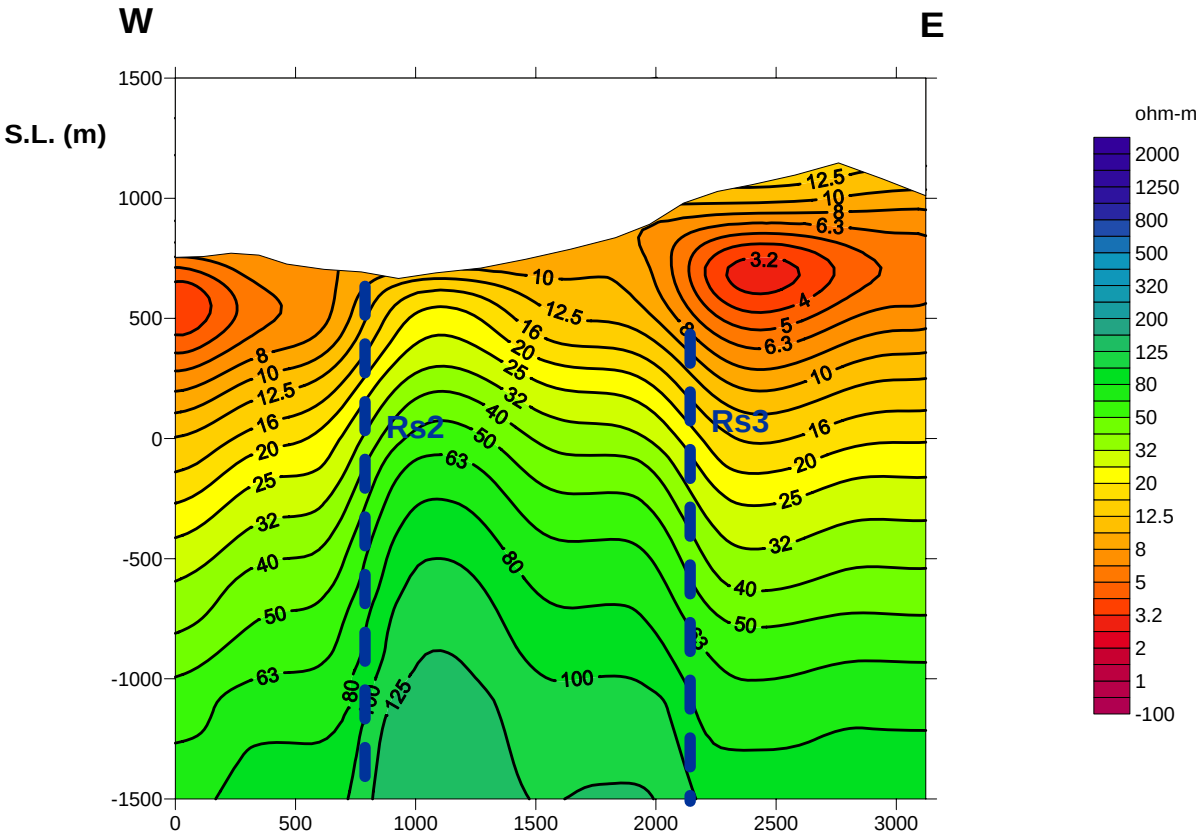

Fig. 4.4.3-17 Resistivity Section Map along line-FF (Sokoria field)

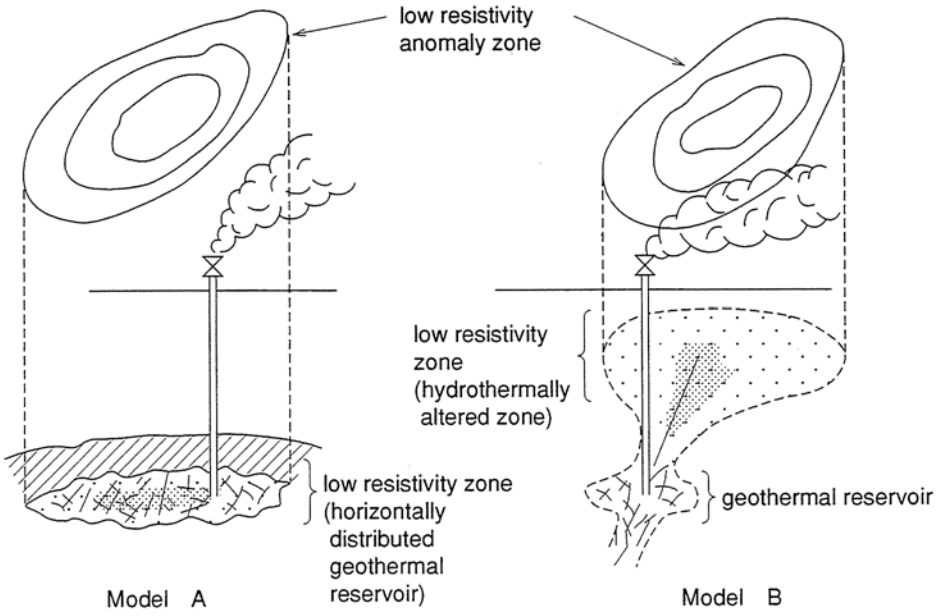

Fig. 4.4.3-18 Conceptual Model of Low Resistivity Zone in Geothermal Field

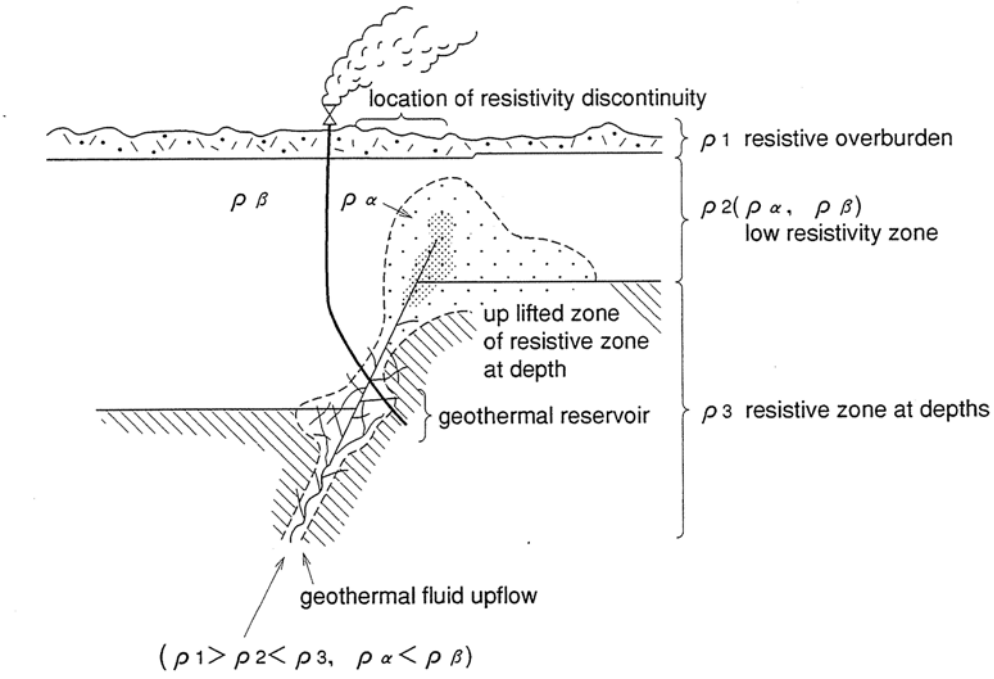

Fig. 4.4.3-19 Conceptual Model of Resistivity Structure in and around Geothermal Reservoir

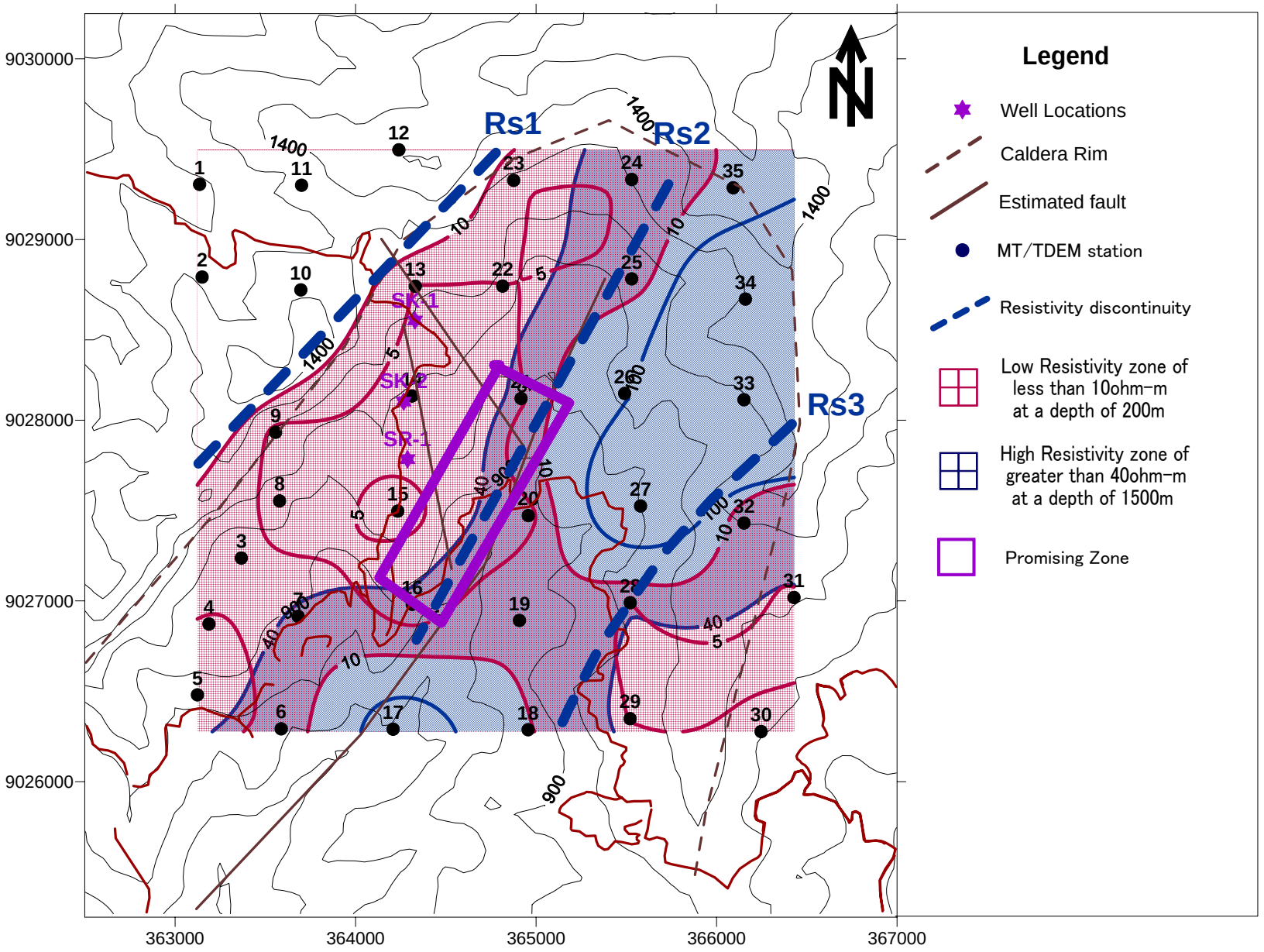

Fig. 4.4.3-20 Synthetic Resistivity Structure Map in the Sokoria geothermal field

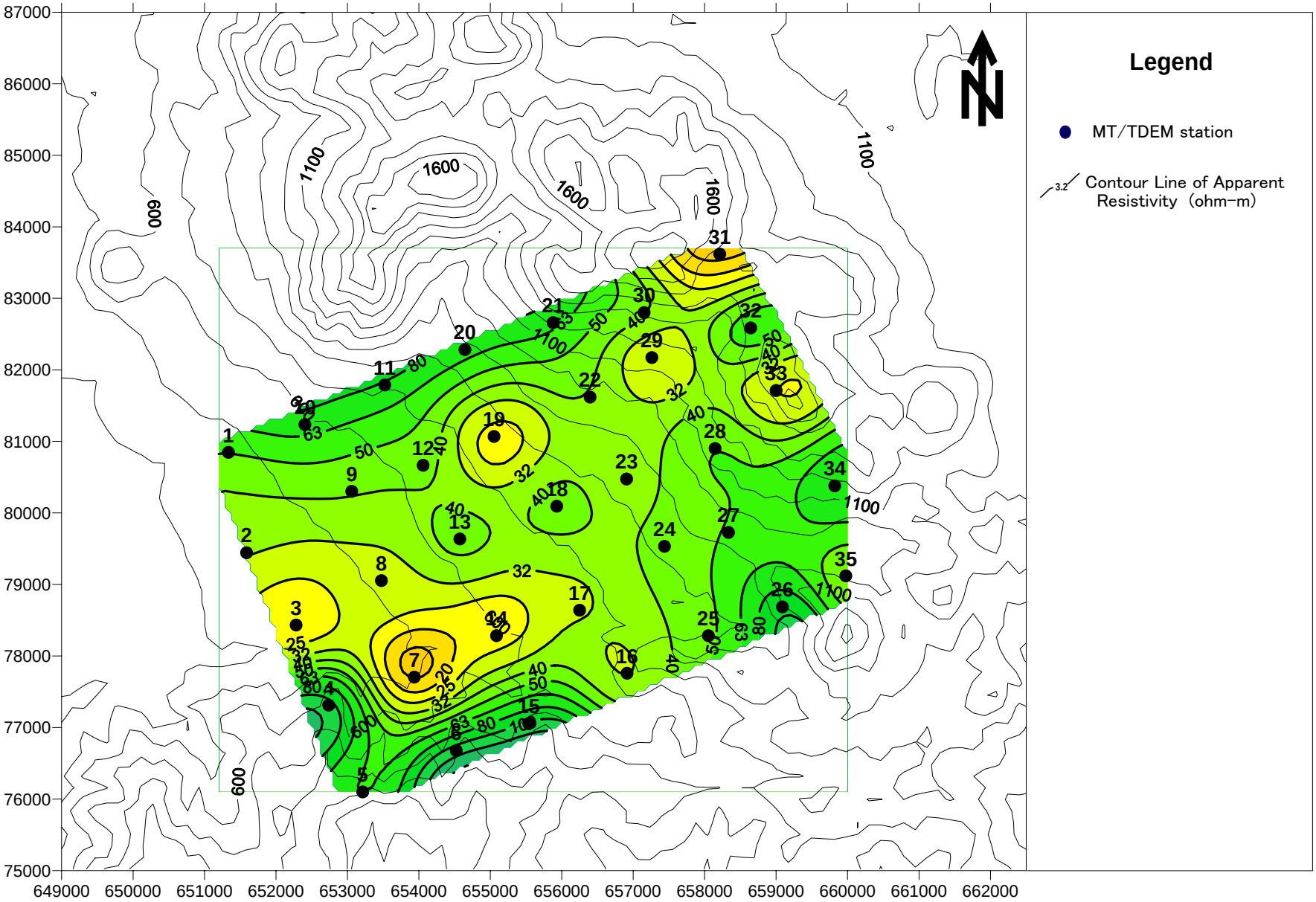

Fig. 4.4.4-1 Apparent Resistivity Map at 100Hz (Kotamobagu field)

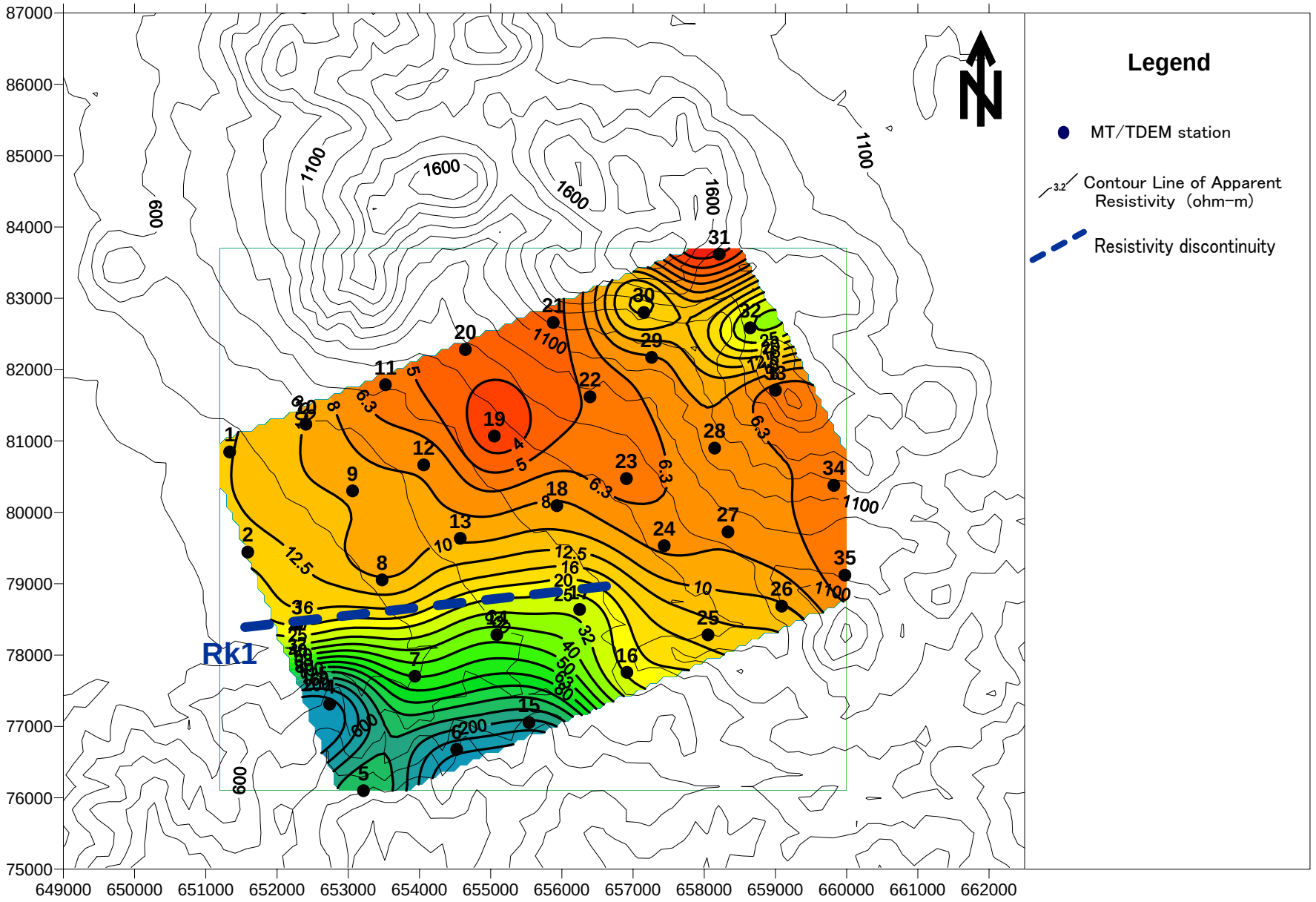

Fig. 4.4.4-2 Apparent Resistivity Map at 1Hz (Kotamobagu field)

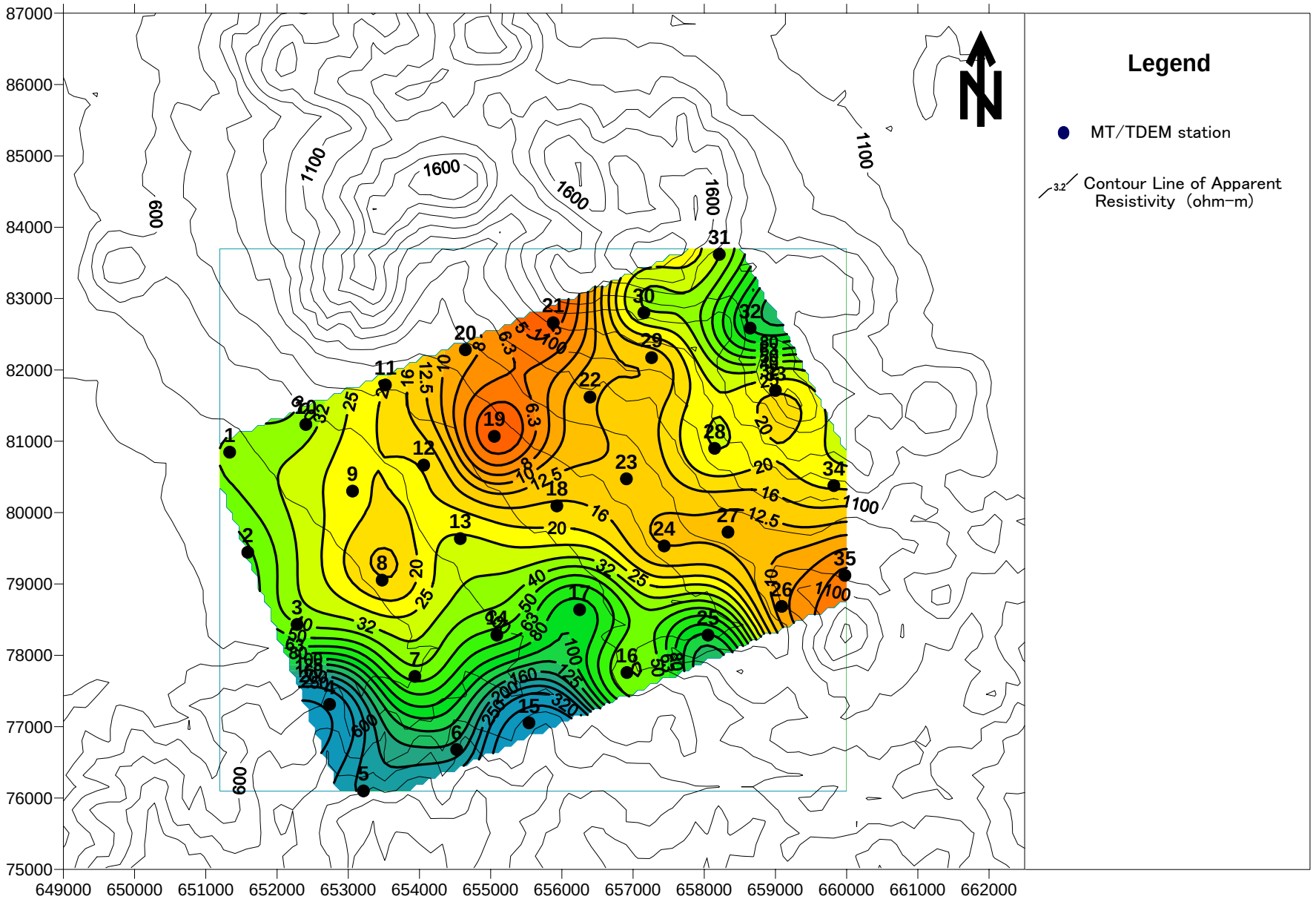

Fig. 4.4.4-3 Apparent Resistivity Map at 0.01Hz (Kotamobagu field)

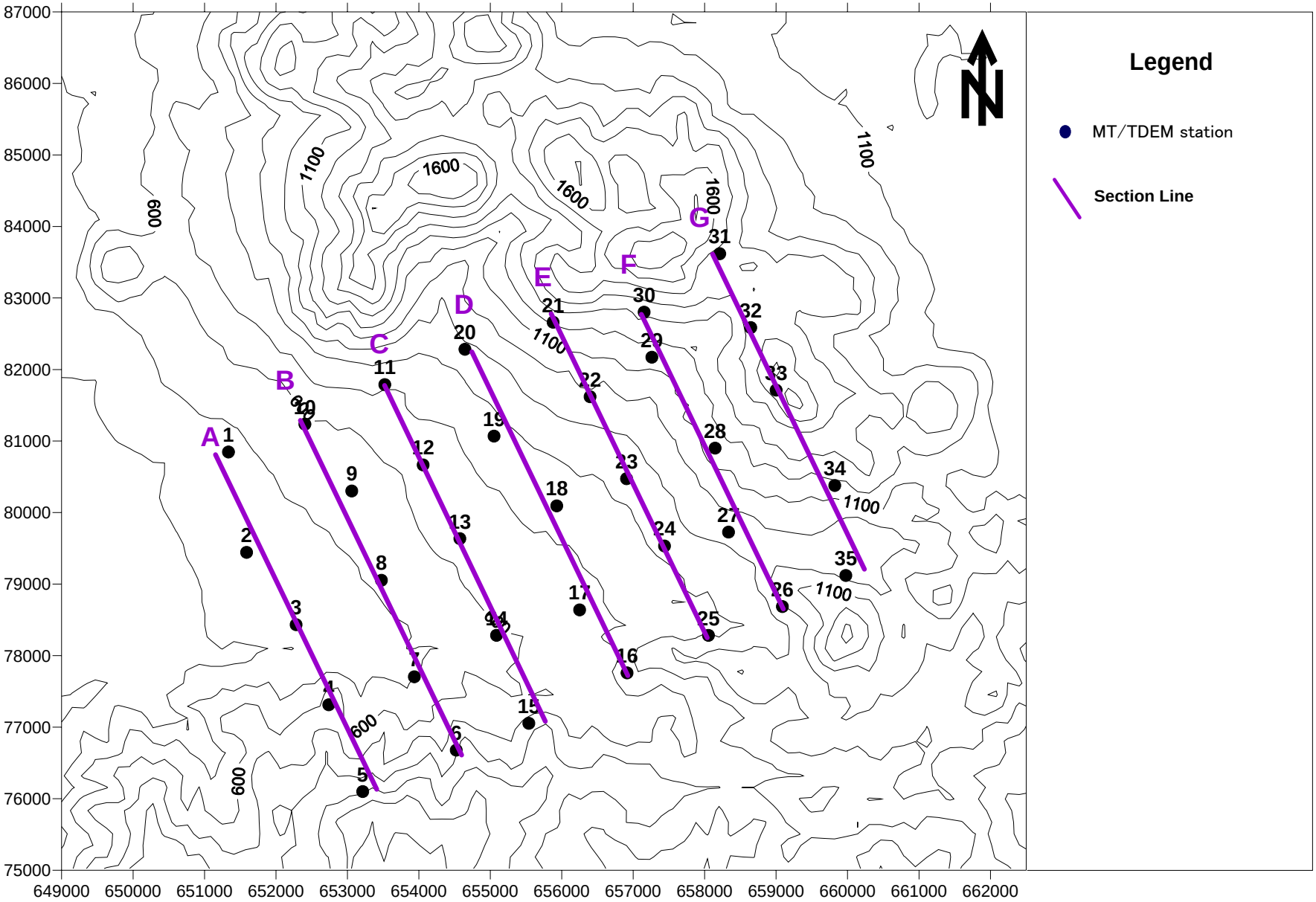

Fig. 4.4.4-4 Location of Section Lines (Kotamobagu field)

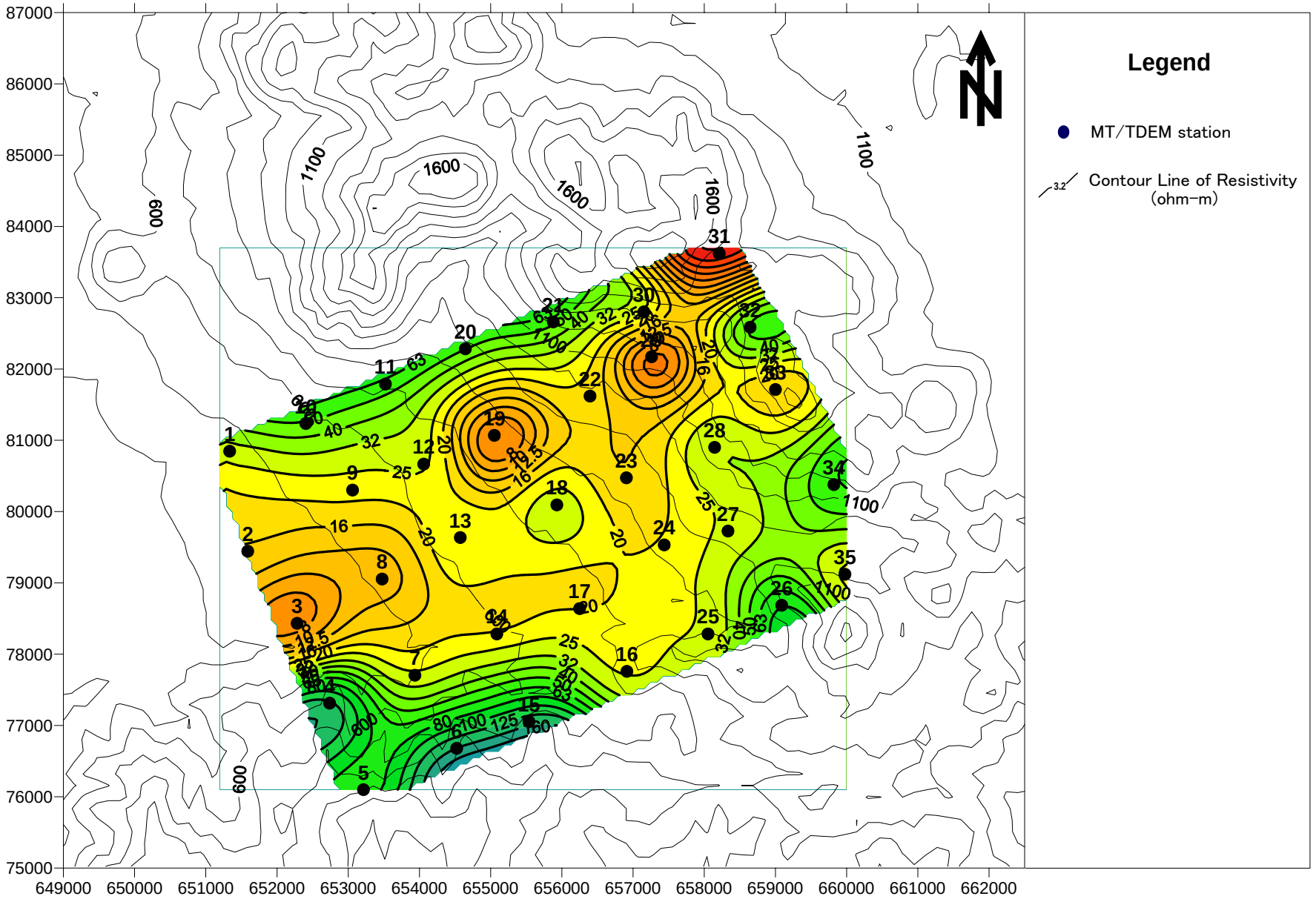

Fig. 4.4.4-5 Resistivity Map at a depth of 200m (Kotamobagu field)

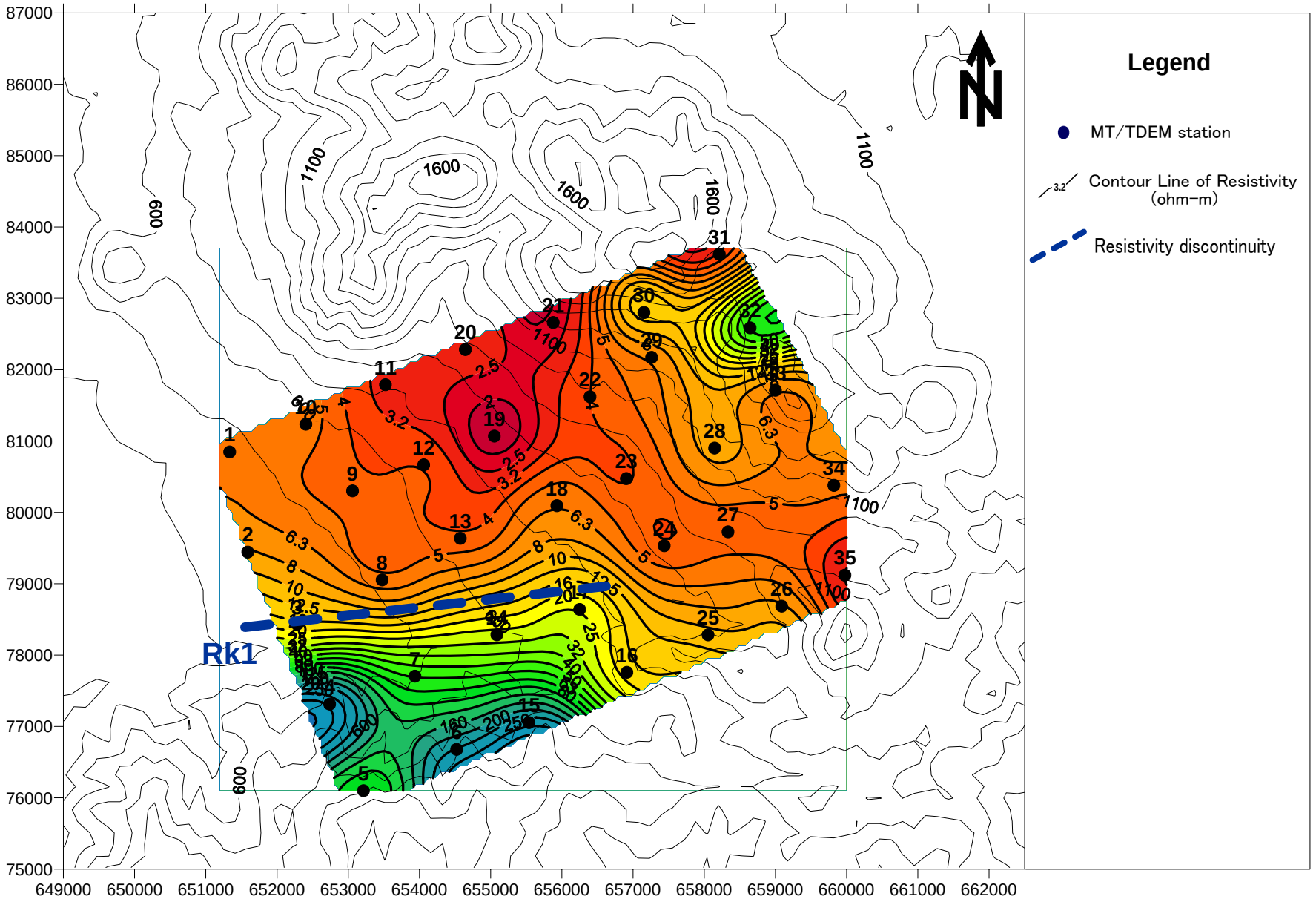

Fig. 4.4.4-6 Resistivity Map at a depth of 500m (Kotamobagu field)

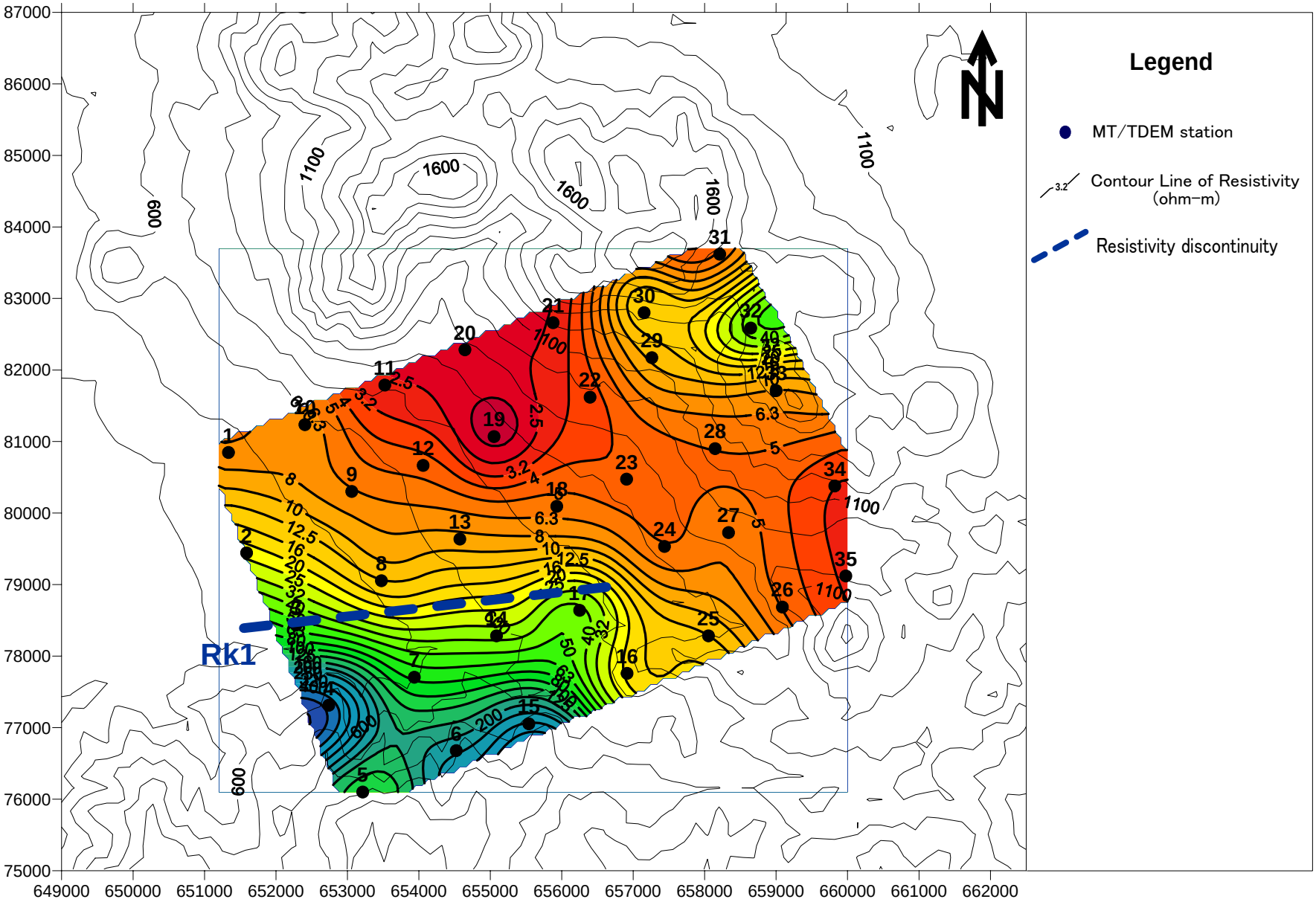

Fig. 4.4.4-7 Resistivity Map at a depth of 750m (Kotamobagu field)

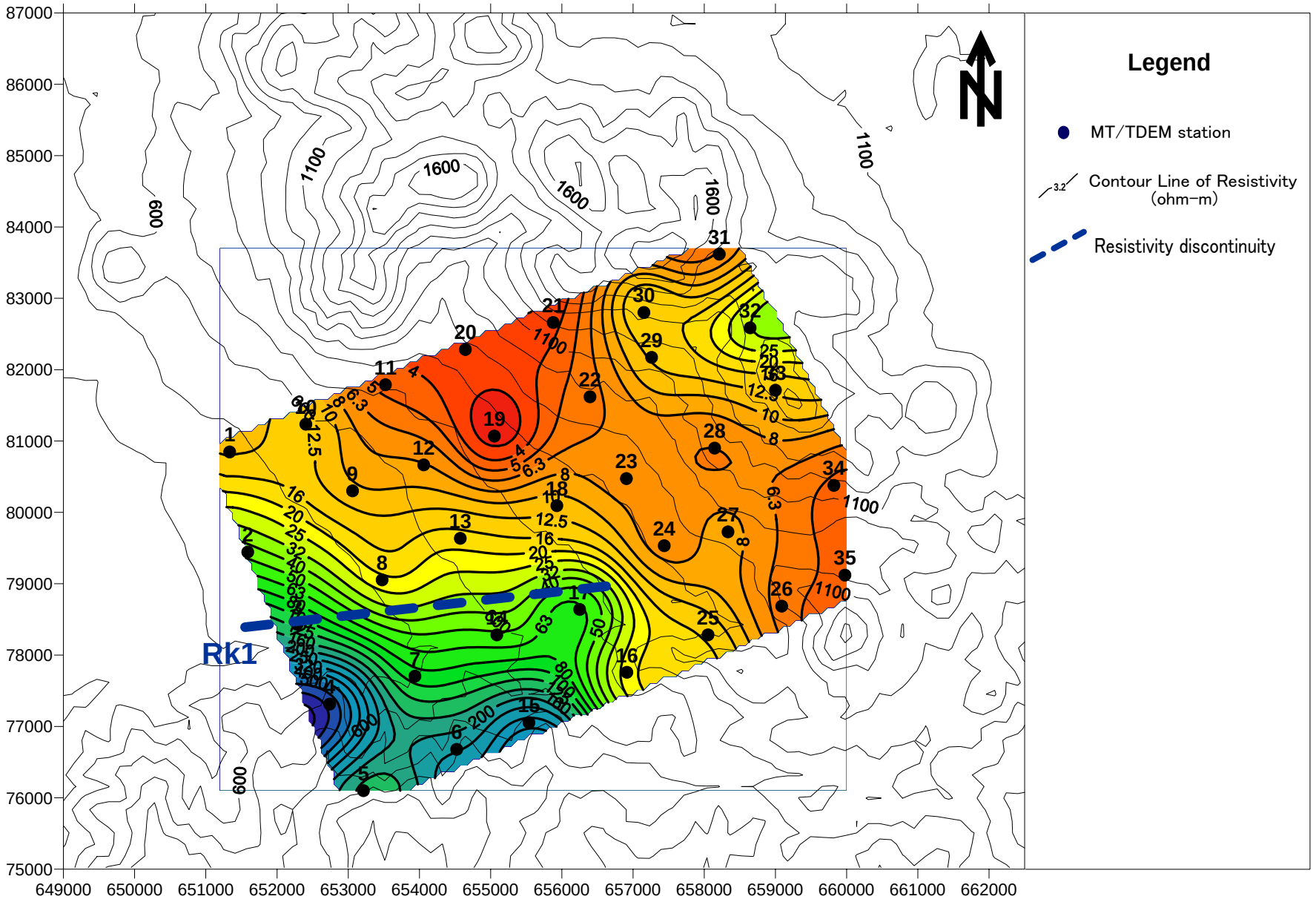

Fig. 4.4.4-8 Resistivity Map at a depth of 1000m (Kotamobagu field)

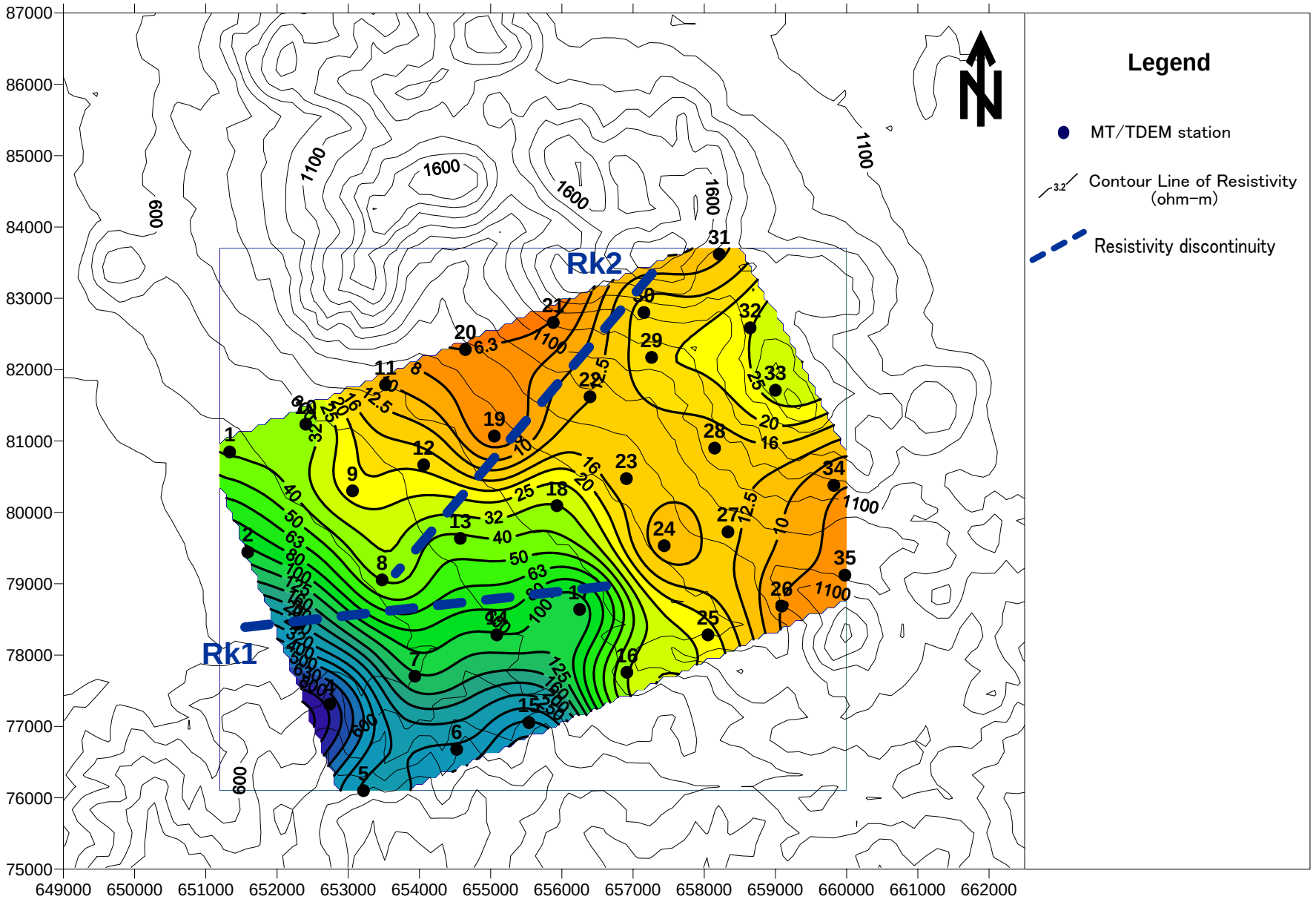

Fig. 4.4.4-9 Resistivity Map at a depth of 1500m (Kotamobagu field)

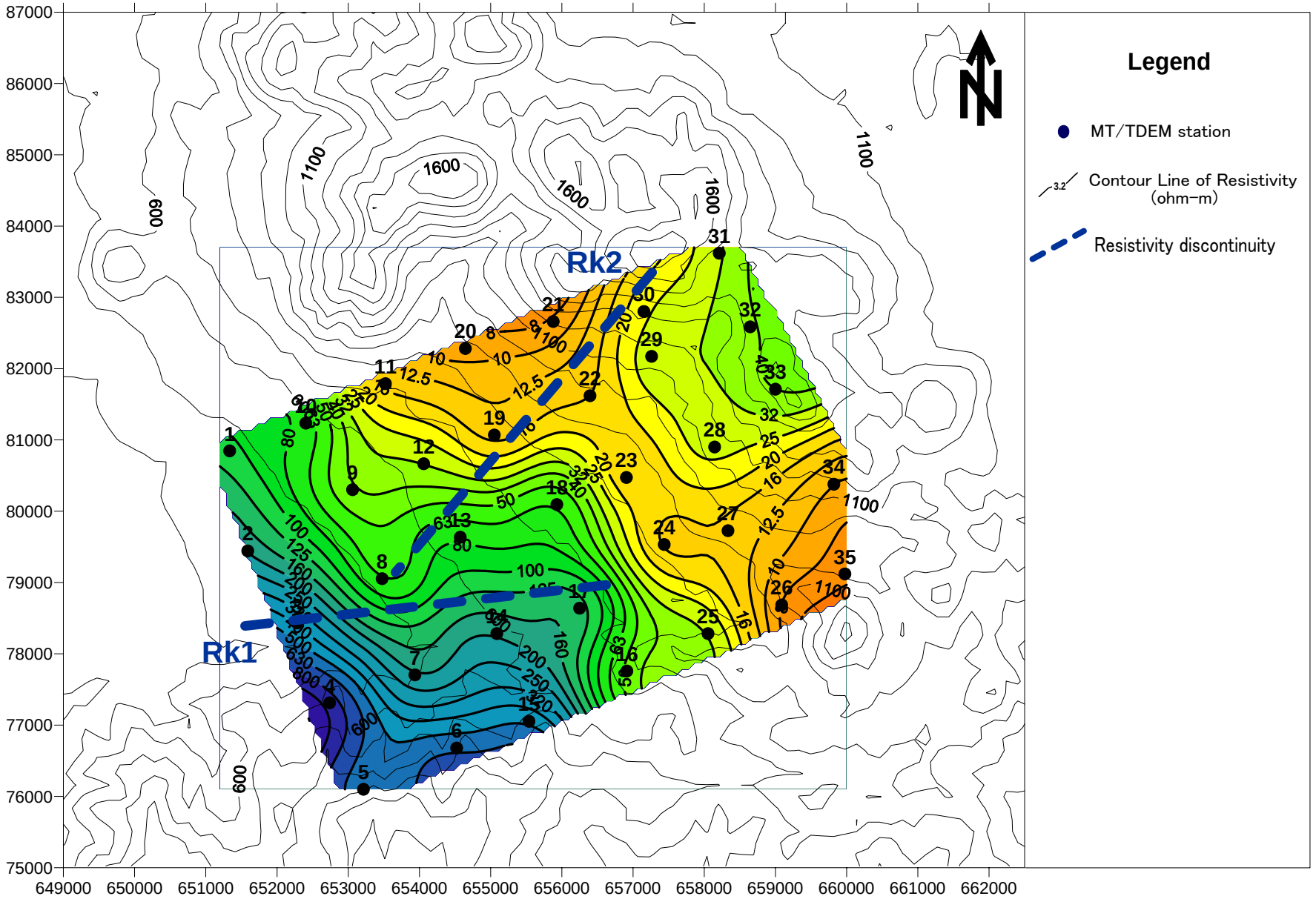

Fig. 4.4.4-10 Resistivity Map at a depth of 2000m (Kotamobagu field)

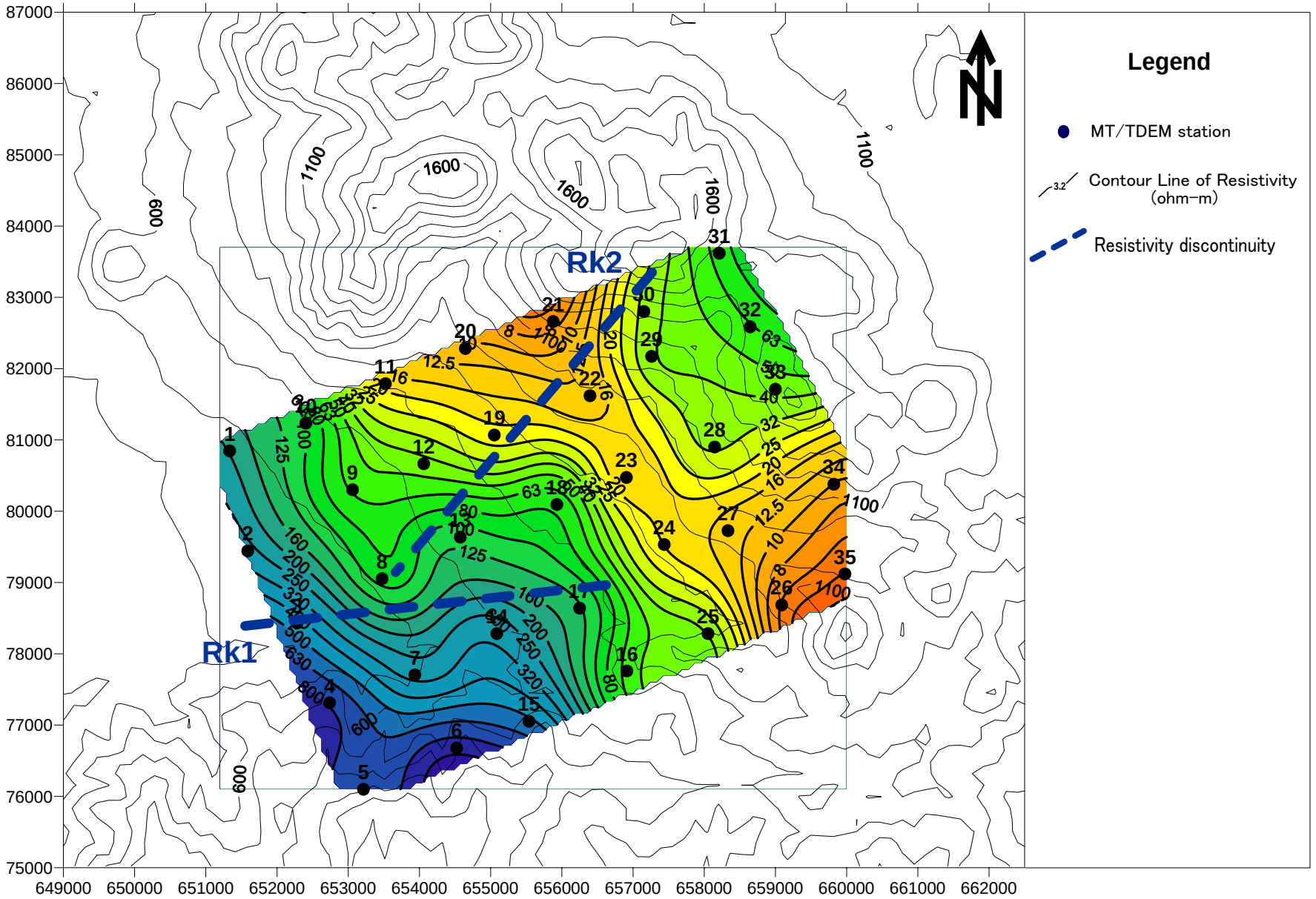

Fig. 4.4.4-11 Resistivity Map at a depth of 2500m (Kotamobagu field)

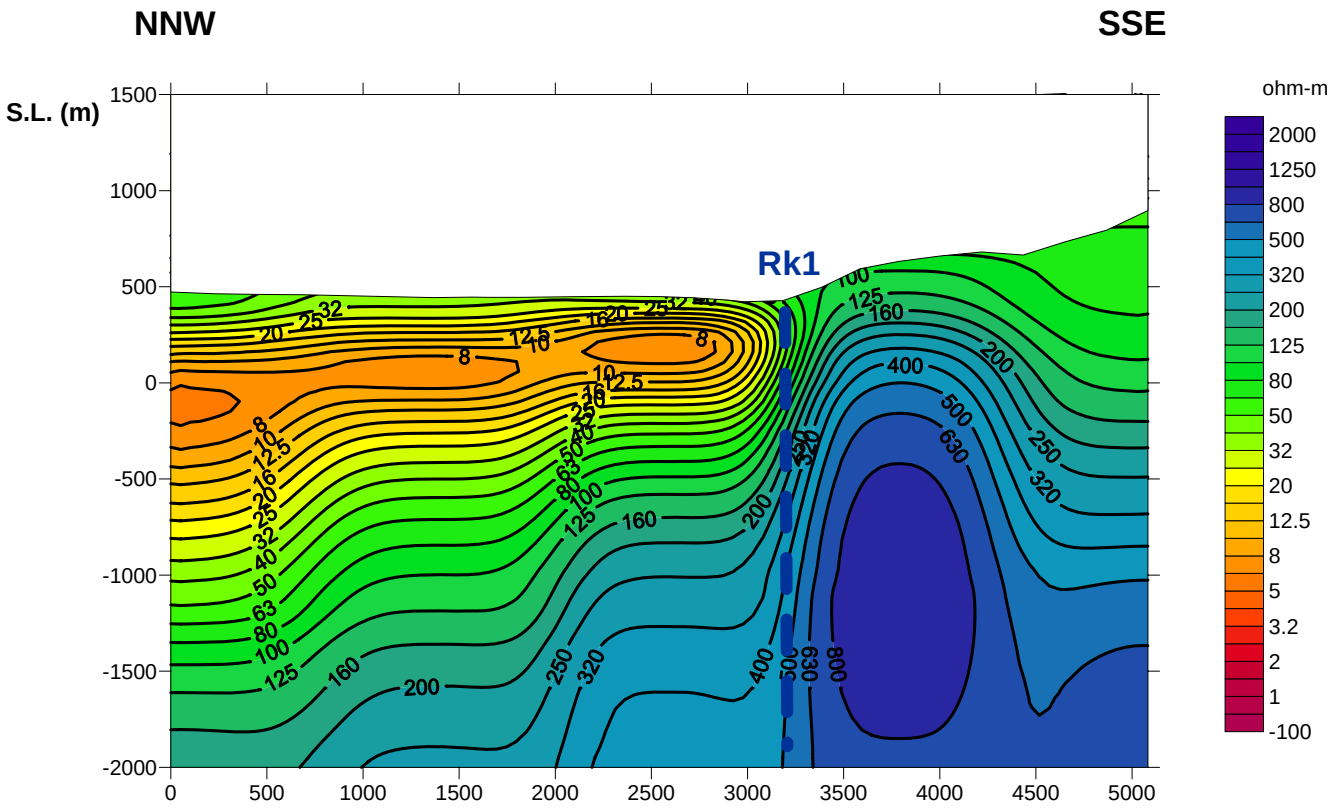

Fig. 4.4.4-12 Resistivity Section Map along line-A (Kotamobagu field)

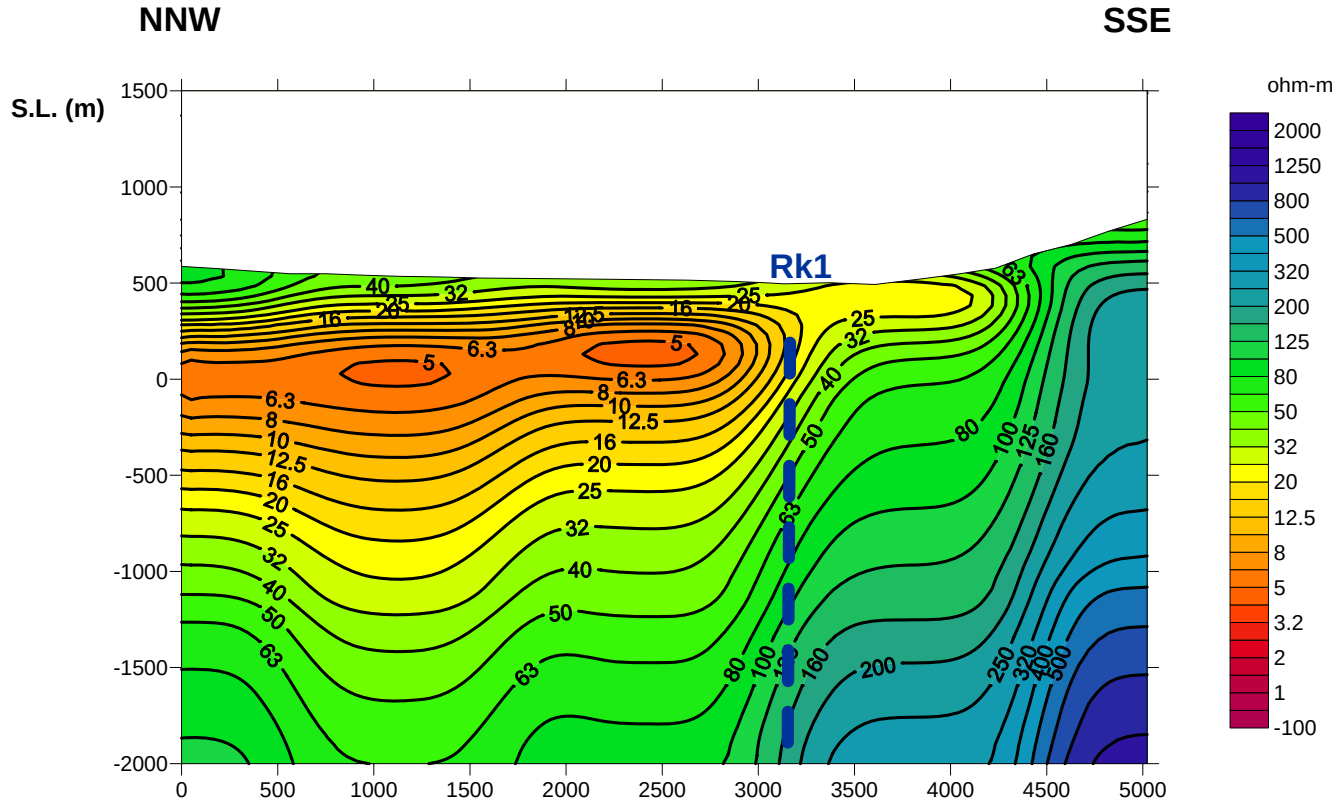

Fig. 4.4.4-13 Resistivity Section Map along line-B (Kotamobagu field)

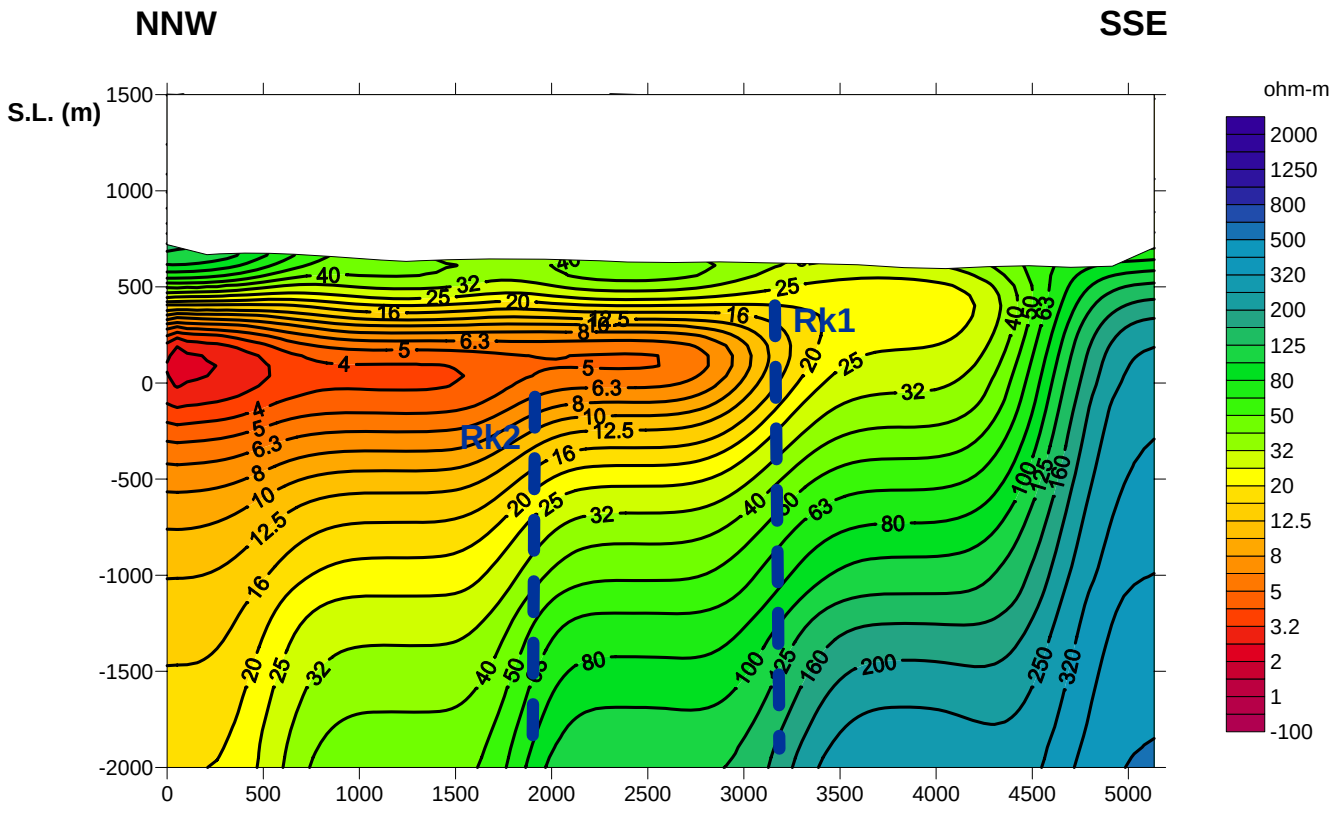

Fig. 4.4.4-14 Resistivity Section Map along line-C (Kotamobagu field)

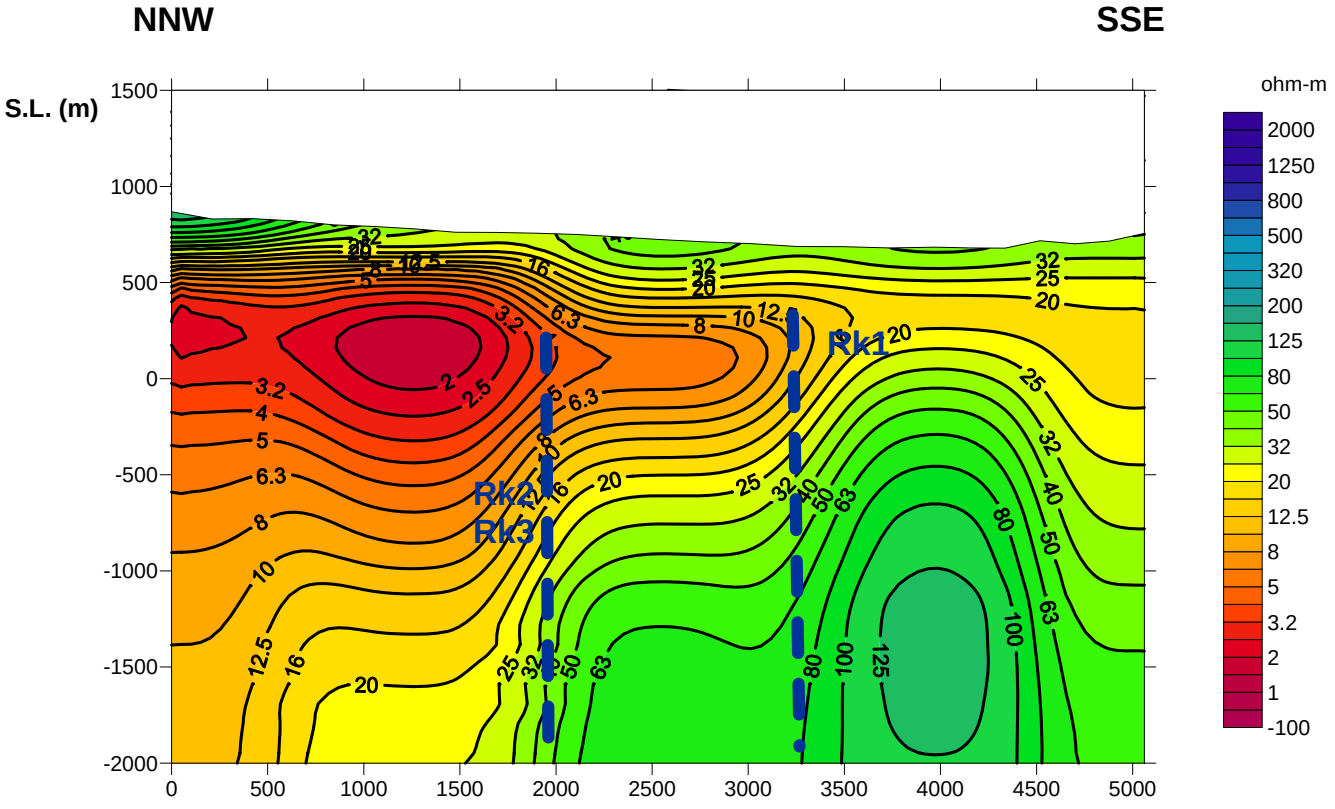

Fig. 4.4.4-15 Resistivity Section Map along line-D (Kotamobagu field)

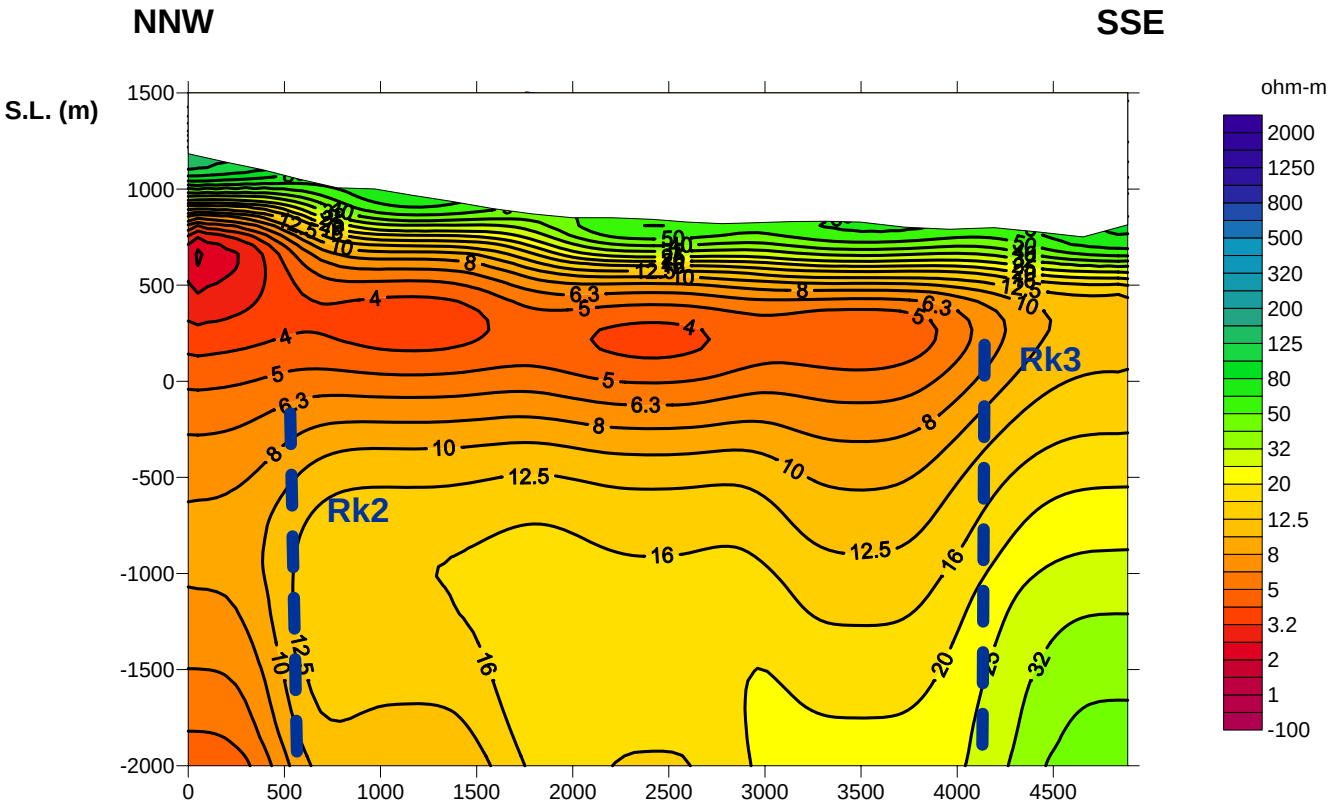

Fig. 4.4.4-16 Resistivity Section Map along line-E (Kotamobagu field)

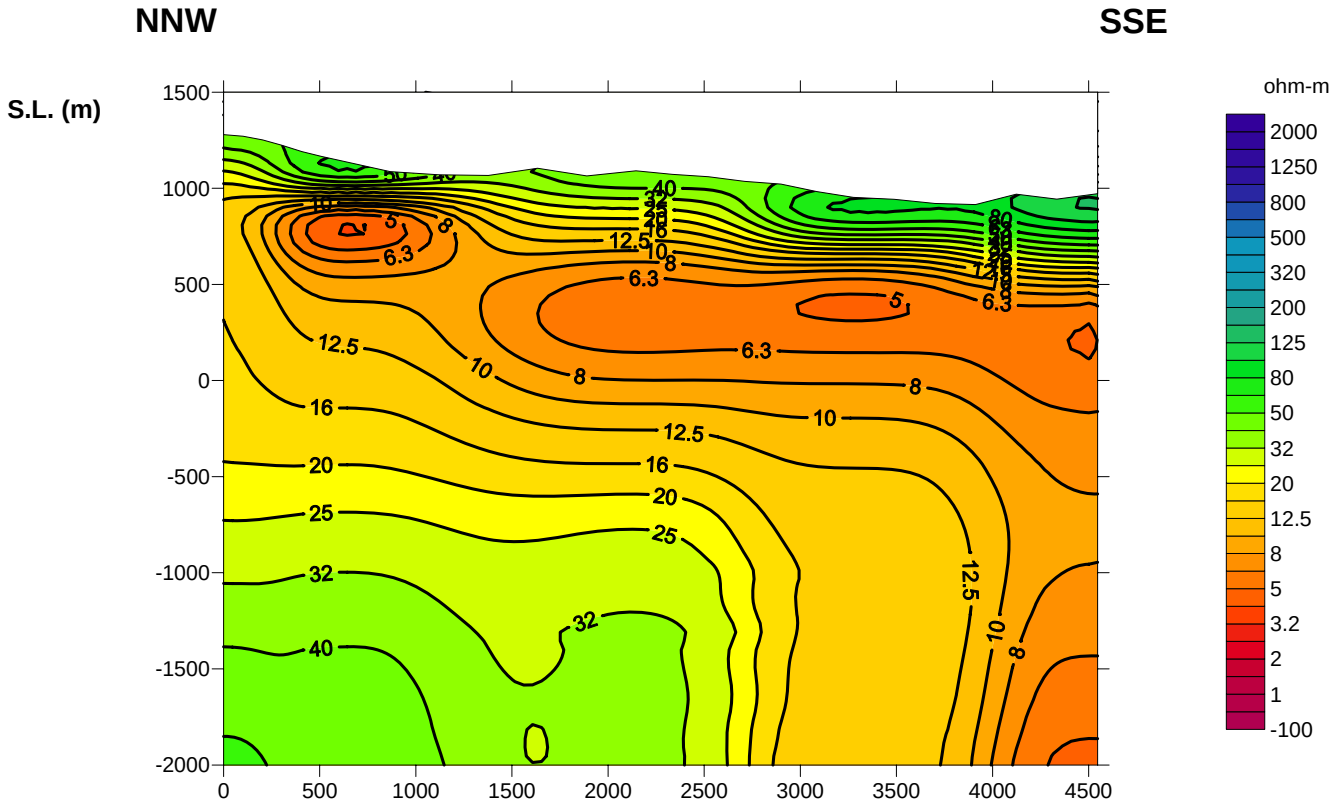

Fig. 4.4.4-17 Resistivity Section Map along line-F (Kotamobagu field)

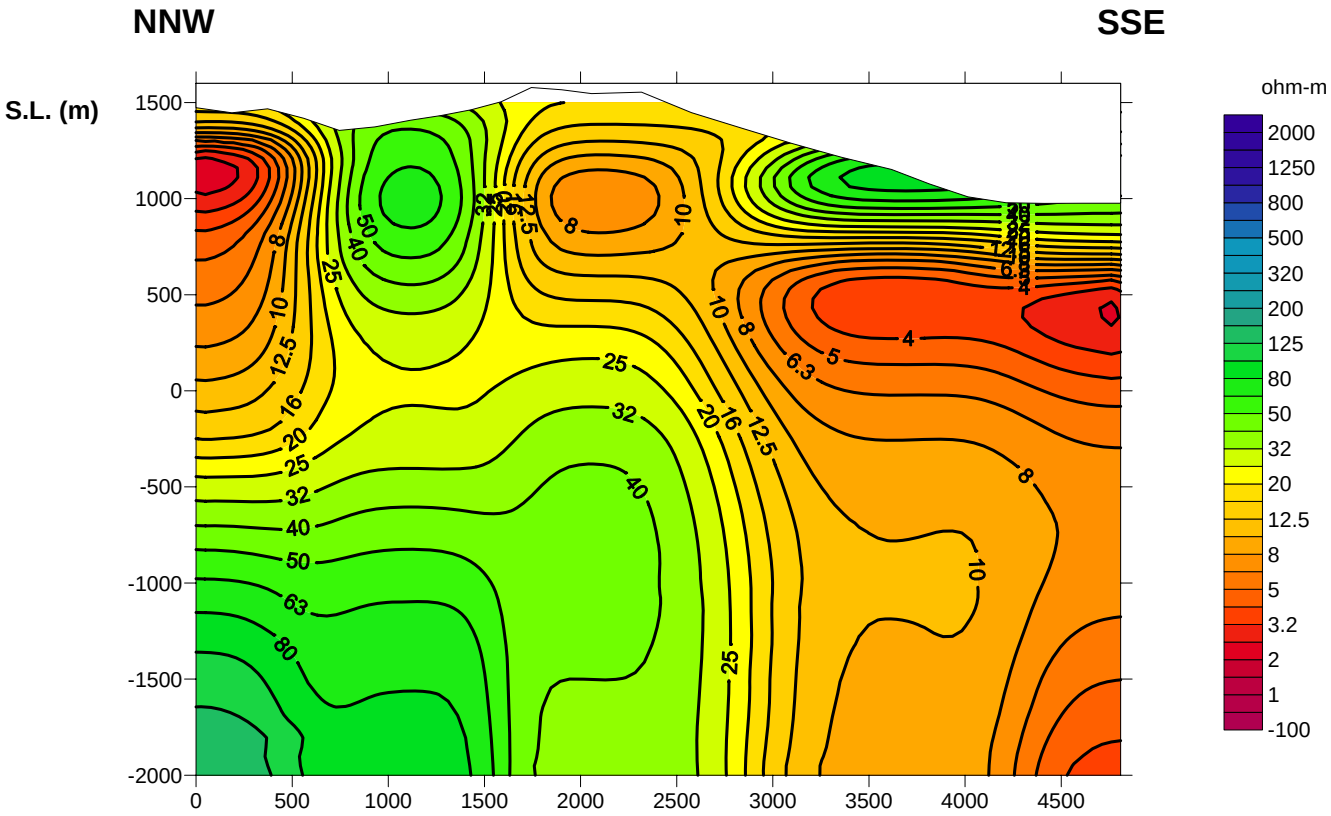

Fig. 4.4.4-18 Resistivity Section Map along line-G (Kotamobagu field)

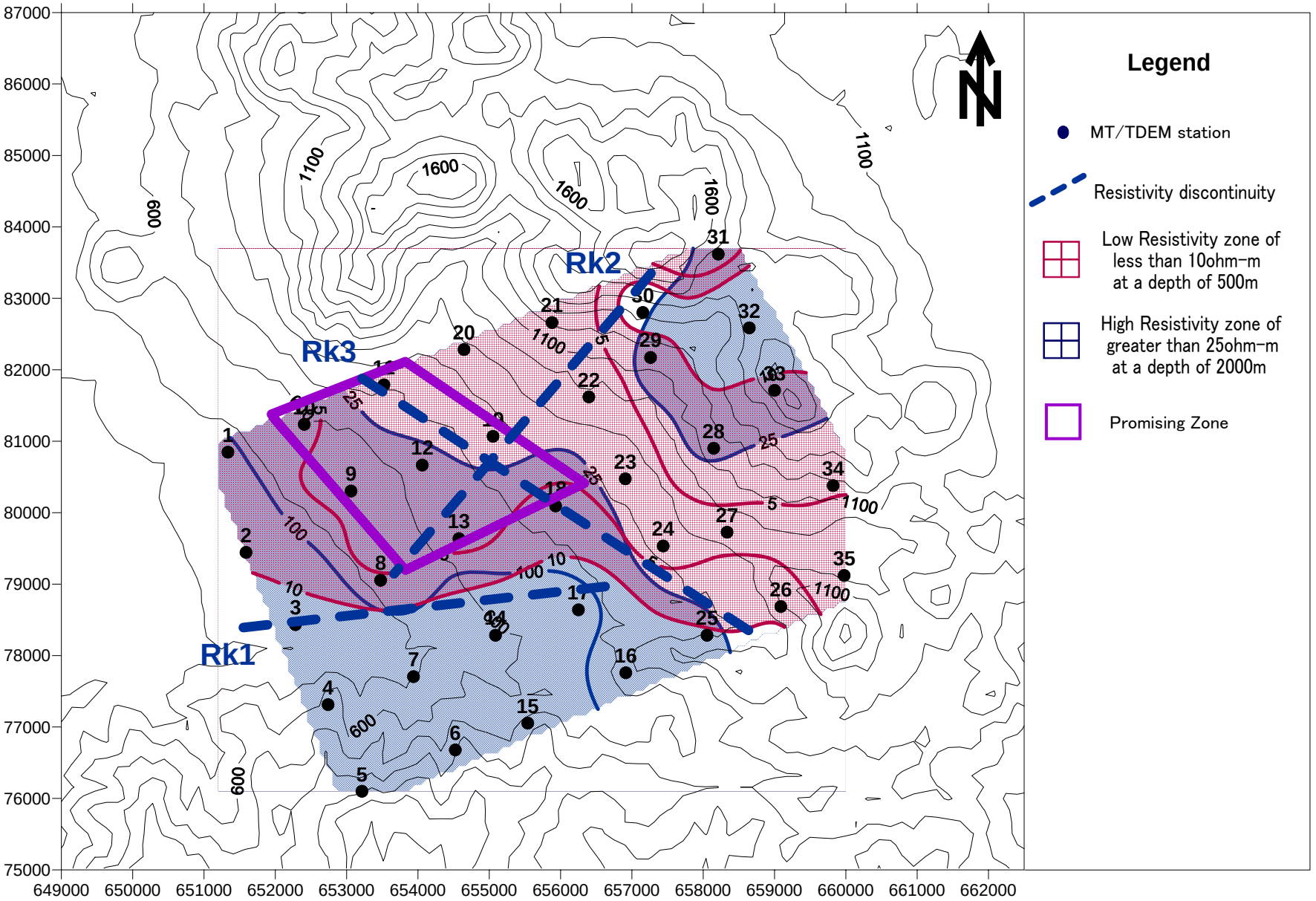

Fig. 4.4.4-19 Synthetic Resistivity Structure Map in the Kotamobagu geothermal field